Performance of a Perovskite-Based Lean-NO_X-Trap Catalyst and Effects of Thermal Degradation and Sulfur Poisoning

by

Crystle Constantinou

A thesis
presented to the University of Waterloo
in fulfillment of the
thesis requirement for the degree of

Master of Applied Science
in
Chemical Engineering

Waterloo, Ontario, Canada, 2012

Author’s Declaration

I hereby declare that I am the sole author of this thesis. This is a true copy of the thesis, including any required final revisions, as accepted by my examiners.

I understand that my thesis may be made electronically available to the public.

Crystle Constantinou

Abstract

Increases in vehicle exhaust emission regulations have led to research, development and improvements in catalytic converter technologies for gasoline-powered vehicles since the 1970s. Nowadays, there are strict regulations and standards for diesel engines as well, and one of the regulated species is nitrogen oxides (NO_X). The lean NO_X trap (LNT) catalyst has been studied and developed for use in lean burn (of which diesel is an example) engine exhaust as a technology to reduce NO_X to N_2. Typical LNT catalysts contain Pt, which catalyzes NO oxidation and NO_X reduction, and an alkali or alkaline earth material for NO_X storage via nitrate formation. The catalyst is operated in a cyclic mode, with one phase of the cycle under oxidizing conditions where NO_X is trapped, and a second phase, which is reductant-rich relative to O_2, where stored NO_X is reduced to N_2. A recently developed catalyst uses a perovskite material as part of the LNT formulation for the oxidation reactions thereby eliminating the need for Pt in a LNT. This catalyst does include Pd and Rh, added to accommodate hydrocarbon oxidation and NO reduction, respectively. Ba was used as the trapping component, and Ce was also part of the formulation.

NO oxidation kinetics over the fully-formulated and bare perovskite material were determined, with NO, O_2 and NO_2 orders being at or near 1, 1 and -1, respectively for both samples. The fully-formulated sample, which contains Ba supported on the perovskite, was evaluated in terms of NO_X trapping ability and NO_X reduction as a function of temperature and reduction phase properties. Trapping and overall performance increased with temperature to 375°C, primarily due to improved NO oxidation, as NO_2 is more readily

trapped, or better diffusion of nitrates away from the initial trapping sites. At higher temperatures nitrate stability decreased, thus decreasing the trapping ability. At these higher temperatures, a more significant amount of unreduced NO_X formed during the reduction phase, primarily due to nitrate instability and decomposition and the relative rates of the NO_X and oxygen storage (OS) components reduction reactions. Most of the chemistry observed was similar to that observed over Pt-based LNT catalysts. However, there were some distinct differences, including a stronger nitrate diffusion resistance at low temperature and a more significant reductant-induced nitrate decomposition reaction.

The perovskite-based lean NO_X trap (LNT) catalyst was also evaluated after thermal aging and sulfur exposure. NO oxidation, NO_X trapping ability and NO_X reduction as a function of temperature and reduction phase properties were evaluated. Similar overall performance trends were seen before and after degradation, however lower performance after thermal aging and sulfur exposure were seen due to sintering effects and possible build-up of S species. Although performance results show that most of the sulfur was removed after desulfation, some sulfur remained affecting the trapping and reduction capabilities as well as the water gas shift (WGS) extent at lower temperatures. The Oxygen storage capacity (OSC) on the other hand was maintained after the catalyst was exposed to thermal aging and sulfur poisoning then desulfation, all of which suggest that the perovskite or Pd components were irreversibly poisoned to some extent.

Acknowledgements

I would like to acknowledge and thank the Natural Sciences and Engineering Research Council of Canada and General Motors for their financial support.

My sincerest thanks and appreciation go to my supervisor, Professor William Epling, for his endless guidance and support. Professor Epling was continuously encouraging and always had my best interest at heart, and for that I am truly grateful.

Those days and nights that never seemed to end in the lab would not have been the same without my lab mates. Thanks to John, Isabella, Ali, Harry and Suad for their useful discussions and support. I would also like to acknowledge the students that assisted in the lab during their co-op terms, Jordan, Melanie, Megan and Keith.

To my good friend Linda, your advice and support throughout my study means more than you know. I thank you for listening, for caring and for the late night coffee breaks. Waterloo would not have been the same without you.

I could not have got through my studies without the constant support and love from my family. Through ups and downs you are always there. Mom, dad, Eva and Paul, I can't thank you enough.

Last, but most certainly not least, to my husband. You are a source of strength and encouragement. I am so grateful for the support and love you give me every day.

Dedication

To my family

Table of Contents

List of Figures

List of Tables

Chapter 1

Background and Objectives

1.1 Research Objectives

The control of harmful gases from vehicle emissions is an ongoing problem around the world. Traditionally, a three-way catalyst (TWC) has been used for gasoline engine exhaust clean-up, and is efficient in the removal and control of hydrocarbons (HC), CO and NO_X exhaust emissions. However for lean-burn engines, running with excess oxygen (such as diesel engines), the reduction of NO_X to N_2 is challenging and the TWC is not efficient enough to meet today's regulations. Two solutions to controlling NO_X are selective catalytic reduction (SCR) catalysis and the lean-NO_X-trap (LNT) catalysis. The SCR catalyst can operate in an O_2 rich environment to selectively reduce NO_X to N_2 and H_2O using ammonia or hydrocarbons as the reductant [1]. The LNT catalyst works in a cyclic manner that oscillates between O_2 rich and fuel rich environments. There has been significant research and development of LNT catalysts [2-4] in response to the inherent challenge of reducing NO_X in an oxidizing environment. A common problem however with the LNT catalyst is that it uses a precious metal component, platinum (Pt) [5], which is expensive. As such, other alternatives to Pt have been studied in the past [5]. General Motors (GM) have developed an alternative to the Pt-based LNT catalyst that is of low cost [6]. The catalyst that was developed includes a rare earth metal, perovskite. The perovskite-based LNT catalyst developed by GM has the chemical formula $La_{1-x}Sr_xMnO_3$ (x=0, 0.1). This catalyst underwent in-house research at GM and their study found NO_X conversion rates of 90% [6].

The focus of this research is on the abilities and limitations of the perovskite-based LNT catalyst manufactured by GM used to control NO_X pollution emitted from lean burn engines. The research goals are:

1. Independently verify performance: this catalyst already underwent in-house research and testing at GM. We studied it at the University of Waterloo to independently verify its NO_X reduction performance.
2. Understand the NO oxidation, and NO_X trap and reduction **chemistry** on the perovskite-based LNT catalyst, and compare these to the standard Pt-based LNT catalyst.
3. Investigate the effects of catalyst deactivation; specifically thermal degradation and sulfur poisoning on the perovskite-based LNT catalyst.

In terms of background, the literature review is presented in Chapter 2 and Chapter 3 outlines the methodologies and procedures used for the experiments that were completed. Chapter 4 presents the results from the NO oxidation and NO_X trapping and reduction experiments over the fresh perovskite-based LNT catalyst and a comparison of these results to the standard Pt-based LNT catalyst. Chapter 5 presents the results and discussion of the effects of thermal degradation and sulfur poisoning over the perovskite-based LNT catalyst. Chapter 6 presents the conclusions to the findings of the experiments presented in Chapters 4 and 5. Lastly, Chapter 7 presents recommendations for future research.

1.2 Background Information

In the United States, the Environmental Protection Agency (EPA) was created to measure and regulate harmful, to both human health and the environment, chemical releases into the environment. The growing amounts of pollutants found in the atmosphere brought about the Clean Air Act (CAA) [7]. The CAA contains regulations that were put into place to protect human health from harmful and hazardous air pollutants [8]. A common environmental discussion topic today is global warming, produced by greenhouse gases trapped in our atmosphere, and the effect it has on global climate change [9]. Greenhouse gases include a variety of emissions with the most common greenhouse gas carbon dioxide (CO_2)[10]. CO_2 is emitted to the atmosphere via a number of processes, which includes the burning of fossil fuels as is the case for automobiles (which are the second highest source of CO_2 emissions) [11]. A suggested approach to reduce CO_2 emissions is the use of diesel engines as they are more fuel efficient; however there are still other pollutants such as NO_X (nitric oxide (NO) or nitrogen dioxide (NO_2)), carbon monoxide (CO) and various hydrocarbons (HC). As automobiles have been highlighted as a key contributor to pollutant emissions, much research has been dedicated to the reduction of pollutants emitted from vehicles. However, the necessity and use of automobiles is currently an inevitable and universal fact in today's society both for personal and commercial uses. Much research therefore, has been dedicated to catalytic converters for the reduction of pollutants emitted from vehicles; specifically the reduction of CO, NO_X and volatile organic compounds (VOCs). Different catalyst technologies will be outlined further in this section.

1.3 Diesel Engine

Dr. W. Addy Majewski and Magdi K. Khair note in their book [12] the most important difference between diesel and gasoline internal combustion engines is the use of compression rather than a spark plug to ignite the fuel and air mixture. Furthermore, the authors explain that the combustion process in diesel engines starts with introduction of air into the combustion chamber by a supercharger, turbocharger, or combination of both. Then, air is compressed by a piston to a high pressure before fuel is injected into the compressed air in the combustion chamber. Fuel could be injected directly into the combustion chamber or it could be injected into a pre-chamber depending on the design of the diesel engine. To produce higher efficiency combustion, the fuel injector ensures that the fuel is broken into small droplets that are easy to evaporate and the fuel is distributed evenly in the combustion chamber. After injecting the fuel, the fuel is ignited by the heat from the compressed air and the droplets vaporize and burn. When it reaches the ignition temperature, the fuel droplets vaporization and combustion causes an increase in the pressure in the combustion chamber. This increase in pressure causes a rapid expansion moving the piston downward supplying power to the crankshaft. The four stages of the combustion process are shown in Figure 1 below.

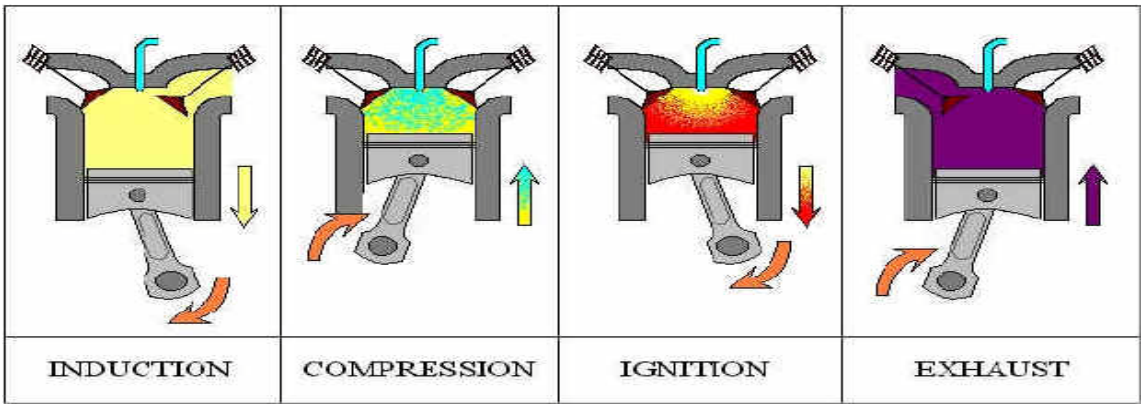

Figure 1: Four stages of the diesel engine combustion process, taken from the Automobiletech website [13]

Diesel engine exhaust gas contains many compounds, such as unburned HC, CO, NO_X, and particulate matter (PM) that are emitted into the atmosphere and are harmful for human and environmental health [12].

1.4 Air Pollution

Compounds that contribute to air pollution are known as air pollutants and can be in the form of gases, liquids or even solid particles. These compounds can be “man-made” or form naturally in the atmosphere.

Primary pollutants are pollutants that are released directly into the atmosphere. Some examples of sources of primary pollutants are industrial processes, factories and emissions from vehicles [8]. Secondary pollutants are formed via chemical and photochemical reactions of primary pollutants. The EPA has listed 6 common pollutants found in the atmosphere and their estimated emission amounts from 1970 to 2012 [8]. There are a variety of sources that emit these pollutants, such as industrial processes and vehicle emissions. Pollutants emitted

from vehicles include all those listed below; however their source in this list is not strictly vehicle emissions. The estimated pollutant data can be found in Table 1.

Table 1: National Emission Estimate Totals for Major Air Pollutants [8]

Pollutant	Millions of Tons Per Year									
	1970	**1975**	**1980**	**1985**	**1990**	**1995**	**2000**	**2005**	**2010**	**2012**
Carbon Monoxide (CO)	197	184	178	170	144	120	102	85	64	52
Nitrogen Oxides (NO_X)	27	26	27	26	26	25	23	19	15	12
Sulfur Dioxide (SO_2)	31	28	26	23	23	19	16	15	8	7
Volatile Organic Components (VOC)	35	31	31	27	24	22	18	18	17	16
Particulate Matter (PM)										
PM_{10}	12	7	6	4	3	3	3	3	3	3
$PM_{2.5}$	N/A	N/A	N/A	N/A	2	2	3	2	2	2
Ammonia (NH_3)	N/A	N/A	N/A	N/A	0.6	0.7	0.5	0.6	0.4	0.3

The pollutants listed in Table 1 are harmful for humans, animals and the environment. SO_2, for example, irritates the eyes and respiratory system that can cause severe respiratory disease [14]. SO_2 and SO_3 can react with water to form acid rain that can lower pH values in lakes and oceans as well as corrode buildings and bridges [8]. CO is produced by incomplete combustion of fossil fuels and can cause sudden illness and death [15]. CO is an odourless and colourless gas that causes dizziness, shortness of breath and eventually death if exposed

to high concentrations. NO_2 is a lung irritant that, if exposed to at high concentrations, will lead to pulmonary edema and death [16]. Nitrogen oxides (NO_X) can also react with water to form acid rain [8].

1.5 Standards and Regulations

Although there has been great progress in reducing pollutant emissions and thus sustaining human and environmental health, there are still significant issues to resolve, with fatalities that can still commonly be associated to air pollutants [17]. As vehicle exhaust emissions add to the pollutants in the atmosphere and there is a growing and continuous use of automobiles, stronger regulations on vehicle exhaust emissions have been set in place over the years. Table 2 (provided by the EPA) shows the amount of change that has happened over the years, due not strictly to vehicle emissions, but from all contributors [18].

Table 2: Percent Change in Emissions (EPA Statistics)

	1980 vs. 2010	**1990 vs. 2010**	**2000 vs. 2010**
Carbon Monoxide (CO)	-71	-60	-44
Lead (Pb)	-97	-60	-33
Nitrogen Oxides (NO_X)	-52	-48	-41
Volatile Organic Compounds (VOC)	-63	-52	-35
Direct PM_{10}	-83	-67	-50
Direct $PM_{2.5}$	N/A	-55	-55
Sulfur Dioxide ($SO_{2)}$	-69	-65	-50
Note: Negative numbers indicate reductions in emissions			

These data show significant improvement in the amount of pollutants found in the atmosphere; however with still growing numbers of cars on the road and the pollutants still found in vehicle exhaust, there is still a growing concern over exhaust emissions.

1.5.1 NO_X Standards and Regulations

Higher NO_X emissions standards have been implemented over the years. Figure 2 shows some NO_X standards for the United Stated and in Europe.

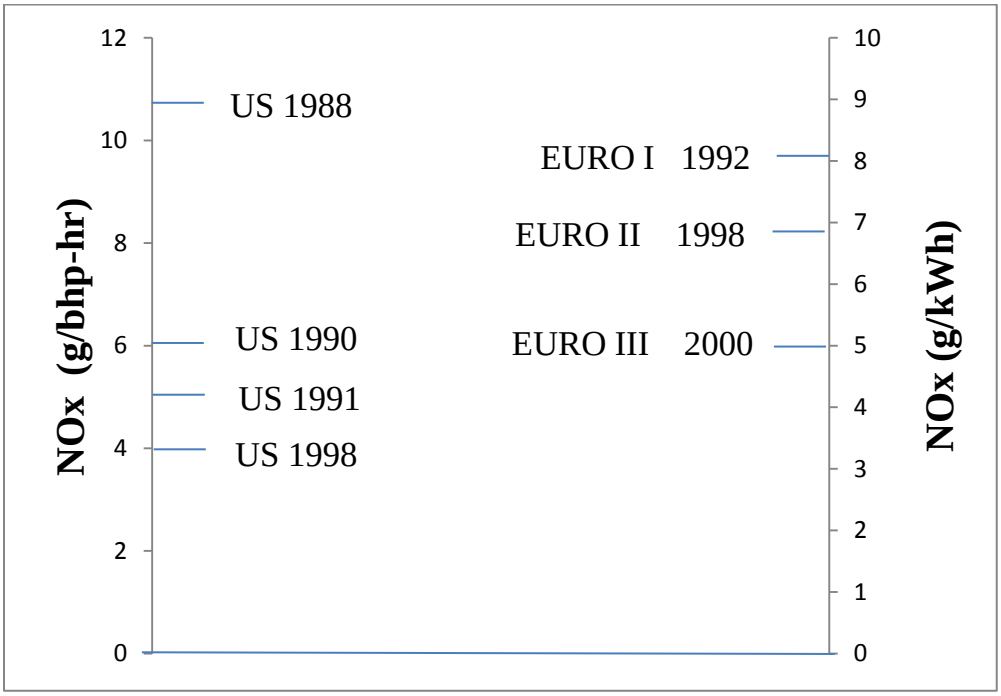

Figure 2: NO_X Emission Standards for Heavy-Duty Engines [19]

NO_X emissions were reduced to below 4 g/bhp-hr in heavy-duty engines in the United States primarily through engine modification (injection timing and charge air cooling). These technologies decrease the cylinder pressure which decreases the amount of heat created and less heat created in turn decreases NO_X emissions [19]. For heavy-duty vehicles manufactured beginning in 2007 the NO_X regulations are as low as 0.2 g/bhp-hr. While diesel engine technologies helped decrease NO_X emissions for heavy-duty engines, exhaust

emissions catalysts were required to hit this lower target – engine modifications have not proven sufficient.

1.6 Sources of NO_X

NO_X is a general term used for NO and NO_2 found in the atmosphere. NO_X gases are highly reactive and toxic. Although there are many sources of NO_X emissions, as seen in Figure 3, the use of automobiles is the main source of NO_X emissions. Much focus has been put on exhaust after-treatment technologies for the removal of NO_X specifically [2-4].

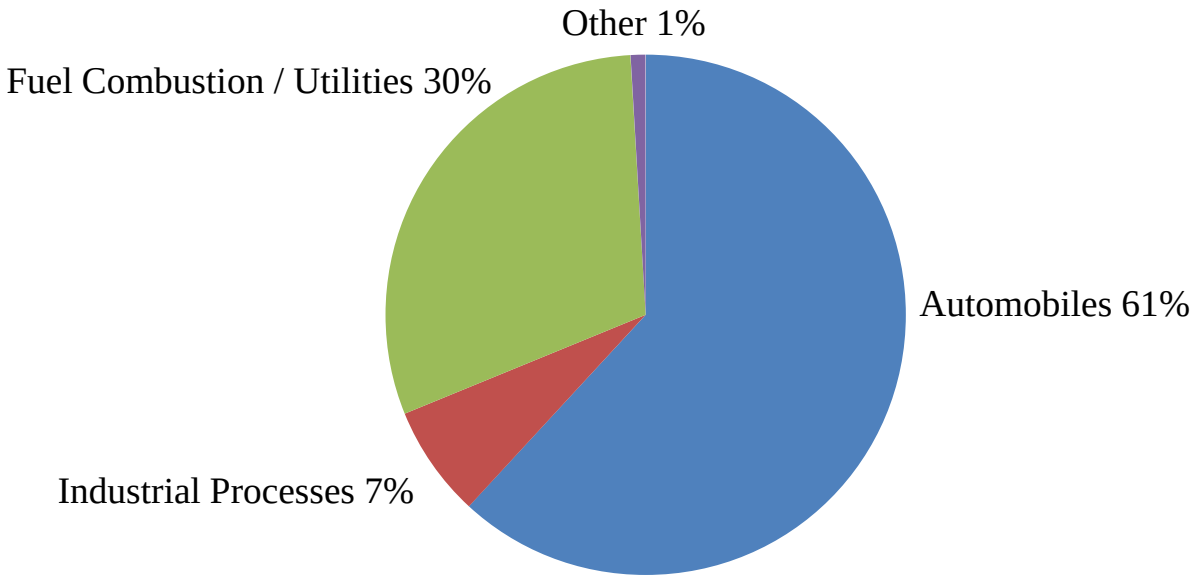

Figure 3: NO_X Emission Sources (EPA Statistics) [20]

1.7 Effects of NO_X

NO_X species are found in the atmosphere and automobile use is the main source. As stated above NO_2 is a lung irritant that can cause pulmonary edema and death [16]. NO_X can also play the role of secondary pollutant, which is reacting with other pollutants or compounds creating another pollutant [8]. For example ground-level ozone forms when NO_X reacts with VOCs in the presence of sunlight: NO_X + VOCs + Sunlight = Ozone. Ozone can kill trees, damage vegetation and cause irritation to the lungs, eyes and nose. Smog can also be formed via NO_X[8]. Much like the reaction creating ozone, smog is created by the reaction between pollutants (NO_X, VOCs and ozone) and sunlight. As stated above NO_X can also play a part in forming acid rain via the formation of nitric acid: $NO_2 + OH = HNO_3$. Acid rain falls into large bodies of water and can kill fish and vegetation. Also, acid rain can corrode buildings and bridges.

1.8 NO_X Reduction Technologies

Lean burn engines, such as diesel engines, running with excess oxygen present a challenge in the reduction of NO_X to N_2. In order to meet today's NO_X emissions regulations, NO_X reduction technologies have been a focus. Three types of technologies are the three-way-catalytic (TWC) converter, selective-catalytic-reduction (SCR) catalysis and the lean-NO_X-trap (LNT) catalyst.

1.8.1 Three-Way-Catalytic (TWC) Converter

Gasoline engine emissions began to be regulated in 1970s to control HC and CO emissions and TWC converters were introduced in the 1980s to meet regulations for NO_X[1]. The TWC is deposited onto a ceramic monolith honeycomb structure, as shown in Figure 4. The honeycomb structure allows for maximum surface area for reactions to occur and while minimizing the amount of catalyst required and keeps the backpressure generated low[21]. The main components of a TWC converter are precious metals, such as Pt, Pd and Rh, and an inorganic carrier called a "washcoat", such as Al_2O_3, that provides a platform for the conversion of HCs to CO_2 and H_2O, NO_X to N_2 and CO to CO_2 [22].

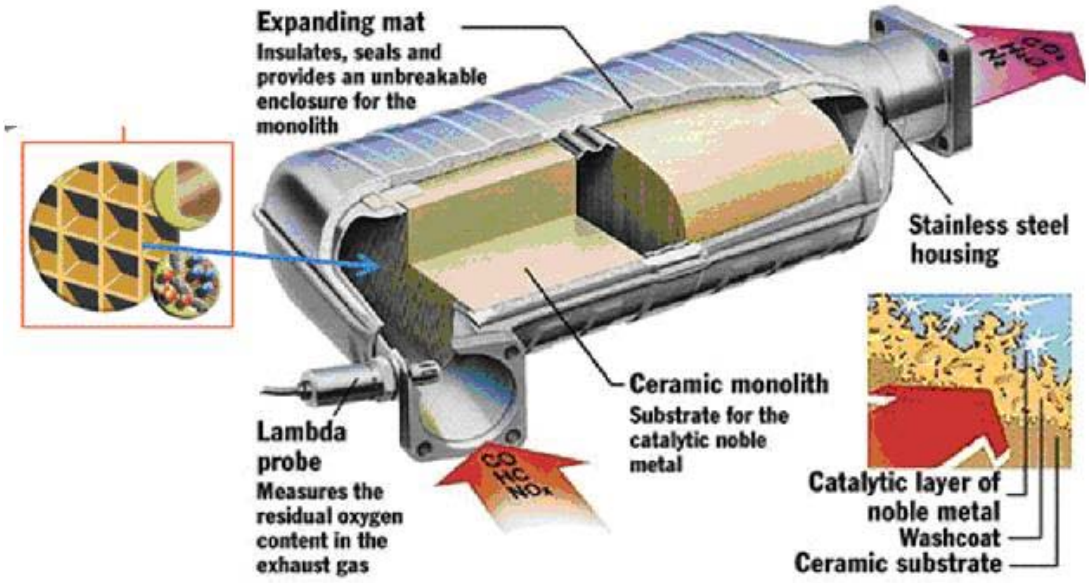

Figure 4: TWC Converter Deconstructed [23]

TWC converters were successful in converting toxic gases to cleaner nontoxic gases for gasoline engines, operating with stoichiometric air to fuel ratio (no O_2 present). Equations (1) to (3) are overall reactions that can occur in the TWC process.

$2NO + 2H_2 \rightarrow N_2 + 2H_2O$ (1)

$2CO + O_2 \rightarrow 2CO_2$ (2)

$2C_XH_Y + (2X + Y/2)\ O_2 \rightarrow 2XCO_2 + YH_2O$ (3)

Some benefits of the TWC converter are its durability, relatively low cost and its low maintenance requirements [1]. However in the case of lean burn engines with an excess of O_2 present, reducing NO_X became problematic (reduction reaction in an oxidizing atmosphere). Other issues with the TWC converters are performance dependence on temperature and loss of activity through thermal deactivation and poisoning [1].

1.8.2 Selective Catalytic Reduction (SCR)

In the 1990s SCR systems were introduced in the US for their use in gas turbines and in coal fired power plants for NO_X emissions control [1]. SCR systems continued to be used in industries such as boilers for chemical processing plants, furnaces, coke ovens, and plant and refinery heaters.

The TWC catalyst operates non-selectively to reduce NO_X by CO and HC with a stoichiometric air-to-fuel ratio (no O_2 present). With respect to emissions from diesel engines, there is an O_2 environment present which does not allow the TWC to effectively reduce NO_X and for this reason cannot be used for NO_X control in lean burn applications; other catalyst applications needed to be employed to selectively reduce NO_X. SCR catalysis

can effectively operate in an O_2 rich environment and can selectively reduce NO_X. SCR catalysts were applied in the automotive industry in 2004 [1]. The SCR process can use two reductant compounds that are injected into the engine exhaust to selectively react and reduce NO_X to N_2 and H_2O; either (a) ammonia (either as pure anhydrous ammonia or urea that decomposes to ammonia) or (b) hydrocarbons [1]. Ammonia-based SCR catalysts have been shown capable of meeting regulations, whereas hydrocarbon-based SCR catalysts are not efficient enough to meet today's regulations. Reactions (4) to (8) below can occur in the ammonia SCR process.

$$6\,NO + 4NH_3 \rightarrow 5N_2 + 6H_2O \quad (4)$$

$$4NO + 4NH_3 + O_2 \rightarrow 4N_2 + 6H_2O \quad (5)$$

$$6NO_2 + 8NH_3 \rightarrow 7N_2 + 12H_2O \quad (6)$$

$$2NO_2 + 4NH_3 + O_2 \rightarrow 3N_2 + 6H_2O \quad (7)$$

$$NO + NO_2 + 2NH_3 \rightarrow 2N_2 + 3H_2O \quad (8)$$

Several ammonia SCR catalysts have been studied over the years and include Pt, which has been found only applicable for low temperature (<573 K) operation, vanadium which is efficient for medium temperature (<700 K) operation but vanadium itself is volatile at high temperature making it less attractive for vehicle use, and metal-doped zeolites, which have proven the industry standard. A common issue is ammonia slip through the catalyst during

operation [1], leading to its release, as well as the lack of a urea infrastructure (urea is used as the NH_3 source, decomposing to NH_3 and CO_2 in the exhaust stream once injected).

1.8.3 Lean-NO_X-Trap (LNT)

Typically LNT catalysts are composed of a precious metal component, such as Pt and Rh, for oxidation and reduction reactions, and an alkali or alkaline-earth metal component, such as Ba, for trapping/nitrate formation reactions. NO_X adsorbs to the surface, and is then transformed to nitrates, thus the NO_X is “trapped”. The overall LNT process is cyclic, where the exhaust stream oscillates between lean (excess O_2) and rich (excess fuel) conditions. Figure 5 below depicts the overall chemistry and process. Through NO oxidation over the Pt component, NO_2 is formed and NO and NO_2 sorb on the surface in the form of nitrites or nitrates. Eventually the catalyst needs to be regenerated to maintain its trapping ability, as otherwise it will simply become saturated with NO_X species. During the regeneration portion of the cycle, the nitrates formed during the trapping phase decompose; NO_X species are released and migrate to reduction sites, to react with reductants such as H_2 and CO or HCs, and are finally reduced to N_2. This restores the surface for trapping. The LNT catalyst has the same ceramic honeycomb structure as the TWC. The overall cycle can be described in five reaction steps [5].

1) NO oxidation to NO_2

2) NO and NO_2 sorption on the surface in the form of nitrites or nitrates

3) Reductant evolution when the exhaust is switched to rich conditions

4) Nitrate and nitrite decomposition - release of NO_X (migration to reduction sites)

5) NO_X finally being reduced to N_2 by the reductants

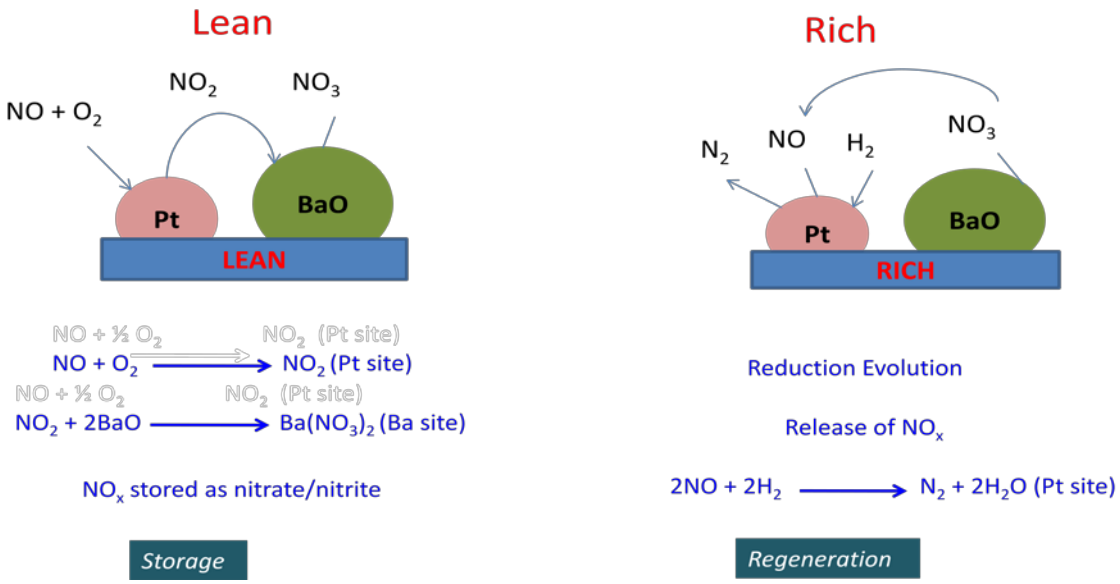

Figure 5: Lean-NO_X-Trap (LNT) Chemistry [24]

1.9 Perovskites as a Lean-NO_X-Trap Component

The most common precious metal component in the make-up of an LNT catalyst is the platinum (Pt) [5]however, Pt is very costly, being roughly $50 / g (retrieved on July 9, 2012)[25]. As such, alternatives for Pt have been studied, such as palladium (Pd) [5]. Perovskite materials have also been investigated. Researchers at General Motors have demonstrated that a perovskite-based catalyst, with no Pt, is efficient for NO_X trapping and reduction and an attractive alternative to Pt-based LNT catalysts, with its thermal stability and low cost [6]. The perovskite structure will be described in the next chapter.

1.10 LNT Deactivation Mechanisms

The activity of a LNT catalyst can decrease over the course of its life; this is known as catalyst deactivation. Catalyst deactivation seems to be a universal problem in automotive catalysis. There are five main catalyst deactivation mechanisms [26] and they are briefly outlined in Table 3.

Table 3: Catalytic Deactivation Mechanisms

Mechanism	Type	Problem	Source
Fouling	Mechanical	Formation of carbon or coke films creating loss of catalytic surface sites	Physical deposits create less active catalytic surface area
Poisoning	Chemical	Loss of catalytic surface sites	Storage of impurities/contaminants creating blockage of site
Thermal Degradation	Thermal	Loss of catalytic surface area, support area and transformation of catalytic phases	Sintering of structure leasing to pore collapse, migration of catalyst particles and reaction of catalyst components
Vapour Formation	Chemical	Loss of catalytic phases	Volatile compounds formed via reaction of gas with catalyst phase
Attrition	Mechanical	Loss of catalytic material	Collision of catalyst particles leads to catalytic loss in surface area

Specifically for LNT catalysts, the two main sources of deactivation are sulfur poisoning and thermal degradation [26]. In LNT chemistry, deactivation results in a decrease in catalyst activity with regards to its ability to trap NO_X and ultimately reduce it to N_2.

Desulfation is a process used to remove the sulfur from the LNT catalyst. Desulfation typically occurs under rich conditions and at high temperatures [27-31], which can lead to thermal degradation.

Not only can thermal degradation occur after desulfation treatment, but to a lesser extent, thermal degradation can also occur during the regeneration portion of the NO_X storage and reduction cycle[5], since the oxidation of hydrocarbons, CO and H_2 (the reductants) are exothermic reactions and generate heat locally. The primary effect of thermal degradation is sintering [32]. Catalyst sintering refers to the loss of surface area of the precious metals (Pt, Pd and Rh) via agglomeration and via washcoat pore collapse [33, 34] which leads to a decrease in catalytic activity.

Chapter 2

Literature Review

This chapter will focus on the perovskite structure and it's abilities as an LNT catalyst, reaction chemistry steps that occur on the LNT catalyst, and the effects of thermal degradation and sulfur poisoning on the performance of LNT catalysts.

2.1 Perovskite-Type Oxides

Mixed metal oxides have the ability to facilitate complex reactions for catalyst applications. In order to achieve the appropriate catalytic reactions, different compounds are researched for their surface, solid state and structural properties, and perovskite-type oxides remain prominent in this research field [35]. The naturally occurring compound Calcium Titanate, $CaTiO_3$ was discovered in the Uran Mountains of Russia 1839 by Gutza Rose and named after L. A. Perovski [36]. The crystal's structure and symmetry play a role in its physical properties such as cleavage, electronic band structure and optical transparency [37]. The general formula of perovskite oxides is ABO_3. *A* and *B* are two cations of very different sizes; the *A* ion is bigger than the *B* ion. The crystallized structure a perovskite oxide takes is ideally a cubic unit cell [38]. An example of this can be seen in Figure 6.

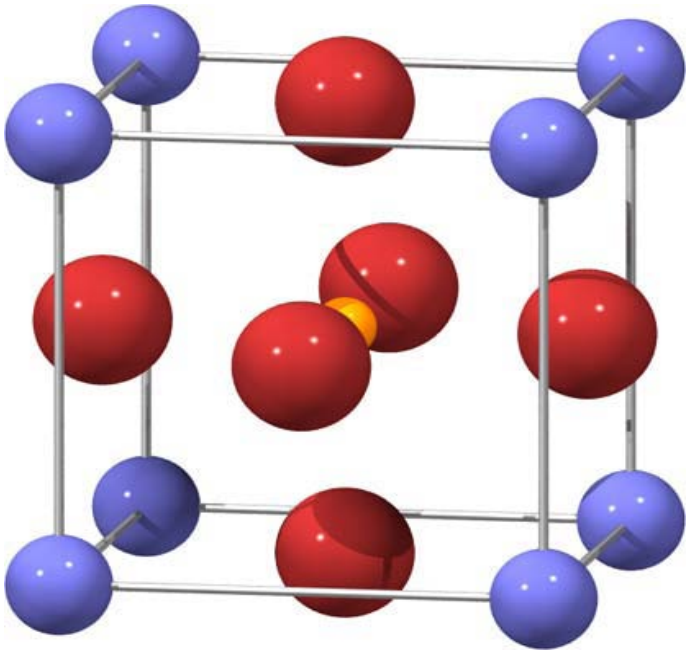

Figure 6: Cubic perovskite unit cell. Blue sphere represent *A* cations, yellow spheres represent *B* cations and red spheres represent the oxygen anions [39]

To tune catalytic capabilities for methane combustion, VOC combustion and NO_X storage and reduction, multi-component perovskite structures have been synthesized by substituting different cations into the perovskite crystal lattice [40 – 43]. About 90% of metallic elements are known to be stable in the perovskite-type oxide crystal lattice structure [35].

The TWC used in vehicle engines commonly include precious metals that are expensive and these precious metals can deactivate due to high temperatures. In general perovskites possess thermal stability and are of low cost, making them a good candidate for TWC catalysts. TWC incorporating perovskites have been seen to exhibit activity comparable to noble metal catalysts [44]. A common noble metal used for catalysis applications is Pt; however similar trends and effective oxidizing capabilities with perovskite-based catalysts have been

observed [6, 42, 43, 45, 46]. Research in LNT catalyst applications using perovskite as a substitute for high cost noble metals has therefore also been done [6]; results show perovskite-based LNT catalyst activity comparable to that of noble metal-based LNT catalysts. The authors in reference [6] showed a perovskite-based catalyst and a Pt-based catalyst had similar NO oxidation activity. In this same study, a fresh perovskite-based sample was evaluated, and re-evaluated after sulfur poisoning and desulfation. The authors concluded that at 350°C the fresh sample achieved 90% NO_X conversion and after the sulfur exposure the catalyst lost approximately 10% of its NO_X conversion efficiency. The authors also concluded however, that after a desulfation process was performed, the NO_X conversion was restored to 90%, suggesting that most if not all of the sulfur was removed. A perovskite-based LNT catalyst, K/La-CoO_3/$Ce_{0.8}Zr_{0.2}O_2$, was also studied and the authors found good NO_X storage capacity and a NO to NO_2 conversion of 44% [45].

2.2 Overview of the Lean-NO_X-Trap Catalyst

As stated in the first chapter, LNT catalysts work in a cyclic manner. An example of the outlet exhaust NO_X as a function of time is depicted in Figure 7. At the beginning of the cycle the excess O_2 levels create an atmosphere for NO to NO_2 conversion. The NO and NO_2, or simply NO_X, is then trapped on the alkaline or alkali earth metal. The catalyst is now acting like a “sponge” and eventually as more exhaust gas passes over it, the catalyst will begin to saturate, leaving no more room for NO_X to be trapped. In order to regenerate the catalyst surface, the NO_X needs to be released so that more NO_X can be stored. However the NO_X that is released must be reduced. Reductants that are in the exhaust gas, such as H_2 and

CO, cannot work efficiently in an O_2 rich environment. To eliminate this O_2 rich environment, an excess of fuel is injected into the system for a short amount of time while simultaneously the air injected into the combustion chamber is lowered to reduce the O_2 levels, creating the "rich" phase. The reductants are at an excess and can reduce the released NO_X; the catalyst surface is replenished and the cycle will start again.

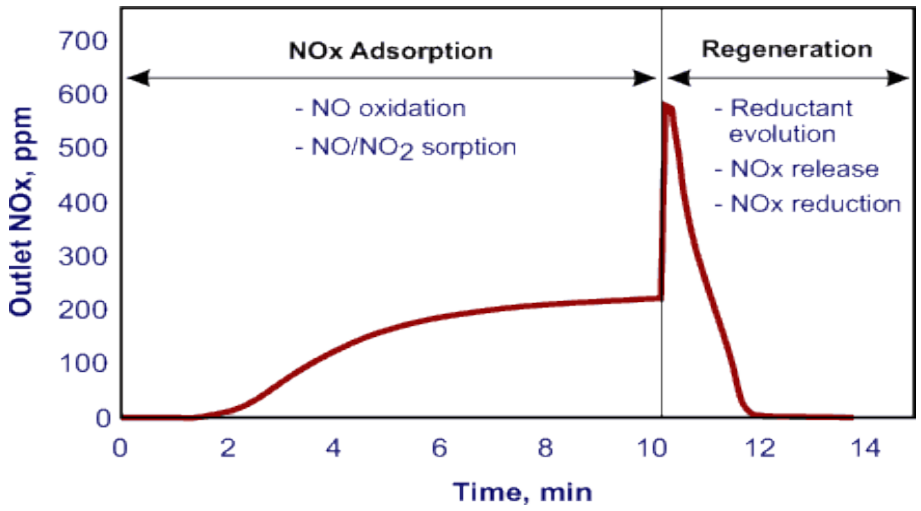

Figure 7: Outlet NO_X concentration profile as a function of time [5]

2.2.1 NO to NO_2 Conversion over the Precious Metal Component

Research has shown that NO_2 is more effectively trapped than NO, and thus NO oxidation over the precious metal sites is a key reaction for the overall LNT process [47 – 51]. NO oxidation over the precious metal occurs via the following reaction:

$$NO + ½\ O_2 \rightarrow NO_2 \qquad (9)$$

The most common LNT oxidation and reduction component is Pt, although other precious metals such as Pd and Rh are also used [5]. Studies have shown that while Pd and Rh are less

active for NO oxidation, they are more active for NO_X reduction [52 – 54]. Another comparative study showed that a Pt-based catalyst showed a 20% maximum NO to NO_2 conversion while no NO oxidation was observed over the Pd-based catalyst under the same experimental conditions [55]. Again, NO oxidation is a vital step and the Pt-based catalyst commonly shows the best NO oxidation results. This is not to say that the NO_X reduction activity of Pd and Rh are not significant effects, as they are commonly added components to LNT catalysts [52]. Perovskites have been studied as oxidation catalysts. The study performed by Kim et al. [6] included a comparison of different perovskite-based catalysts for diesel oxidation catalyst and lean NO_X trap catalyst performance. The study focused on NO_X trapping and reduction, NO to NO_2 conversion and sulfur poisoning. They observed that substituting Sr into La-based perovskites proved to be efficient in increasing the surface area and acting as a structural promoter. In the General Motors study [6], the $La_{1-x}Sr_xMnO_3$ (x = 0, 0.1) catalyst performed the best and was chosen as a good competitor to the Pt-based catalyst for LNT applications. The perovskite catalyst had similar NO oxidation activity as a Pt-based catalyst tested. For example, at 300°C, NO to NO_2 conversion was 86% for the perovskite-based catalyst, which was actually higher than the Pt-based catalyst studied at the same temperature. López-Suárez et al. have also studied Sr-based perovskite LNT catalysts and showed good NO to NO_2 conversion [43]. He et al. [45] also showed significant NO to NO_2 conversion over La-based perovskites.

Studies performed on the conventional Pt-based catalyst by Mulla et al. [56] and a Pd-based catalyst by Weiss et al. [57] determined reaction orders for NO, O_2 and NO_2 which were 1, 1

and -1 respectively. In both studies, NO_2 inhibition of the NO oxidation reaction was noted. Mulla et al. attributed the NO_2 inhibition to the fact that NO_2 preferentially adsorbs to the surface due to a high sticking coefficient [47]. This in turn prevented adsorption of NO and O species thus decreasing NO oxidation. Below is an example of a proposed kinetic scheme by Mulla et al. [56]:

$$NO + * \overset{k_1}{\leftrightarrow} NO* \quad (10)$$

$$NO_2 + 2* \overset{k_2}{\leftrightarrow} NO* + O* \quad (11)$$

$$O_2 + * \overset{k_3}{\rightarrow} O_2* \quad (12)$$

$$O_2* + * \overset{k_4}{\rightarrow} 2O* \quad (13)$$

Where * is a Pt site and k_i is the rate constant at the i^{th} step.

2.2.2 NO_X Sorption over Trapping Components

The next step in the LNT process, after NO oxidation, is the storage of NO_X (NO and NO_2) in the form of nitrates (NO_3^{-1}) and nitrites (NO_2^{-1}). Common components used for NO_X storage are alkaline and alkali earth metals, most commonly Ba. As Ba is the most common trapping component used, below are examples of NO_X adsorption mechanisms using Ba. NO_2 reacting with barium peroxide to form nitrates [51], NO reacting with Ba oxide to form nitrates [58], NO_2 reacting with BaO to form nitrates and nitrites [59] and NO_2 reacting with BaO to form nitrates and NO [5] reactions are, respectively;

$BaO_2 + 2NO_2 \rightarrow Ba(NO_3)_2$ (14)

$BaO + 2NO + 3O \rightarrow Ba(NO_3)_2$ (15)

$2BaO + 4NO_2 \rightarrow Ba(NO_2)_2 + Ba(NO_3)_2$ (16)

$BaO + 3NO_2 + 3O \rightarrow Ba(NO_3)_2 + NO$ (17)

There are different components that can be used as the trapping material and selection is important. Components such as perovskites, mixed oxides and inorganic oxides have been tested as trapping materials [60]. López-Suárez et al. have studied Sr-based perovskite LNT catalysts and showed good NO_X storage ability [43]. He et al. [45] also showed significant NO_X trapping results on La-based perovskites. Generally however, alkali and alkaline earth metals still prove to have better performance. One study using Ba shows that when introducing NO_2 over $Pt/Ba/Al_2O_3$, nitrates are formed [61]. Another study using Ba showed both nitrites and nitrates being stored over $Pt/Ba/Al_2O_3$ when both NO and O_2 were introduced at low temperatures [62]. Other NO_X trap performance studies over Ba/Al_2O_3 showed NO_2 effectively sorbed while NO in the presence of O_2 did not [48, 51, 63]. Again, NO_2 overall traps better than NO [47 – 51]. NO_2 has also been seen to adsorb to washcoat (or support) components [64]. In this Fourier Transform Infrared (FTIR) study, BaO/Al_2O_3, Pt/Al_2O_3 and $Pt/BaO/Al_2O_3$ catalysts were all tested and NO_2 adsorbed on Al_2O_3 over all three catalysts. It was also shown however, that only 1% of the NO_X trapped was trapped on washcoat components, the rest by Ba [58].

Not only does the type of trapping component affect the trapping ability, but the temperature does as well. In a study using a thermogravimetric analyzer (TGA), experiments were carried out that compared the amount of NO_X trapped, correlated to the amount of weight change at different temperatures [5]. The study showed that at 200°C the weight change was 0.431g while at 450°C the weight change was 0.135 g, thus more NO_X was trapped at 200°C. This demonstrates that at high temperatures, there is low nitrate and nitrite stability.

Lastly, the presence of other gases in the exhaust gas mixture can also influence trapping ability. Components such as H_2O, CO_2 and O_2 have been seen to affect trapping. One research study showed that the presence of CO_2 during the trapping phase over a Pt/potassium (K)/Al_2O_3 catalyst caused a 45% decrease in trapping capacity at 250°C [65]. This study also showed similar negative effects on trapping ability in the presence of H_2O during the trapping phase [65]. At 300°C adding 5% H_2O led to a 16% decrease in trapping. The reason for the decrease was competition for Ba sites, with Ba carbonates and hydroxides forming when CO_2 and H_2O were added to the feed gas. Lastly, it has been seen that an increase in O_2 concentration can increase the amount of NO_X stored [66]. There are two proposed reasons for this; first the presence of O_2 increases the amount of NO to NO_2 conversion, and second it can also increase oxidation of surface NO_X to nitrates.

2.2.3 Reduction Evolution

In order to reduce the trapped NO_X to N_2, reductants such as H_2, CO and HC, must be delivered. This is accomplished in a reducing or “rich” environment. The source of the rich

environment is a short injection of excess fuel into the exhaust stream or managing the in-cylinder conditions such that the combustion actually runs rich.

Along with stored NO_X, stored O_2 can be reduced as well by the reductants, providing competition for reductant. Thus there must be enough fuel injected into the system in order to account for both the NO_X and oxygen stored. This factor is based on the Oxygen Storage Capacity (OSC) of a particular catalyst; this will be discussed in a later chapter. Most of the competition occurs at higher temperatures as the reductants are used up reducing the surface of the catalyst [67]; whereas at lower temperatures most of the reductant is used to reduce stored NO_X.

At low temperatures H_2 proves to be more efficient in reducing NO_X than CO and propylene [68, 69], however all are comparable at higher temperatures. CO can act either as a direct reductant via equation (18), or an indirect reductant in the presence of H_2O via the Water Gas Shift (WGS) reaction depicted in equation (19). The WGS reaction results in the formation of H_2 that later acts as a reductant.

$$2CO + 2NO \rightarrow N_2 + 2CO_2 \quad (18)$$

$$CO + H_2O \rightarrow H_2 + CO_2 \quad (19)$$

The WGS reaction occurs over precious metals thus it is expected to occur over LNT catalysts as well [70].

2.2.4 Nitrate and Nitrite Decomposition – Release of NO_X

In order to reduce NO_X, it first has to be released from the storage sites and this can occur via two driving forces [5]. First the injection of fuel, (the fuel contains reductants) results in

exothermic reactions which create heat via oxidation of the reductants by stored oxygen on the catalyst surface or O_2 present in the gas stream [5]. Heat generated can decrease nitrate and nitrite stability and thus results in NO_X release. In a past study involving rapid reductant pulse cycling experiments, the heat generated in the middle of the catalyst sample during the reductant phase was monitored. A 150°C temperature rise was observed as a result of the exothermic oxidation reactions between the reductant (H_2) and oxygen that was also present, as the authors "simply" added the reductant to the lean phase composition [71]. A second driving force for NO_X release is the absence of NO and O_2 which results in a net-reducing environment creating a lack of nitrate stability that leads to NO_X release [5]. It has been seen in the past that O_2 increases nitrate and nitrite stability over a Pt-based catalyst [72]. Thus the absence of O_2 can destabilize nitrates and nitrites.

Other components can affect the amount of NO_X released; for example H_2O and CO_2. An increase in gas-phase CO_2 was seen to increase the amount of NO_X released [73]. With CO_2 present carbonates form [74] and the formation and stability of carbonates create competition for nitrate formation and stability. Another study investigated the effect of the presence and absence of H_2O during the regeneration phase on NO_X release [74]. The authors found that with H_2O present the amount of NO_X released was lower than when H_2O was not present. However, the authors also noted that less NO_X was trapped when H_2O was present compared to when it was absent thus there was already less NO_X to be released in the first place. Overall the authors concluded that the presence or absence of H_2O showed that multiple NO_X release mechanisms exist on the Pt-based catalyst surface.

LNT performance can also be impacted by the release of unreduced NO_X [5]. A close proximity of the precious metal (reducing site) and the storage component can decrease the amount of unreduced NO_X. In a comparison of nitrate decomposition over $Pt/Ba/SiO_2$, Pt/SiO_2 and Ba/SiO_2 catalysts [75], the authors showed that more decomposition occurred when the Pt site was close to the Ba site, thus decomposition is easier when Pt and Ba are in close proximity.

2.2.5 NO_X Reduction to N_2

The final and ultimate goal of the LNT process is to reduce the NO_X stored in the lean phase to N_2 during the rich phase. As stated above, unreduced NO_X can be released at the onset of the rich phase, thus there is a small window of opportunity to actually reduce released NO_X. Common factors that can affect NO_X reduction are amount of reductant, type of reductant and temperature [5]. One study showed that increasing the amount of CO by decreasing the air/fuel ratio can increase NO_X conversion [76]. Another study showed that using a combination of 0.75% H_2 and 2.25% CO resulted in a 40% conversion[77], where under the same conditions, using only 3% CO led to a conversion of only 22% showing H_2 is a better reductant, and commonly H_2 and CO are better reductants than hydrocarbons. A study over three BaO/Al_2O_3 samples; the first containing Pt, the second Rh, and the third Pd, showed that in general using H_2 and CO as reductants resulted in better NO_X conversions than when using hydrocarbons as reductants[78]. The study showed that H_2 and CO were better reductants because H_2 and CO were in general able to reduce stored NO_X, whereas the hydrocarbons used reduced stored NO_X only at specific test conditions and not over all

catalysts. For example, H_2 was able to reduce stored NO_X at all temperatures tested (test temperatures ranged from 150 - 350°C) for the first sample and at all but one temperature for the second and third samples. Whereas using a hydrocarbon as a reductant, such as propylene (C_3H_6), reduction only occurred at 350°C over the third catalyst sample. CO ranks as a good reductant because it can act as a direct reductant or an indirect reductant in the presence of water via the WGS reaction. WGS reactions have been seen over TWC catalysts [26] and since WGS reaction occurs over precious metals it is also expected to occur over LNT catalysts as well[70].

There are two main mechanisms for NO_X reduction to N_2 over a Pt-based LNT catalyst [5]. Firstly, it has been suggested that the reductant reduces the Pt site and then Pt can actually decompose NO [79, 80]. The second mechanism is a direct reaction between NO_2 and the reductant. This implies that NO oxidation is the first step and is involved in this mechanism [81, 82].

2.3 Catalyst Deactivation

Catalyst deactivation commonly occurs in LNT catalysis and is an issue that is researched. The causes of deactivation are classically divided to three categories: chemical, thermal and mechanical [33]. The five main catalyst deactivation mechanisms were briefly outlined in the Introduction section in Table 3.

2.3.1 Sulfur Poisoning

With sulfur present in the fuel exhaust [5], there is opportunity for S species to sorb to an LNT catalyst. Literature results show that SO_2 can also sorb onto the trapping components of the general LNT catalyst, Pt/alkali-alkaline-earth metal/Al_2O_3, to form sulfate, sulfites and sulfides, which is also the case for perovskite based catalysts [83, 84]. Specifically, research on a La-based perovskite catalyst shows lanthanum oxides react with SO_2 creating the corresponding sulfate [85]. These species have also been seen to migrate from the surface to the bulk [86].

NO_X and S species competition for available trapping sites occurs due to the fact that S species can sorb to the catalyst as well as NO_X. Furthermore, sulfates are more stable than the corresponding nitrates on Pt/Ba-based LNT catalysts [5, 87 – 90]. $BaSO_4$ has been observed on the surface of a Pt/Ba LNT for small SO_2 doses [28, 91] and at high doses bulk sulfates can form[92, 93]. As well as storage component poisoning, sulfur has been observed to bond with the washcoat component, such as Al_2O_3, forming Al sulfates[28], which in turn have been observed to plug catalyst pores ultimately limiting activity[94, 95]. Research has shown that noble metal addition to perovskite-based catalysts can not only increase catalyst activity, but also sulfur resistance [84, 96].

2.3.2 Desulfation

The removal of sulfur from the LNT catalyst surface is known as desulfation. The desulfation process occurs under rich conditions and at high temperatures [27 – 31], which unfortunately can lead to thermal degradation, which will be discussed below. $BaSO_4$ can be created after

sulfur exposure, and bulk $BaSO_4$ decomposes at 1600°C [97]. Surface sulfates can be removed at lower temperatures than bulk sulfates and a reducing environment also significantly lowers the temperature for S removal [5]. Nitrate/nitrite reduction is more efficient when H_2 is the reductant, relative to CO [98] and the same has been seen in reducing sulfates/sulfites [29, 87, 91].

The catalyst used in this research does not include Pt. One study found that using H_2 with no Pt present decreased the amount of S removed [31]. As well as temperature of desulfation, the desulfation time and amount of reductant are important [99, 100]. For example in one study no S was removed during a desulfation at 600°C for 2 hours in a lean environment, however desulfation in a rich environment increased activity [100].

The catalyst used in this research was a perovskite-based LNT catalyst, $La_{0.9}Sr_{0.1}MnO_3$, with precious metal loadings of 1.8 Pd/0.2 Rh g liter^{-1}. In a previous study with the same catalyst, the fresh sample was evaluated after sulfur poisoning [6, 101]. The authors concluded that at 350°C the fresh sample achieved 90% NO_X conversion and after the sulfur exposure used the catalyst lost approximately 10% of its NO_X conversion efficiency. The authors also concluded however, that after a desulfation process was performed, the NO_X conversion was restored to 90%, suggesting that most if not all of the sulfur was removed.

2.3.3 Thermal Degradation

As stated above, desulfation leads to thermal degradation since high temperatures are required. Another cause of thermal degradation is the heat generated via the exothermic reactions of hydrocarbons, CO and H_2, during the regeneration portion of the NO_X storage

and reduction cycle [5]. The primary effect of thermal degradation is sintering [32]. A loss of surface area of the precious metals (Pt, Pd and Rh) via agglomeration and via washcoat pore collapse [33, 34] is the result. Studies have shown that with a $Pt/Ba/Al_2O_3$ catalyst, Pt sintering can decrease the Pt and Ba interaction, which decreases NO_X storage and reduction performance [5, 102, 103]. More specifically, Uy et al. found aging resulted in the storage component, Ba, separating and acting "independently" from Pt/Al_2O_3 [102]. Other effects are reactions between storage and support materials resulting in mixed metal oxides [103]. Casapu et al. studied high temperature effects over $Pt/Ba/Al_2O_3$ and $Pt/Ba/CeO_2$ catalysts and showed that $BaAl_2O_4$ formed at 850°C and $BaCeO_3$ formed at 800°C [103]. Perovskite-based catalysts usually have lower surface areas and also exhibit sintering tendencies which can lower activity [45, 104, 105].

Chapter 3

Experimental Methods

3.1 Experimental Description

3.1.1 Catalyst

The perovskite-based catalyst, that was used in this study was provided by General Motors and described in a previous paper [6]. The catalyst was 1.8 cm in diameter and 2.6 cm in length, and had a 400 cell per square inch (cpsi) cell density. The catalyst was first tested “as-is” (fresh) then the catalyst was thermally aged and the same tests were repeated for comparison. Lastly the catalyst was poisoned by sulfur and most of the same tests were completed before and after desulfation for comparison again. Some were not run after S exposure (prior to desulfation) to ensure no S release during the evaluation prior to desulfation.

3.1.2 Reactor

The catalyst was wrapped in a 3M high temperature matting material and placed in a quartz tube reactor for testing and this tube was then placed in a Lindberg/Blue Mini-Mite tube furnace. The wrapping secured the catalyst and prevented any gas by-pass. Two thermocouples were placed in the reactor tube; one at the inlet and one at the outlet of the catalyst, in order to monitor temperature. A picture of the reactor used is found below in Figure 8.

Figure 8: Reactor tube and Lindberg/Blue Mini-Mite tube furnace

3.1.3 Gas Feed and Delivery System

Nitrogen was used as the balance gas for all experiments. The nitrogen was generated using an OnSite N_2 generator. As H_2O was involved in most of the experiments, the tubing downstream of the mass flow controller manifold was heated to above 100°C, and then H_2O was added to the gas mixture using a Bronkhorst CEM system. The rest of the feed gases used were provided by PraxAir and streamed to the reactor via Bronkhorst mass flow controllers.

3.1.4 Analysis

For the NO oxidation, cycling, water gas shift (WGS), and oxygen storage capacity (OSC) experiments, the reactor outlet gases were monitored with a Fourier Transform Infrared (FTIR) analyzer. The instrument was a MKS MultiGas^{TM} 2030.The following compounds were monitored using this instrument: NO, NO_2, N_2O, CO, CO_2, H_2O, and NH_3.

3.2 Experiments and Tests

Each experiment, with the exception of experiments completed after sulfur poisoning and before desulfation (to be explained later), was completed over a conditioned catalyst. The reactor was brought to 500°C and higher and H_2 gas was used to clean the catalyst of any residual surface nitrates.

3.2.1 NO Oxidation Procedures

The NO oxidation experiments were carried out under lean conditions. A 50,000 h^{-1} (STP) space velocity was used and the temperature range was 200-500°C. A constant flow of 200 ppm NO, 10% O_2, 10% CO_2, 10% H_2O and a balance of N_2 was held at each temperature. The target temperatures were held constant until a steady-state NO to NO_2 conversion was achieved, at which point the following calculation was applied:

$$NO_2\ Conversion = \frac{NO}{NO+NO_2}\ X\ 100 \qquad (20)$$

The NO oxidation experiments completed for the kinetic study were conducted on conditioned catalyst samples and followed the same procedure laid out in reference [56].

Table 4 lists the gas components and amounts used during the kinetic study. Conversions were noted once steady-state NO to NO_2 conversion was achieved. The NO to NO_2 conversions were maintained near and below 10%.

Table 4: Kinetic Study - Experimental procedure and conditions

Components	NO Order Test	O_2 Order Test	NO_2 Order Test	Ea Test
NO	100-450 ppm	300 ppm	300 ppm	300 ppm
O_2	10%	4 – 12%	10%	10%
NO_2	170 ppm	170 ppm	80 – 180 ppm	170 ppm
Temperature	300°C	300°C	300°C	240 – 320°C

The rate of a chemical reaction can be defined by the reaction rate equation:

$$r = k[A]^{\alpha}[B]^{\beta}C^{\gamma} \quad (21)$$

Where *r* is the rate of the reaction, *k* is the reaction constant, *A*, *B* and *C* are the reaction components and α, β and γ are their respective reaction rate orders.

To determine the order of either NO, O_2 and NO_2, two of the three components were held constant and the other was varied during NO oxidation experiments as per Table 4 procedures. By taking the natural logarithm of the reaction rate equation, the expression then becomes:

$$ln(r) = ln(k) + \alpha ln(A) + \beta ln(B) + \gamma ln(C) \quad (22)$$

Because two of the components are held constant and the variable *k* is already a constant, equation (22) is in the form of a "slope-intercept" equation:

$$y = mx + b \quad (23)$$

Where the dependent variable *y* is represented by $ln(r)$, the independent variable *x* can be represented by either $ln(A)\ or\ ln(B)\ or\ ln(C)$ (depending on which variable is varying while the others are constant), the slope, *m*, is represented by either α, β or γ (again depending on which variable is varying while the others are constant) and *b* is represented by the constant variable expressions + $ln(k)$.

Thus, to determine the reaction rate orders for NO, O_2 and NO_2, plots of the natural logarithmic of NO oxidation rates vs. the natural logarithmic of concentrations of NO, O_2 and NO_2 were graphed. The slope of each plot provided the reaction rate order of each component. For example, below is the expression used to calculate the NO reaction rate order:

$$ln(r) = K + \alpha ln(A) \quad (24)$$

Where the dependent variable *y* is represented by *r* (found by the steady-stated NO to NO_2 conversion during NO oxidation experiments where NO_2 and O_2 were held constant while NO concentrations were varying), *K* is the constant sum of $ln(k) + \alpha ln(A) + \beta ln(B)$ which represents the *y*-intercept, $ln(A)$ represents the independent variable *x* and α represents the slope of the $y = mx + b$ equation.

To determine the activation energy, the steady-state NO to NO_2 conversion data were fit using the Arrhenius expression:

$$k = Ae^{\frac{-Ea}{RT}} \quad (25)$$

Where *k* is the rate constant, *Ea* is the activation energy, *A* is the pre-exponential factor, *R* is the universal gas constant and *T* is temperature. NO oxidation experiments were completed and steady-state NO to NO_2 conversions were recorded at varying temperatures while NO, NO_2 and O_2 concentrations were held constant. As with determining the reaction rate orders, in order to determine the activation energy equation (25) was transformed:

$$ln(k) = ln(A) + \frac{-Ea}{RT} \quad (26)$$

The reaction rate *r* and the reaction rate constant *k* are scalars of each other as seen in equation (21). The slope of equation (26) is what was desired in order to determine the *Ea*; thus the reaction rate was calculated and was used instead of *k*, as the slope would not change whether the value of *r* or *k* was used. Plots of the natural logarithmic of NO oxidation rates vs. $\frac{-1}{T}$ were graphed.

$$ln(r) = ln(A) + \frac{-Ea}{RT} \quad (27)$$

Where $ln(r)$ represents the dependant *y* variable, $ln(A)$ is the *y*-intercept, $\frac{-1}{T}$ represents the independent *x* variable and $\frac{Ea}{R}$ represents the slope.

The slope of the plot is the value of $\frac{Ea}{R}$, thus the Ea was found via:

$$Ea = m(slope)\ x\ R \quad (28)$$

3.2.2 Cycling

3.2.2.1 Short Cycles

LNT catalysts operate in cycles, oscillating between fuel lean and fuel rich phases. The lean, oxygen rich, phase lasts about 1 to 2 minutes, and the rich, reductant rich, phase is short, 1 to 5 seconds. Similar, in terms of cycle times, experiments were used to evaluate the perovskite-based catalyst performance. The catalyst was cleaned at 500°C with 1% H_2, 10% CO_2, 10% H_2O and a balance of N_2 before it was cooled to each target test temperature. The test temperatures were 200, 300, 400 and 500°C and experiments were run at a 50,000 h^{-1} (STP) space velocity. The catalyst was first exposed to the lean phase, which consisted of 200 ppm NO, 10% O_2, 10% CO_2, 10% H_2O and a balance of N_2 and lasted 60 seconds. The conditions were then switched to the rich phase that consisted of 1% H_2, 3% CO, 10% CO_2, 10% H_2O and a balance of N_2 and lasted 5 seconds. Equations (29) to (35) were used to calculate values of NO_X stored, NO_X released, NO_X converted from NO_X that was trapped, NO_X converted overall, NH_3 formed, N_2O formed, and N_2 formed.

Stored NO_X (ppm*s) = Total NO_X in – Total NO_X out (29)

NO_X released (ppm*s) = NO_X released - NO_X released during lean phase (30)

$$NO_X \text{ converted from trapped (\%)} = \frac{Total\ NO_X\ trapped - NO_X\ released\ in\ rich}{Total\ NO_X\ trapped} X\ 100 \quad (31)$$

$$\text{Total } NO_X \text{ converted (\%)} = \frac{Total\ NO_X\ in - Total\ NO_X\ Released}{Total\ NO_X\ in} X\ 100 \quad (32)$$

$$NH_3\ formed\ (\mu mole) = \frac{NH_3\ in\ rich(ppm*s)\text{X}\ 3.308\left(\frac{\text{L}}{\text{min}}\right)\ \text{X}\ 1{,}000{,}000\ \frac{\mu\text{mole}}{\text{mole}}}{1{,}000{,}000(ppm)X\ 60\left(\frac{s}{min}\right)X22.4\ (STP)} \quad (33)$$

$$N_2O\ formed\ (\mu mole) = \frac{N_2O\ in\ rich(ppm*s)\text{X}\ 3.308\left(\frac{\text{L}}{\text{min}}\right)\ \text{X}\ 1{,}000{,}000\ \frac{\mu\text{mole}}{\text{mole}}}{1{,}000{,}000(ppm)X\ 60\left(\frac{s}{min}\right)X22.4\ (STP)} \quad (34)$$

$$N_2\ formed\ (\mu mole) = NO_X stored - NO_X released - NH_3 formed\ stored\ in\ rich -$$

$$2XN_2O formed\ stored\ in\ rich(ppm * \text{s})\text{X}\frac{3.308\left(\frac{\text{L}}{\text{min}}\right)\ \text{X}\ 1{,}000{,}000\ \frac{\mu\text{mole}}{\text{mole}}}{1{,}000{,}000(ppm)X\ 60\left(\frac{s}{min}\right)X22.4\ (STP)} \quad (35)$$

3.2.2.2 Long Cycles

It may be difficult to identify the chemistry occurring over the catalyst in such short time periods. Thus the lean and rich phases were stretched to longer time periods to allow for a more thorough evaluation of the reaction chemistry. The long-cycles completed in this study followed a specific protocol provided by the Cross-Cut Lean Exhaust Emissions Reduction Simulations (CLEERS) group. The protocol is laid out in a way that allows an evaluation of the effect of temperature, NO_X source (NO or NO_2) and surface NO_X species decomposition either in the presence or absence of reductant. The catalyst was first cleaned at 550°C with 1% H_2, 5% CO_2, 5% H_2O and a balance of N_2, before any long cycle experiments were completed. Once cleaning was complete, the catalyst was brought to the test temperatures and first exposed a lean phase that lasted 15 minutes then a rich phase that lasted 10 minutes. The lean phase consisted of 300 ppm NO or NO_2, 10% O_2, 5% CO_2, 5% H_2O and a balance of N_2. The rich phase consisted of 375 ppm H_2, 625 ppm CO, 5% CO_2, 5% H_2O and a balance of N_2. To compare reductant present and reductant free conditions, three reductant-

present cycles were completed and then the 4th (last) cycle completed had no reductant in the rich phase. Specific conditions are described in Table 5. All calculated values are the same as in the short cycle section of this Experimental Methods section and were calculated the exact same way.

Table 5: CLEERS protocol - experimental procedure and conditions for long cycle experiments

Run #	Temp	Gas Mix	SV (h^{-1})	Lean Period (s)	Reductant	Regen Peak	Regen Period (s)	# of Cycles
1	550	1	30,000	0	H_2	1%	600	1
2	550	2/3	30,000	900	CO/H_2	1000 ppm	600	3
3	550	2/4	30,000	900	None	0	600	1
4	550	1	30,000	0	H_2	1%	600	1
5	463	2/3	30,000	900	CO/H_2	1000 ppm	600	3
6	463	2/4	30,000	900	None	0	600	1
7	550	1	30,000	0	H_2	1%	600	1
8	375	2/3	30,000	900	CO/H_2	1000 ppm	600	3
9	375	2/4	30,000	900	None	0	600	1
10	550	1	30,000	0	H_2	1%	600	1
11	288	2/3	30,000	900	CO/H_2	1000 ppm	600	3
12	288	2/4	30,000	900	None	0	600	1
13	550	1	30,000	0	H_2	1%	600	1
14	288	2A/3	30,000	900	CO/H_2	1000 ppm	600	3
15	288	2A/4	30,000	900	None	0	600	1
16	550	1	30,000	0	H_2	1%	600	1
17	200	2/3	30,000	900	CO/H_2	1000 ppm	600	3
18	200	2/4	30,000	900	None	0	600	1
19	550	1	30,000	0	H_2	1%	600	1
20	200	2A/3	30,000	900	CO/H_2	1000 ppm	600	3
21	200	2A/4	30,000	900	None	0	600	1

3.2.3 Water Gas Shift (WGS)

The CO levels during the regeneration phase of the long cycling experiments were monitored. The following equation was used to calculate the WGS extent:

$$WGS\ extent\ (\%) = \frac{CO\ in - CO\ out}{CO\ in} \text{ X } 100 \quad (36)$$

3.2.4 Oxygen Storage Capacity (OSC)

The objective of this test was to evaluate and quantify, via CO consumption experiments, the amount of catalyst OSC. The catalyst was exposed to a lean gas stream consisting of 10% O_2, 5% CO_2, and a balance of N_2 for 60 seconds, and then the gas was switched to the rich gas stream consisting of 5% CO_2, 1% CO and a balance of N_2 for 90 seconds. H_2O was not included in this experiment in order to eliminate the WGS effect. The outlet CO concentrations were used to calculate the amount of O_2 being consumed via:

$$CO\ (\mu mole) = \frac{CO\ pulse(ppm*\text{s}) \text{X } 3.308\left(\frac{\text{L}}{\text{min}}\right) \text{X } 1{,}000{,}000\ \frac{\mu\text{mole}}{\text{mole}}}{1{,}000{,}000(ppm) X\ 60\left(\frac{s}{min}\right) X 22.4\ (STP)} \quad (37)$$

$$CO\ converted\ (\mu mole) = Co\ in - Co\ out \quad (38)$$

$$O_2\ stored\ (\mu mole) = \frac{CO\ converted\ (\mu mole)}{2} \quad (39)$$

3.3 Effects of Deactivation

3.3.1 Thermal Aging Tests

After the fresh catalyst was tested it was thermally aged and the same tests and calculations were repeated. The catalyst was thermally aged in the pilot reactor for 8 hours at a temperature of 750°C with 10% H_2O, 19% O_2 and a balance of N_2.

3.3.2 Sulfur Poisoning and Desulfation Tests

After the thermal aging process and post-evaluation, the catalyst was tested after exposure to sulfur and then after simulated desulfation. For the sulfur exposure, in the pilot reactor the catalyst was exposed to lean conditions consisting of 200 ppm NO, 10% O_2, 10% H_2O, 10% CO_2, 10 ppm SO_2 and a balance of N_2 at 300°C for 85 minutes, which resulted in an exposure of 1 g sulfur / L of catalyst (as outlined in[101]).

The desulfation was carried out under rich conditions with 1% H_2, 3% CO, 10% H_2O, 10% CO_2 and a balance of N_2. The temperature was ramped from 300 to 700°C at a rate of 10°C/min. Once the temperature reached 700°C it was held there for 30 minutes (as outlined in [101]). The same experiments completed when the catalyst was fresh and thermally aged were also completed once the catalyst underwent sulfur poisoning and desulfation. Lastly, the catalyst was exposed to sulfur yet again, however without undergoing desulfation. Again the same experiments were performed. During the sulfur poisoning and desulfation procedures some gases such as N_2, H_2, H_2S, COS and CS_2 were monitored using an OMNI Star gas analysis mass spectrometer by Pfeiffer.

Chapter 4

Evaluation and Characterization of a Fresh Perovskite-Based Lean-NO_X-Trap Catalyst

4.1 NO Oxidation over Fresh Perovskite-based LNT catalyst

Previous work has shown that NO_2 will sorb on LNT materials more efficiently than NO [47 – 51], which suggests that NO oxidation (NO to NO_2 conversion) is a critical step in improving the overall performance of a LNT catalyst. Pt-based catalysts have proven efficient and are commonly used; however similar trends and effective oxidizing capabilities with perovskite-based catalysts have been observed [6, 42, 43, 45, 46]. While NO_2 sorption increases the efficiency of the overall LNT catalyst performance, NO_2 itself inhibits NO oxidation over Pt-based catalysts [56, 106]. It has been suggested that NO_2 absorbs easily to the oxidation sites, due to its high sticking coefficient [47, 56, 107], and oxidizes the Pt, thereby preventing NO adsorption and oxidation.

NO oxidation as a function of temperature data, over the fully-formulated perovskite sample, are shown in Figure 9. At low temperatures, low conversions were attained, due to kinetic limitations. NO to NO_2 conversion began to increase after 200°C, increased until 350°C, where the conversion began to drop due to thermodynamic limitations and the reaction then followed the equilibrium curve. In comparing these results to literature data, the same conversion trends are noted.

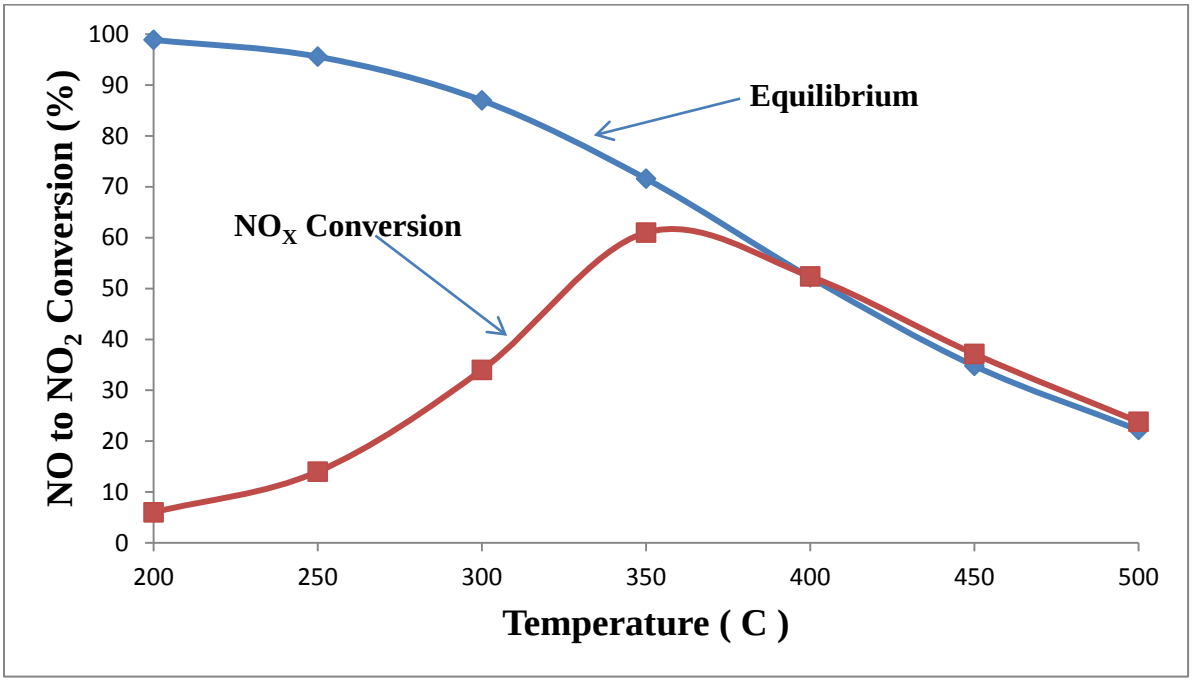

Figure 9: NO oxidation as a function of temperature at 50,000 h^{-1} space velocity; 200 ppm NO, 10% O_2, 10% CO_2, 10% H_2O and a balance of N_2

The NO oxidation kinetic behavior for the fully-formulated perovskite-based sample was evaluated and the results are shown in Figure 10. These NO oxidation experiments were conducted on a cleaned catalyst at 300°C, with details listed in Table 4, and followed the procedure described in reference [56]. The rates were found and plotted against the respective varying component concentrations. The reaction orders for NO, O_2 and NO_2 were determined to be 1.13 ± 0.25, 1.06 ± 0.06, and -1.01 ± 0.26, respectively (Statistical error calculations found in Appendix A).

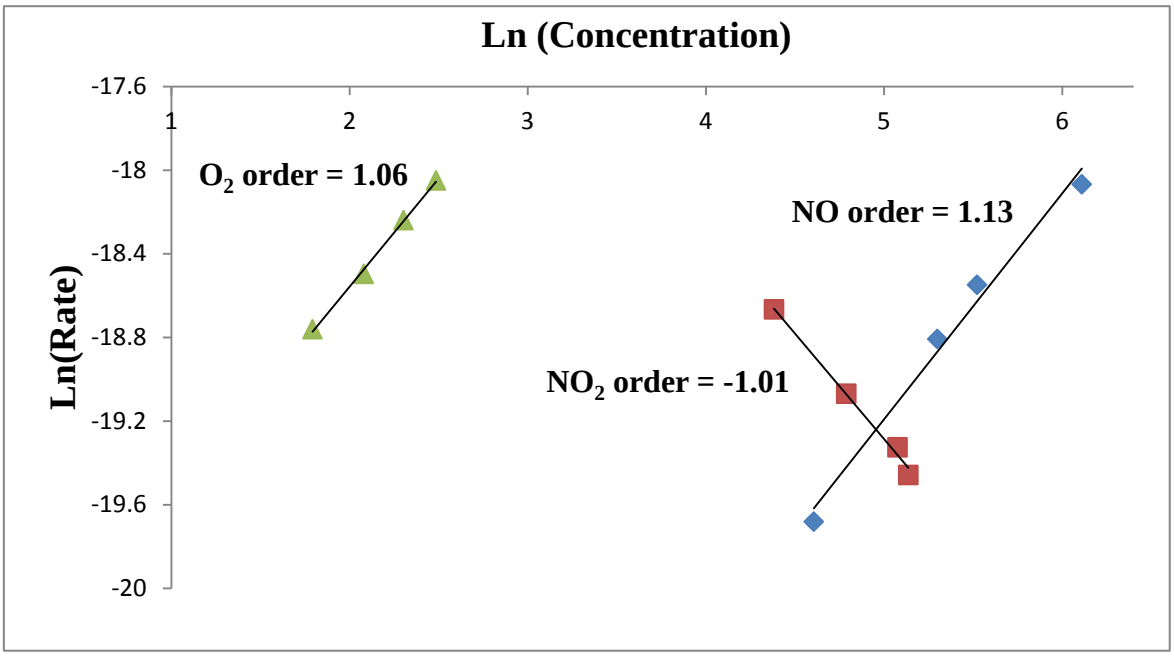

Figure 10: Natural logarithm of NO oxidation rate vs. natural logarithm of concentrations of NO, O_2 and NO_2; fully formulated perovskite

These results are consistent with literature data for the conventional Pt-based catalyst [56] and a Pd-based catalyst [57], which suggests that the kinetic steps are the same over the perovskite, Pt- and Pd-based catalysts. A separate set of NO oxidation experiments was performed in order to determine the activation energy. The target temperatures were held constant until a steady-state NO to NO_2 conversion was achieved. Some previous activation energy (Ea) values found in literature data for the Pt/Al_2O_3 catalysts were 82 ± 9 kJ/mol as per Mulla et al. [56]and 75.9 kJ/mol as per Bhatia et al.[108], whereas Weiss and Iglesia [57] studied the NO oxidation reaction over a Pd/Al_2O_3 catalyst and reported an Ea of 152 kJ/mol. The catalyst used in our study contains Pd, but no Pt. The activation energy calculated for the fully-formulated perovskite-based catalyst (containing Pd) was 82 ± 11 kJ/mol. The activation energy reported in reference [57] is much higher than the activation energy

calculated using the perovskite-based sample, suggesting that the Pd itself does not play as much as of role in the reaction pathway, with the perovskite itself catalyzing the reaction. To qualitatively verify that Pd is not significantly contributing to the reaction pathway, the exact same NO oxidation experiments were completed on a bare perovskite sample (no precious metal included). The NO oxidation kinetic behavior for the bare perovskite-based sample was evaluated and the results are depicted in Figure 10.

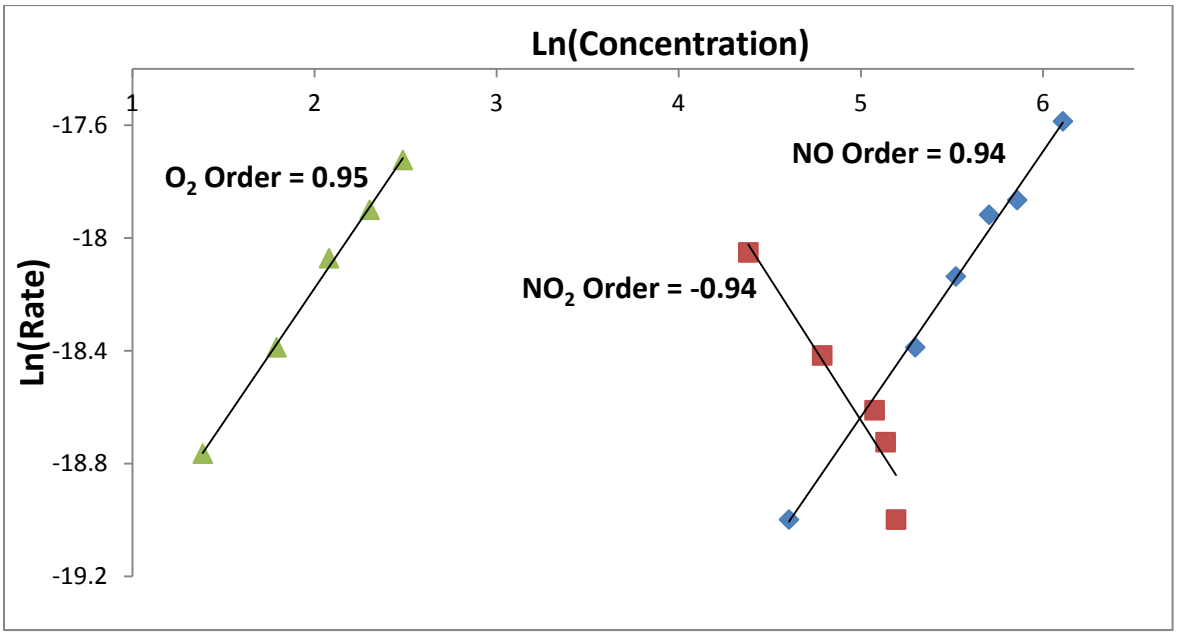

Figure 11: Natural logarithm of NO oxidation rate vs. natural logarithm of concentrations of NO, O_2 and NO_2; bare perovskite

The reaction rate orders were all found to be quite similar for NO, O_2 and NO_2; 0.94 ± 0.09, 0.95 ± 0.07 and -0.94 ± 0.29, respectively. Furthermore, the activation energy over the bare perovskite sample was 81 ± 11 kJ/mol, which is still in the same range as the activation energy found in the fully formulated perovskite sample and previously tested Pt/Al_2O_3 samples [56, 108]. The NO to NO_2 conversions over the bare perovskite, in the temperature

range of the kinetics tests, were actually higher, but by only 2-3%, from 260 to 320°C than those of the fully-formulated sample. This demonstrates that the perovskite itself was indeed likely acting as NO oxidation catalyst.

4.2 NO_X Storage and Reduction over Fresh Perovskite-based LNT catalyst

The storage or trapping ability of a LNT catalyst varies with temperature as does NO to NO_2 oxidation, a key step that goes hand-in-hand with the amount of NO_X stored. Past proposed trapping mechanisms involve NO_2 as the primary reactant for nitrate formation via the disproportionation reaction [4, 109]. Also, Kwak et al. [110] have demonstrated that after NO_X begins to break through, the rate of uptake is determined by the gas/solid equilibrium between NO_2 and the available trapping sites. Thus more NO to NO_2 conversion will also affect the overall NO_X trapped. As shown in Figure 9, at low temperatures NO oxidation is poor over the fully-formulated perovskite-based catalyst due to kinetic limitations. Although sites are available and nitrates are more stable at lower temperatures, the lack of NO_2 formation will lead to poor storage. In general, as the temperature increases, NO oxidation extent also increases, but nitrate stability will decrease [109]. At higher temperatures the amount of NO_X trapped can therefore be limited by nitrate stability. Between 200°C and 400°C, significant NO to NO_2 conversion typically occurs (as depicted in Figure 9) and the loss in nitrate stability is not significant, thus a maximum in NO_X storage is usually observed in this temperature range. In order to depict this, below in Figure 12 are results from a temperature programmed desorption (TPD) experiment. 300ppm of NO, 10% O_2, 10% H_2O,

10%CO_2 and a balance of N_2 flowed over the fresh perovskite-based catalyst at 100°C until the catalyst was completely saturated with NO_X. The NO and O_2 were shut off and any physically adsorbed NO_X was released leaving behind only chemically adsorbed NO_X. The temperature was then ramped at 10°C/min until 550°C. At around 300 °C NO_X begins to release showing that stability is decreasing and by around 450 °C no NO_X is stable at all. This shows that at higher experimental temperatures performance is limited by nitrate stability.

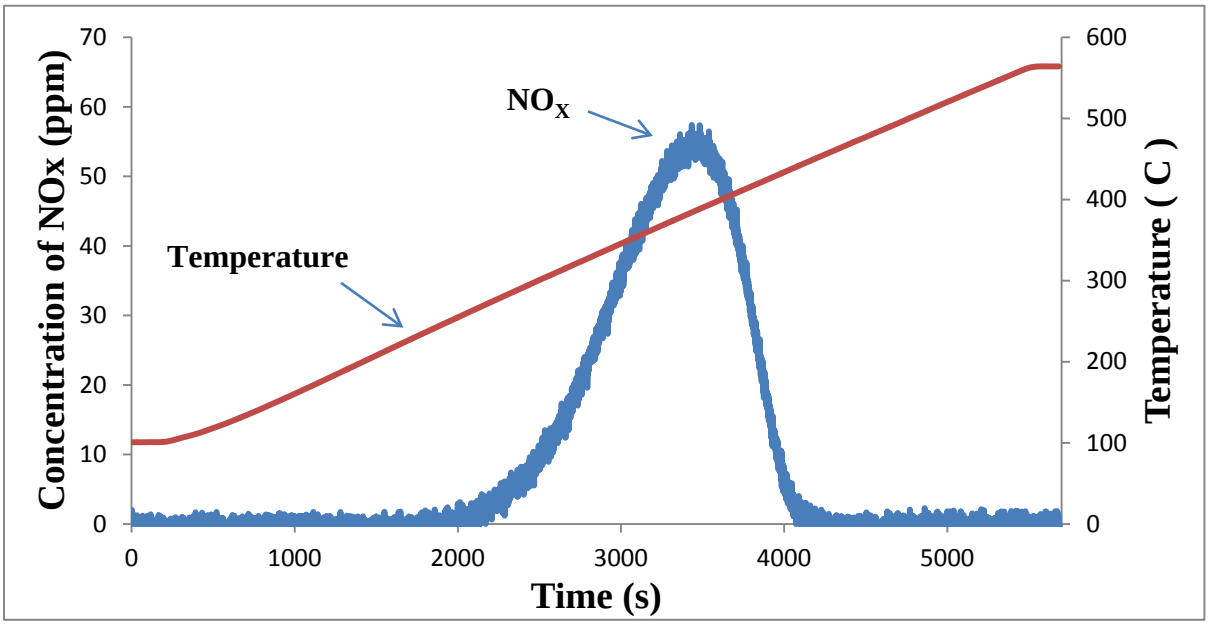

Figure 12: Temperature programmed desorption over the fresh perovskite catalyst

4.2.1 Short Cycling Results

The short cycle storage profiles, shown as NO_X concentration as a function of time, at four different temperatures are shown in Figure 13.

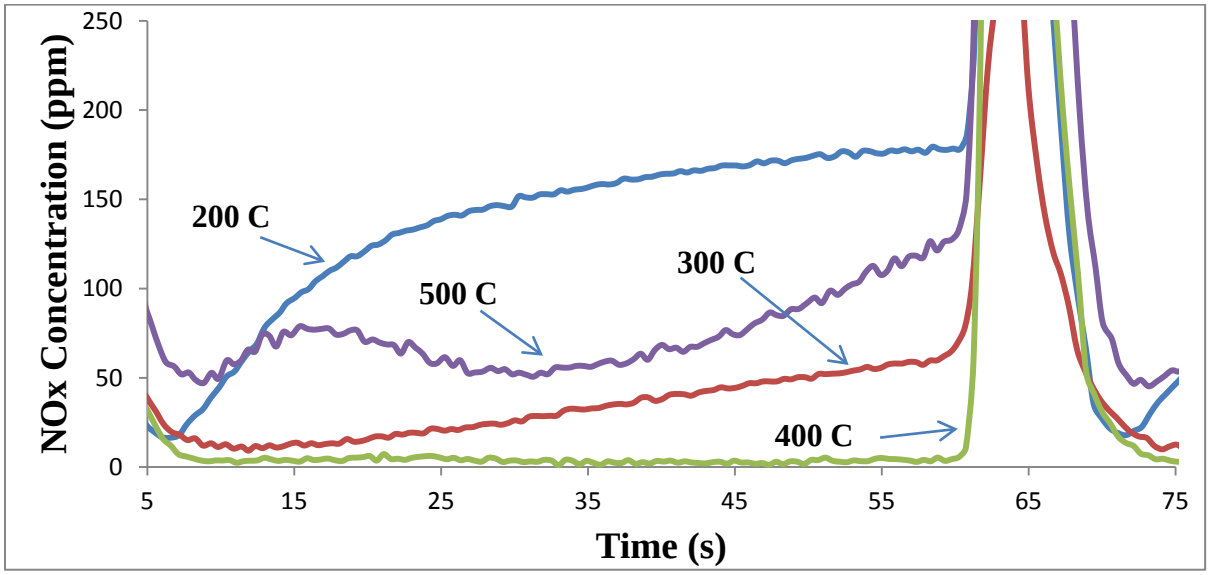

Figure 13: Short cycling NO_X ($NO + NO_2$) concentration profiles for temperatures 200, 300, 400 and 500°C; 200 ppm NO, 10% O_2, 10% CO_2, 10% H_2O, balance N_2 at 50,000 h^{-1} space velocity

Table 6 summarizes the data obtained during the short cycling experiments. The catalyst trapped the least amount of NO_X at the two temperature extremes, 200 and 500°C, 14 and 22 µmoles, respectively, with the onset of slip (NO_X breakthrough) occurring near the very beginning of the lean phase. At 200°C, zero slip was not attained, with residual NO_X being released during the regeneration phase having to also be trapped at the onset of the lean phase. The best trapping performance was observed at 400°C, with slip not observed during the lean phase. The amount of NO_X trapped increased from 200 to 400°C, which follows the NO oxidation extent trend. The best overall NO_X conversion efficiency, 71%, was observed at 300°C. At 400 and 500°C, 58% and 9% were reduced, respectively, and at the lowest temperature, 200°C, reduction was the lowest, 2%. In terms of the amount of stored NO_X that

was reduced, only 4% was reduced at 200°C, 87% at 300°C, 64% at 400°C and 18% at 500°C.

Table 6: Short cycle storage and reduction performance results using NO as the NO_X source: 200 ppm NO, 10% O_2, 10% CO_2, 10% H_2O and a balance of N_2 in the lean phase (60 seconds); 3% CO, 1% H_2, 10% CO_2, 10% H_2O and a balance of N_2 in the rich phase (5 seconds)

Temp (°C)	NO_X trapped (µmoles)	NO_X released (µmoles)	NO_X Converted (µmoles)	NO_X Converted (%)	NH_3 formed (µmoles)	N_2O formed (µmoles)	N_2 formed (µmoles)	NO_X Converted (%) – Using 4% H_2 as reductant
200	14	13.4	0.7	2	0.1	0.1	0.5	41
300	39	5	34	71	16	2	16	84
400	45	16	29	58	0	0	29	59
500	22	18	4	9	0.1	0.3	3.6	11
*Some experimental error is included in these data								

In the 500°C data set, there is a non-monotonic concentration change with respect to time. This pattern has been previously observed on a commercial LNT catalyst [111] and was attributed to a temperature wave moving through the catalyst, initially formed during the regeneration phase via exothermic oxidation reactions forming H_2O and CO_2. This heat generated was then conducted along the solid at a relatively slow rate and thus appeared during the lean phase. As the temperature increased, nitrates became more unstable, thus there was decreased trapping with the increase in solid temperature. This occurred at 500°C over the perovskite sample as well.

The same experiment was repeated with only H_2 as a reductant and even better conversion results were observed; overall NO_X conversions are also tabulated in Table 6. This is consistent with previous observations, where H_2 has proven to be a better reductant than a combination of CO and H_2 [98]. Again, the best overall conversion efficiency was observed at 300°C, with a very significant gain at 200°C obtained. The reason for the large gain at 200°C is due to better reduction during the regeneration phase. As shown in Figure 13, there are significant releases of NO_X during the regeneration phase, and the H_2 performed much better in reducing this released NO than the CO/H_2 mixture. This in turn resulted in better trapping as less NO_X originating from the regeneration phase needed to be "re-trapped" at the onset of the lean phase, thus contributing to the overall better performance observed. Overall, the results show that the perovskite LNT capabilities are good, especially at 300 and 400°C. At higher temperatures, i.e. 500°C, lower trapping and conversion values are due to the lack of nitrate stability. At lower temperatures, i.e. 200°C, there is a much lower NO_X conversion likely due to poor NO oxidation or poor regeneration. When comparing the perovskite catalyst to a Pt-based catalyst with respect to short cycling, the trends appear the same[109, 112]. In order to investigate the LNT chemistry further, long cycles were performed; that is longer time periods in the lean and rich phases.

4.2.2 Long Cycling Results

The storage profiles, shown as NO_X concentration as a function of time, at five different temperatures are shown in Figure 14. The plotted profiles are those of the third cycle of the protocol, by which time cycle-to-cycle stability was reached. Again, the catalyst trapped the

least amount of NO_X at the two temperature extremes. 35 µmoles of NO_X were trapped at 550°C, with the onset of slip (NO_X breakthrough) at merely 4 seconds. At 200°C, about the same amount was trapped and slip also began close to the beginning of the lean phase. A summary of the trapped amounts are listed in Table 7. The best trapping performance was observed at 375°C, with 90 seconds elapsed prior to slip.

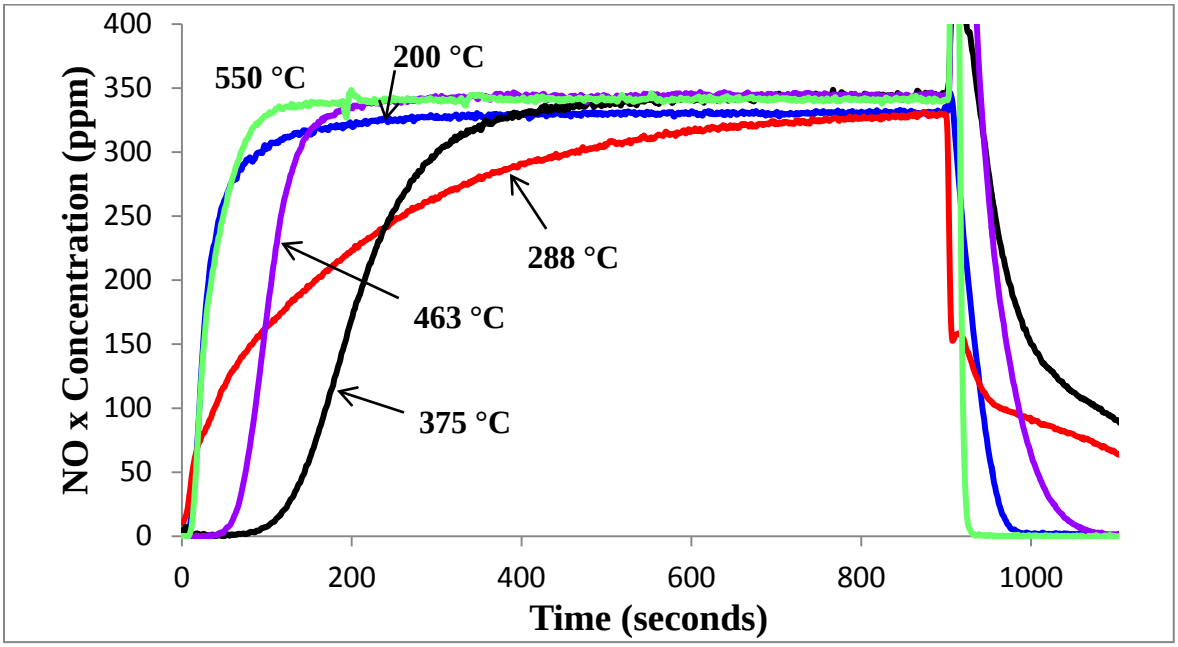

Figure 14: Long cycling NO_X (NO + NO_2) concentration profiles of third cycle during the storage period for temperatures 200, 288, 375, 463 and 550°C; 300 ppm NO, 10% O_2, 5% CO_2, 5% H_2O, balance N_2 at 30,000 h^{-1} space velocity

Ba is a common trapping component added to NSR catalysts, and was part of the perovskite catalyst formulation used in this study for this very reason. Previous research has shown that with $Pt/Ba/Al_2O_3$ catalysts, trapping performance decreases with increasing temperature above 375°C due to decreasing nitrate stability [109, 110]. The same trend at higher temperature was observed here, suggesting that the poor performance at high temperature

was again due to low nitrate stability. Poor performance at lower temperatures can be attributed to poor trapping due to poor NO oxidation performance or slow nitrate diffusion. Another possibility is lack of regeneration, such that trapping sites became saturated after multiple cycles, which has been seen in previous work [113].

In order determine if it was regeneration or trapping performance, the first cycle (where the catalyst was previously cleaned and therefore NO_X-free) and the third cycle (where nitrate/nitrite build-up could have occurred) were compared. As seen in Figure 15, the first and third cycles overlap. If there was limited regeneration, then nitrates would build-up on the surface with each cycle. With such a build-up, the trapping performance would change between regenerations, which was not observed. This therefore demonstrates that it was not regeneration limiting the low temperature efficiency, but it was the trapping ability. NO_2 was still being formed and trapping sites were still available at these low temperatures. One cause for poor trapping can be diffusion limitations as nitrates build up around the oxidation sites. In previous Pt-based catalyst work similar limitations were noted [107, 109], although at lower temperatures the overall NO_X conversion limitation was still attributed to a more significant effect of a lack of regeneration. In these previous studies, it was observed that even when reductant break through began there was leftover NO_X on the surface of the catalyst, confirming a limitation due to regeneration. In the case of the perovskite-based catalyst the limitation was due to trapping ability instead.

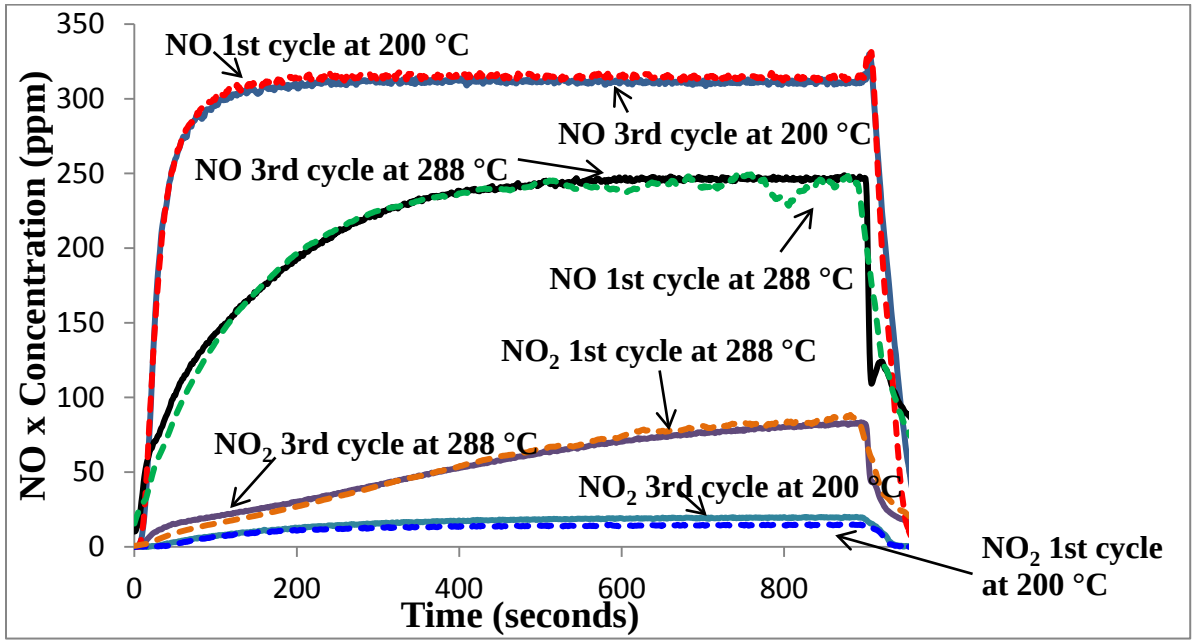

Figure 15: Long cycling, 1st vs. 3rd cycles of NO_X storage at 200°C and 288°C. NO and NO_2 profiles shown. 300 ppm NO, 10% O_2, 5% CO_2, 5% H_2O, balance N_2 at 30,000 h^{-1} space velocity

Table 7 summarizes the data obtained during the long cycling experiments and Figures 16-18 are examples of the regeneration phase; NO, NO_2, N_2O, NH_3 and CO outlet concentration data as a function of time at different temperatures.

Table 7: Long cycle storage and reduction performance results using NO as the NO_X source: 300 ppm NO, 10% O_2, 5% CO_2, 5% H_2O and a balance of N_2 in the lean phase (15 minutes); 625 ppm CO, 375 ppm H_2, 5% CO_2, 5% H_2O and a balance of N_2 in the rich phase (10 min)

Temp (°C)	Total NO_X trapped (µmoles)	NO_X trapped (%) - at 20% BT	NO_X Released (µmoles) - no reductant	NO_X released (µmoles) - with reductant	NH_3 formed (µmoles) - With Reductant	N_2O formed (µmoles)	N_2 formed (µmoles)
200	36	21	27	28	11	0	0
288	137	56	36	70	44	3	17
375	188	92	119	136	30	0.44	22
463	93	55	90	90	0.1	0	3
550	35	18	32	33	0.07	0	2

The amount of NO_X trapped increased from 200 to 375°C, which follows the NO oxidation extent trend again. In terms of the amount of NO_X trapped that was reduced during the regeneration phase, the best efficiency was observed at 288°C, but still only 49% was reduced. At 375°C and 200°C, only 28% and 22% of the trapped NO_X were reduced, respectively, and at the other temperatures reduction was quite poor. For example, at 550°C the amount of NO_X released is very close to the amount trapped. At the higher temperatures this is in part due to a poor reduction rate relative to the nitrate decomposition rate. Similar trends were observed with a Pt-based commercial LNT catalyst [109] following the same CLEERS protocol as this study, where incomplete reduction was observed at 550 and 463°C. The authors concluded that there was a slower reductant delivery rate than the rate of nitrate decomposition and NO_X release. There was sufficient reductant delivery during the regeneration phase of the cycle taken as a whole. For example, Table 7 shows that at 550°C,

35 µmols of NO_X were stored, so 87.5 µmols of reductant were needed for nitrate reduction. There was a 150 µmols/min reductant flux, so it should have taken just over half a minute for the stored NO_X to be reduced. However, as can be seen in Figure 16, there was a sharp and rapid release of the stored NO_X (both with reductant and without reductant present) at the onset of the regeneration phase, and within several seconds release had ended. This confirms that decomposition rate outpaced the reduction rate at this temperature. Complimenting this observation, the data in Figure 16 show no difference between results when the reductant was present and absent – thus clearly nitrate decomposition dominates. Although there was no surface NO_X species reduction, there was significant reductant consumption, which must be related to reducing stored oxygen on the surface. Since the catalyst has measurable oxygen storage capacity (OSC), to be discussed below, competition arose between the stored oxygen and NO_X for the reductant. At 463°C calculations of the amount of NO_X released and trapped also show little difference, for the same reasons. The release of NO_X at the outlet, via nitrate decomposition was slower compared to 550°C, but still quite rapid at the onset of the regeneration phase (data not shown for brevity). At both 463 and 550°C, neither N_2O nor NH_3 was produced, as expected given the lack of NO_X reduction. These trends are consistent with the Pt-based catalyst studied previously [109].

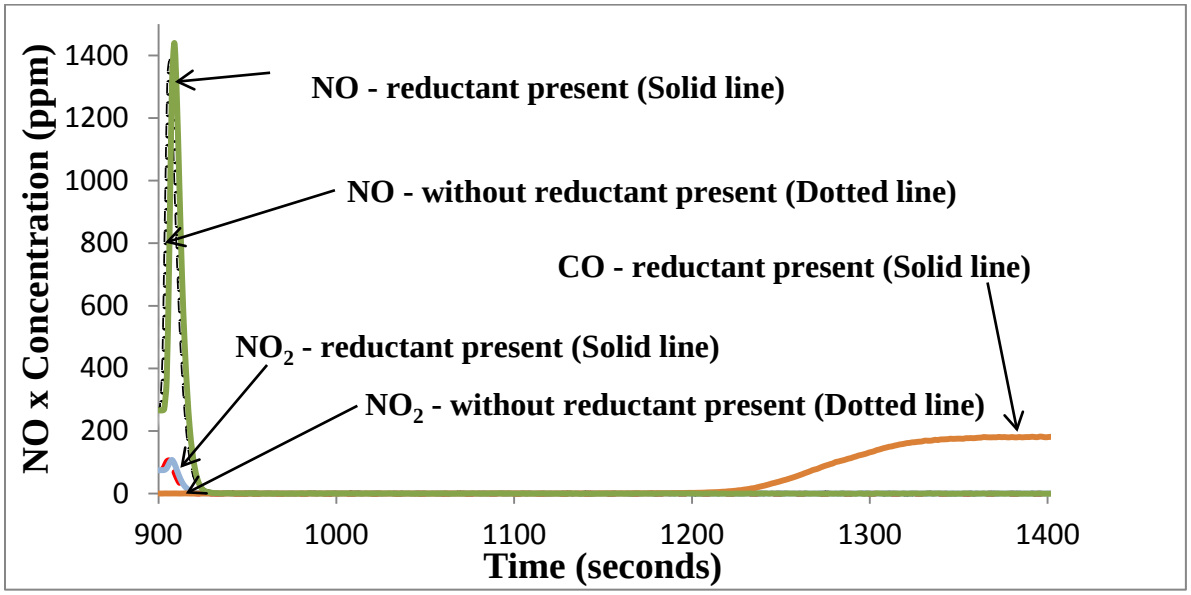

Figure 16: Long cycling, NO (with reductant), NO (without reductant), NO_2 (with reductant), NO_2 (without reductant), NH_3, N_2O and CO concentration profiles at 550°C for the regeneration phase. With 625 ppm CO, 375 ppm H_2, 5% CO_2, 5% H_2O, balance N_2 at 30,000 h^{-1}

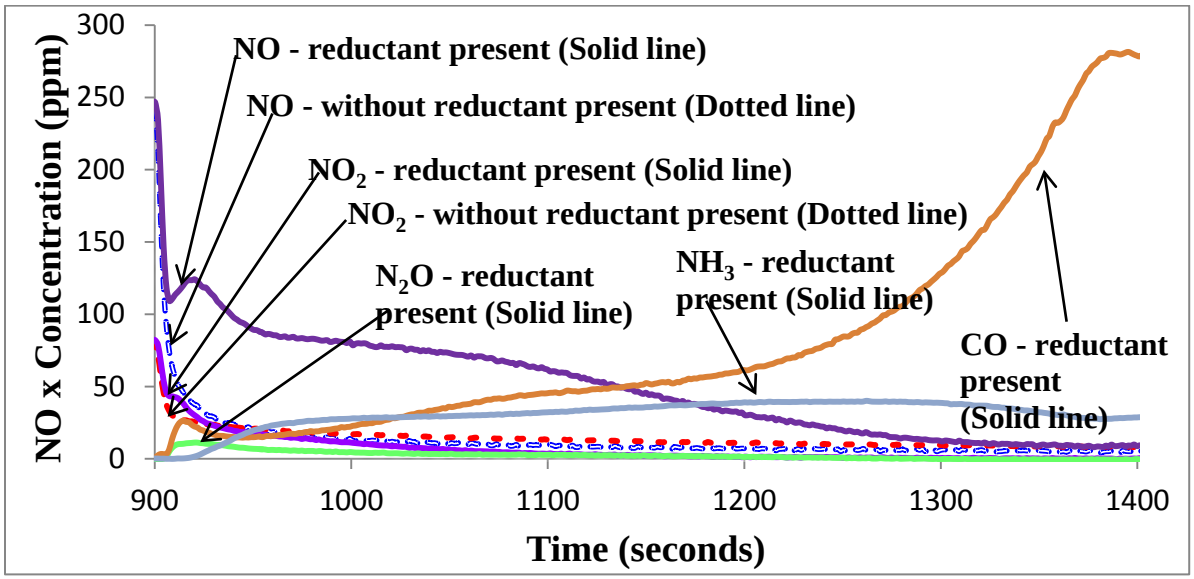

Figure 17: Long cycling, NO (with reductant), NO (without reductant), NO_2 (with reductant), NO_2 (without reductant), NH_3, N_2O and CO concentration profiles at 288°C for the regeneration phase. With 625 ppm CO, 375 ppm H_2, 5% CO_2, 5% H_2O, balance N_2 at 30,000 h^{-1}

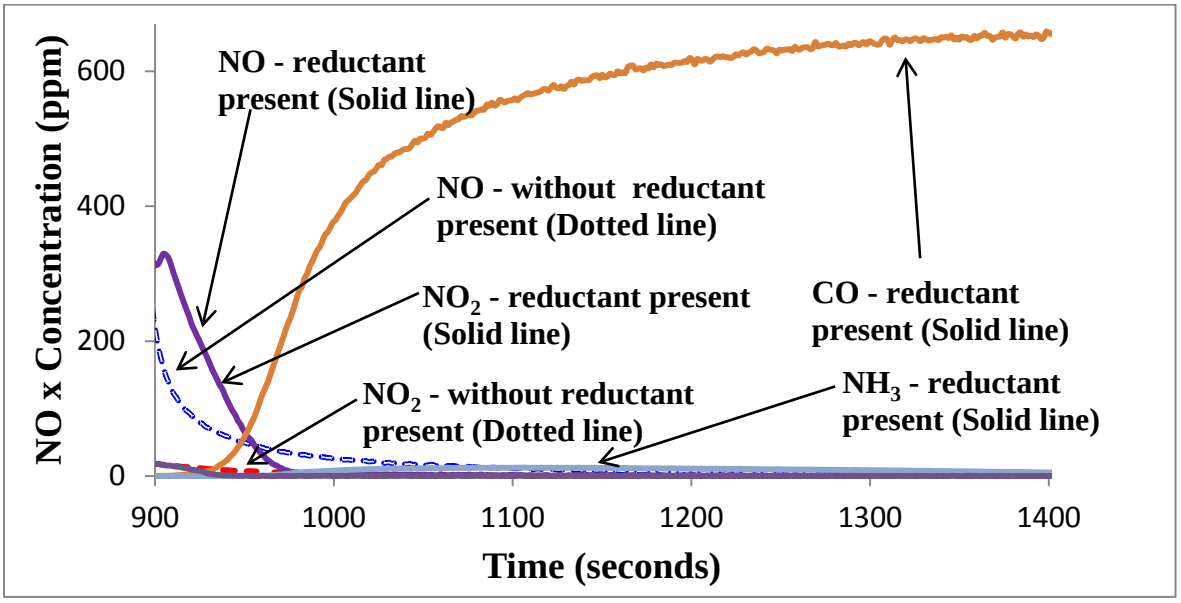

Figure 18: Long cycling, NO (with reductant), NO (without reductant), NO_2 (with reductant), NO_2 (without reductant), NH_3, N_2O and CO concentration profiles at 200°C for the regeneration phase. With 625 ppm CO, 375 ppm H_2, 5% CO_2, 5% H_2O, balance N_2 at 30,000 h^{-1}

The data listed in Table 7 show that at 200, 463 and 550°C there was little to no difference in the amount of NO_X released when comparing the presence and absence of reductant during the regeneration phase. The reason for such at high temperatures was discussed above. As shown in Figure 18, at 200°C, reduction of stored nitrates occurs, with high selectivity to NH_3, when reductant was added. Without reductant, the amounts released were similar, which indicates that reductant must induce nitrate decomposition, leading to more being released, of which some is reduced. Here, it is simply coincidence that the values were similar. At 288 and 375°C, nitrate decomposition was not as rapid and therefore there are still nitrates on the surface that can be reduced by the reductants. And when no reductant was added, these nitrates can still decompose thus resulting in some release. There was release

without reductant present, but it was much slower than at higher temperatures, demonstrating the increase in stability of nitrates at these lower temperatures. To further confirm this, the amount of NO_X stored at 375 and 288 °C differs from the amount released with and without reductant present. When a reductant was present, (Table 7), NO_X was reduced.

At 375°C, there was a much smaller NO_X "puff" at the onset of regeneration with reductant and no "puff" in the absence of reductant. The data obtained at 288°C, shown in Figure 17, shows a small "puff" with reductant and none in the absence of reductant added. These results demonstrate reductant induced nitrate decomposition, with more NO_X released at the beginning of the regeneration phase compared to that without reductant added. This effect was also seen on a model $Pt/Ba/Al_2O_3$ system by Nova et al.[114]. It should be noted that although reductant induced nitrate decomposition was demonstrated in this study there are other factors that affect nitrate stability. The absence of O_2 makes the nitrates/nitrites less stable and thus decompose [115] and also the presence of CO_2 has been seen to affect the stability of nitrates/nitrites [65].

Little to no N_2O was formed during the regeneration phase at any temperature. In terms of NH_3, at 375°C, NH_3 release was observed after about 30 seconds from the onset of regeneration. The delay in the NH_3 observation can be attributed to a high NO_X to reductant ratio. Once the ratio begins to decrease, NH_3 formation becomes more favorable. The fact that NH_3 was still being released at the end of the regeneration phase shows that there was still some NO_X left on the surface. In testing Pt-based LNT catalysts, reductant breakthrough typically coincides with NH_3 observed [109]. Over the perovskite sample, a CO breakthrough

profile was observed at about the same time as NH_3, but CO was also observed almost immediately after the onset of regeneration, rather than being delayed through reduction of OSC and nitrate consumption. Its concentration then decreased, before increasing again when NH_3 was also observed. These results suggest that surface NO_X species may be initially inhibiting CO reaction with OSC. At 288°C, Figure 17, CO was also observed at the onset of regeneration, and then the outlet concentration decreased, again indicating surface nitrates inhibit consumption of CO in OSC or nitrate reduction.

At 200°C, there was some NH_3 formed during the regeneration phase and this amount increased at 288°C and then decreased with increasing temperature. When NH_3 was produced, it was observed when reductant breakthrough began, as shown in Figures 17 and 18, beyond the initial slip peak due to OSC reduction inhibition, and in addition there must have been leftover NO_X on the surface of the catalyst since NH_3 formation was still observed at the end of the regeneration phase. This was again also seen in previous research with a Pt-based catalyst[109]. It has been proposed that when no more OSC is being reduced, the H_2 can react with either NO or other surface N-species to form NH_3 [116] and since there is no more OSC, NH_3 is therefore observed in the outlet, i.e. NH_3 is now not also consumed in reducing stored oxygen. Over the perovskite sample, the fact that NH_3 was formed at or after CO breakthrough (so little to no OSC was being reduced) and after NO_X was no longer being released supports such a mechanism. Previous research has also shown that NH_3 formation is dependent on the reductant to stored NO_X ratio [117]. The higher the ratio, the more NH_3 is formed. The data shown here follow the same trend. As the stored NO_X was reduced, less

was present and thus deeper reduction was observed. Furthermore, NH_3 is a known reductant in NSR chemistry. It is able to reduce stored nitrates [118, 119]. Thus, as the amount of stored NO_X decreased, less NH_3 was consumed via NO_X reduction and was therefore observed. At a device level, it is formed at upstream sites early during the regeneration phase [98], but is consumed at downstream sites where stored NO_X still exists. Once these are consumed, NH_3 is observed. At higher temperatures, where nitrate decomposition is rapid, less stored NO_X is available to react with the reductant and thus less NH_3 is formed.

In all, most of the trends are similar to those observed over a Pt-based NSR catalyst, where a decrease in temperature led to a decrease in the amount of NO_X released relative to the amount of NO_X trapped. For both catalysts trapping was limited by both NO oxidation and nitrate formation diffusion at lower temperatures. At higher temperatures both catalysts are limited by nitrate stability. NH_3 formation was observed with reductant breakthrough or high reductant to stored NO_X ratios. There was a substantially higher level of NO_X conversion during short cycling than long cycling in the middle operating temperature region. Short cycling led to better overall conversions due to more reductant readily available for reduction relative to all being consumed for OSC reduction, as well as less NO_X stored during the shorter lean phase. However, there were some differences noted. At lower temperatures, the perovskite still did not perform as well suggesting a diffusion limitation that is stronger on the perovskite than that of the Pt catalyst. Furthermore, low temperature trapping performance was not limited by regeneration, but by this diffusion limitation. Another difference was the amount of NO_X released in the presence and absence of reductant, where

the perovskite demonstrated a stronger dependence on reductant induced nitrate decomposition than that observed with the Pt-based sample [109]. Finally, the reductant breakthrough at the onset of the rich phase has not been previously noted, indicating that OSC consumption, or nitrate reduction, is inhibited likely by the presence of the nitrates themselves.

4.3 Water Gas Shift (WGS) Extent over Fresh Perovskite-based LNT catalyst

Water gas shift (WGS) is a common reaction occurring during the regeneration step of LNT cycling experiments and in practice [70, 77, 98, 120]. The regeneration gas stream included a mixture of CO and H_2 as reductants and the entire cycle included water, and during the cycling experiments WGS did occur during the regeneration portion of the cycle. The effect of the WGS reaction is the reduction of CO levels in the rich or regeneration gas stream via the following reaction: $CO + H_2O \rightarrow H_2 + CO_2$. Previous work shows that H_2 can more effectively reduce trapped NO_X than can CO at lower temperatures [98, 121], thus the more H_2 being used as a reductant the more efficient the entire process is. This is also evident based on the data listed in Table 6.The WGS extent is shown in Table 8 at the five temperatures used during the long cycling experiments.

Table 8: Amount of WGS extents at 200, 288, 375, 463, 550 °C

Temperature (°C)	WGS Extent (%)
200	3
288	55
375	*
463	85
550	70
*Note: * Denotes that a WGS extent value was undetermined due to the fact that a CO value did not reach steady state when the rich phase was complete*	

The WGS data were calculated using the CO levels at the end of the regeneration phase of the 3rd long cycle. Since high extents of WGS would ultimately help reduction, as H_2 is a better reductant better than CO, it would be ideal to have high extents of WGS at all temperatures, but especially at lower temperatures. The data show that the WGS extent increased with an increase in temperature, but dropped between 463 and 550°C. At high temperatures (463 and 550°C) there was little storage and still little reduction demonstrating that although more H_2 was available for better reduction it did not overcome the fact that there is too little nitrate stability at those high temperatures and thus rapid release of NO_X. At 200°C there was insignificant WGS activity. It is important to note that CO can reduce NO_X directly via $2CO + NO \rightarrow N_2 + CO_2$ and indirectly via the WGS reaction. Thus, it is difficult to confirm which route dominates. The trend observed here matches that previously observed over the Pt-based catalyst [109], although the values attained with the perovskite sample are lower.

4.4 Oxygen Storage Capacity (OSC) over Fresh Perovskite-based LNT catalyst

Commercial LNT catalysts can contain ceria, which acts as an oxygen storage component. During the regeneration phase of the cycling experiments, the reductants, and intermediate NH_3, can react with the ceria, reducing it, and thereby decrease the amount of available reductant for regeneration and NO_X reduction. This is especially critical at high temperatures, where nitrate decomposition is rapid and a lack of reductant leads to substantial NO_X release. Since the amount of O_2 stored can play a significant role in the regeneration phase, the OSC of the perovskite LNT catalyst was quantified via CO consumption experiments to evaluate the possibility of OSC competition over this system. The results are listed in Table 9.

Table 9: of O_2 stored at 200, 288, 375, 463, 550 °C

Temperature (°C)	O_2 Stored (mmoles)
200	0.06
288	0.11
375	0.31
463	0.41
550	0.44

The experiment was conducted on a cleaned catalyst and in cycles. The catalyst was exposed to a lean gas stream consisting of 10% O_2, 5% CO_2, and a balance of N_2 for 60 seconds, and then the gas was switched to the rich gas stream consisting of 5% CO_2, 1% CO and a balance of N_2 for 90 seconds. H_2O was not included in this experiment in order to eliminate the WGS effect. Thirty cycles were completed in order to achieve/guarantee cycle-to-cycle stability. The outlet CO concentrations were used to calculate the amount of O_2 being consumed.

Table 9 shows that the amount of O_2 stored increased with increasing temperature. Clearly there is a substantial amount of OSC, for example 0.44 mmole O_2 stored compared to that of NO_X trapped, 0.035 mmole, at 550°C. These data show that there will be competition for the reductants between surface oxygen and nitrate decomposition or NO_X reduction. This is true for all temperatures (with different extents of OSC and therefore competition).

4.5 NO_2 as a NO_X Source – Long Cycling

Literature evidence shows that typical LNT catalysts can trap NO_2 more easily than NO. This includes rates of trapping as well as extents [47 – 51, 56, 109]. In testing the perovskite-based sample, using NO_2 as the NO_X source rather than NO also significantly increased the amount of total NO_X trapped, as observed by comparing Figures 15 and 19, and in comparing the values in Table 10.

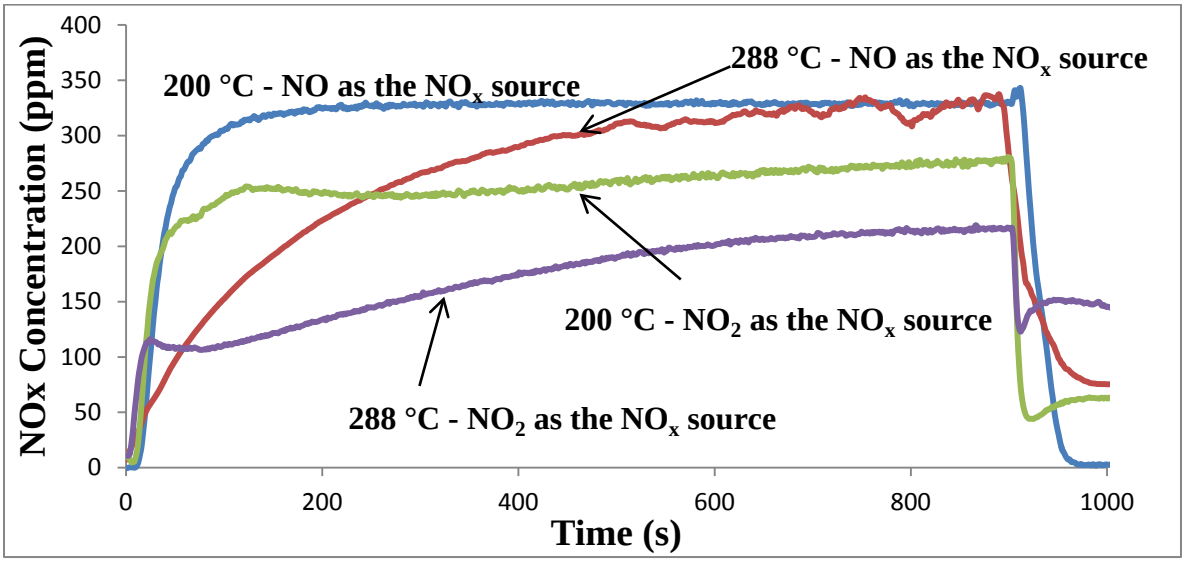

Figure 19: Long cycling, NO + NO_2 (NO_X) concentration profile at 200 and 288°C with NO as the NO_X source and 200 and 288 °C with NO_2 as the NO_X source. 300 ppm NO or NO_2, 10% O_2, 5% CO_2, 5% H_2O, balance N_2 at 30,000 h^{-1} space velocity

For example, at 200°C when the NO_X source was NO or NO_2, 36 and 178 µmoles of NO_X were trapped, respectively, and at 288°C, 137 µmoles and 353 µmoles of NO_X were trapped, respectively. These results follow the same trends observed with Pt-based LNT catalysts, where limiting factors at low temperatures are NO oxidation and nitrate diffusion[107], as well as the increased NO_2 gas to solid phase equilibrium[113].

Table 10: Long cycle storage and reduction performance results using NO and NO_2 as the NO_X source: 300 ppm NO and/or NO_2, 10% O_2, 5% CO_2, 5% H_2O and a balance of N_2 in the lean phase; 625 ppm CO, 375 ppm H_2, 5% CO_2, 5% H_2O and a balance of N_2 rich phase

Temp (°C)	NO_2 as NO_X source NO_X Trapped (µmoles)	NO as NO_X source NO_X Trapped (µmoles)	NO_2 as NO_X source NO_X Trapped - at 20% BT	NO as NO_X source NO_X Trapped - at 20% BT
200	178	36	35	21
288	353	137	67	56

Chapter 5

Effects of Thermal Degradation and Sulfur Poisoning on the Performance of a Perovskite-Based Lean-NO_X-Trap Catalyst

5.1 Effects of Thermal Aging and Sulfur Poisoning on NO Oxidation

NO oxidation experiments were carried out to evaluate NO to NO_2 conversion over the catalyst when fresh, and after thermal aging and desulfation after sulfur poisoning. An NO oxidation experiment was also carried out when the catalyst was exposed to sulfur poisoning before desulfation, however only for temperatures between 200 and 300°C in order to avoid S release. The inlet gas consisted of 200 ppm NO, 10% O_2, 10% CO_2, 10% H_2O and a balance of N_2. The data shown were attained once steady state NO to NO_2 conversion was reached. Previous work has shown that NO_2 will sorb on LNT materials more efficiently than NO [47 – 51], demonstrating that NO oxidation (NO to NO_2 conversion) is a critical step in improving the overall performance of a LNT catalyst. Consequently, investigating the effects of aging and sulfur poisoning on this LNT catalyst process is critical.

NO oxidation data as a function of temperature when the catalyst was in its fresh, thermally aged and desulfated after sulfur poisoning states, are shown in Figure 20. When the catalyst was fresh it attained low conversions at low temperatures due to kinetic limitations. After

thermal aging and desulfation the conversions were slightly lower. The conversion trends for all states were similar with NO to NO_2 conversion increasing after 200°C until 350°C. After 350°C conversion dropped due to thermodynamic limitations and the reaction then followed the equilibrium curve. After thermal aging, the low temperature NO to NO_2 conversions decreased relative to when the catalyst was fresh. Two possible degradation routes are likely. First, precious metal sintering could have occurred causing a loss in dispersion and leading to a drop in activity. Secondly, sintering of the washcoat could occur, possibly causing a collapse in the pore structure or in loss of active site dispersion. Sintering of La-based perovskites doped with Pd has been previously observed [122]. Based on the NO oxidation Ea findings from when the catalyst was fresh, and the likelihood that it is the perovskite itself catalyzing NO oxidation, it seems more likely that the perovskite did suffer some loss in performance, but this does not exclude Pd dispersion loss if it contributed to NO oxidation. A similar sintering effect has also been seen when evaluating a commercial Pt-based LNT catalyst [123].

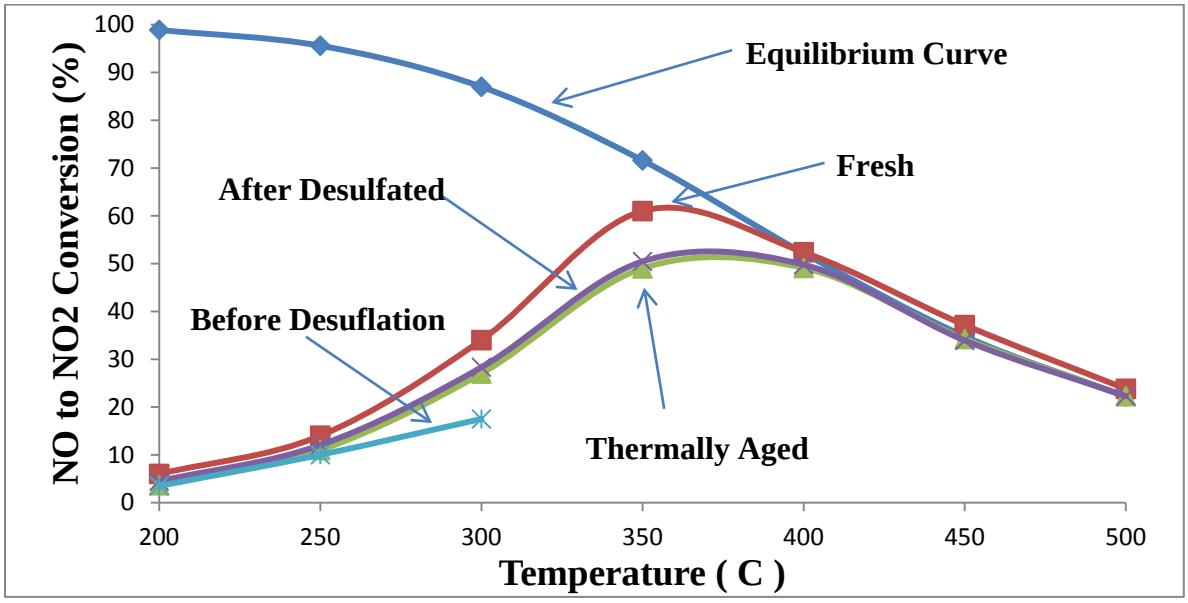

Figure 20: NO oxidation as a function of temperature at 50,000 h^{-1} space velocity; 200 ppm NO, 10% O_2, 10% CO_2, 10% H_2O and a balance of N_2. For fresh, thermally aged and before and after desulfating the catalyst

After sulfur exposure and then desulfation, the NO to NO_2 conversion values matched the values of when the catalyst was thermally aged only. The match between the desulfated and thermally aged data sets suggests that there were no irreversible S poisoning effects, while prior to desulfation, S build-up on the surface did inhibit NO oxidation, as has been previously observed for Pt-based samples [124, 125]. However, this was not a permanent deactivation, with S desorption resulting in a return to previous performance.

As stated above, NO_2 will sorb on LNT materials more efficiently than NO [47 – 51]. Literature evidence also shows that NO_2 is a key reactant for nitrate formation via the disproportionation reaction on LNT catalysts [109]. Thus an increase in NO to NO_2 conversion leads to better overall NO_X trap performance. Figure 20 shows that at low temperatures there were low NO oxidation extents due to kinetic limitations. Although

nitrates are more stable at lower temperatures and sites are available for trapping, a lack of NO_2 formation ultimately leads to poorer storage. In the case of higher temperatures, NO oxidation increases, but at the same time nitrate stability decreases ultimately decreasing NO_X storage [50]. The best NO_X storage abilities are typically seen between 300 and 400°C where the temperatures are low enough for nitrate stability yet high enough for good NO to NO_2 conversion (Figure 20).

5.2 Effects of Thermal Aging and Sulfur Poisoning on NO_X Storage and Reduction

Previous research has shown that thermal aging and sulfur poisoning affect Pt-based LNT performance during cyclic operation [91, 93, 124, 126]. This section focuses on the effects of sulfur exposure and thermal aging on the LNT cycling capabilities of the perovskite-based sample.

5.2.1 Short Cycles

Short duration cycle experiments were completed over the catalyst in the fresh, thermally aged and desulfated (after S exposure) states. The overall NO_X conversion had the same trend in all instances, as seen in Figure 21, however when the catalyst was fresh it had the best overall efficiency.

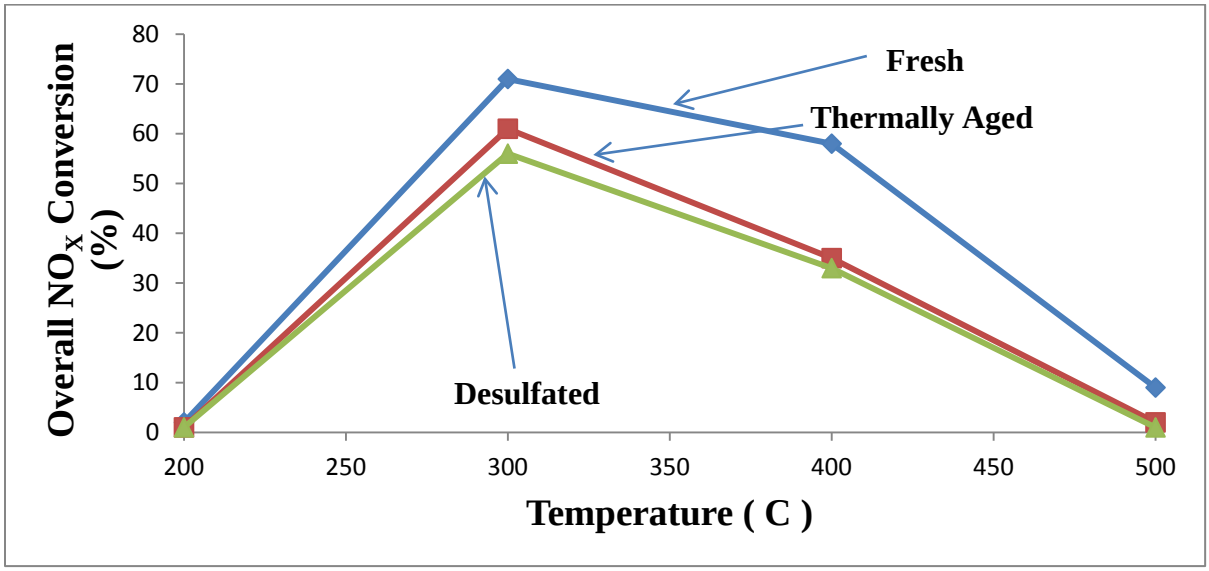

Figure 21: Short cycling NO_X ($NO + NO_2$) conversion profiles as a function of temperature (200, 300, 400 and 500°C) for the fresh, thermally aged, sulfur exposed and desulfated catalyst; 200 ppm NO, 10% O_2, 10% CO_2, 10% H_2O, balance N_2, at 50,000 h^{-1} space velocity

The overall lower NO_X conversion values at 500°C are due to the lack of nitrate stability and at 200°C to poor NO oxidation (Figure 20) and nitrate diffusion, as discussed below. Results obtained from the short cycling experiment data are tabulated in Table 11. Figures 22 and 23 show the outlet NO_X concentration profiles as a function of time for experiments at 300 and 400°C, respectively. Once the catalyst was thermally aged, the NO_X conversion dropped from 71% to 61% at 300°C and 58% to 35% at 400°C.

Table 11: Short cycle storage and reduction performance results using NO as the NO_X source: 200 ppm NO, 10% O_2, 10% CO_2, 10% H_2O and a balance of N_2 in the lean phase (60 seconds); 3% CO, 1% H_2, 10% CO_2, 10% H_2O and a balance of N_2 in the rich phase (5 seconds)

Catalyst State	Temp (°C)	NO_X trapped (µmoles)	NO_X released (µmoles)	NO_X Converted (µmoles)	Overall NO_X Converted (%)	NH_3 formed (µmoles)	N_2O formed (µmoles)	N_2 formed (µmoles)
Fresh	**200**	14	13.4	0.7	2	0.1	0.1	0.5
	300	39	5	34	71	16	2	16
	400	45	16	29	58	0	0	29
	500	22	18	4	9	0.1	0.3	3.6
Thermally Aged	**200**	11	10	1	1	0.52	0.1	0.1
	300	38	6	32	61	16	2	12
	400	42	25	17	35	10	2	5
	500	17	15	2	2	0.08	0.09	1.7
Sulfur Poisoned – Before Desulfation	**200**	2.4	2	0.45	1	0.25	0	0.2
	300	8.7	2.6	6.1	13	3.5	0.03	2.5
Desulfation – After Sulfur Poisoning	**200**	11	10.4	0.6	1	0.5	0.1	0.01
	300	39	9	30	56	22	2	5
	400	44	30	14	30	12.5	1.4	0.1
	500	17	16.6	0.4	1	0.1	0.1	0.1

As shown in Figures 22 and 23, the trapping ability was poorer after thermal degradation, which leads to the poorer overall reduction. Taken together with the NO oxidation results, the data suggest that a loss in oxidation ability and trapping ability occurred. This can be attributed to precious metal or perovskite material sintering as discussed above, but the high temperature treatment may also impact the trapping component [106]. Precious metal sintering can decrease the interaction between the storage component and precious metal site which decreases NO_X storage and reduction performance, as observed with Pt-based LNT catalysts [102, 103, 127]. Another possibility is a reaction between the storage and support materials resulting in mixed metal oxides [102, 103, 127]. These data do not distinguish between these different degradation models, but it is likely a combination of the above. NO oxidation loss due to perovskite activity degradation leads to decreased NO_2 levels and thus decreased trapping rates. This in turn leads to poorer performance, which can be confounded by a loss in interaction between the trapping and reduction sites, leading to poorer trapping extent and regeneration.

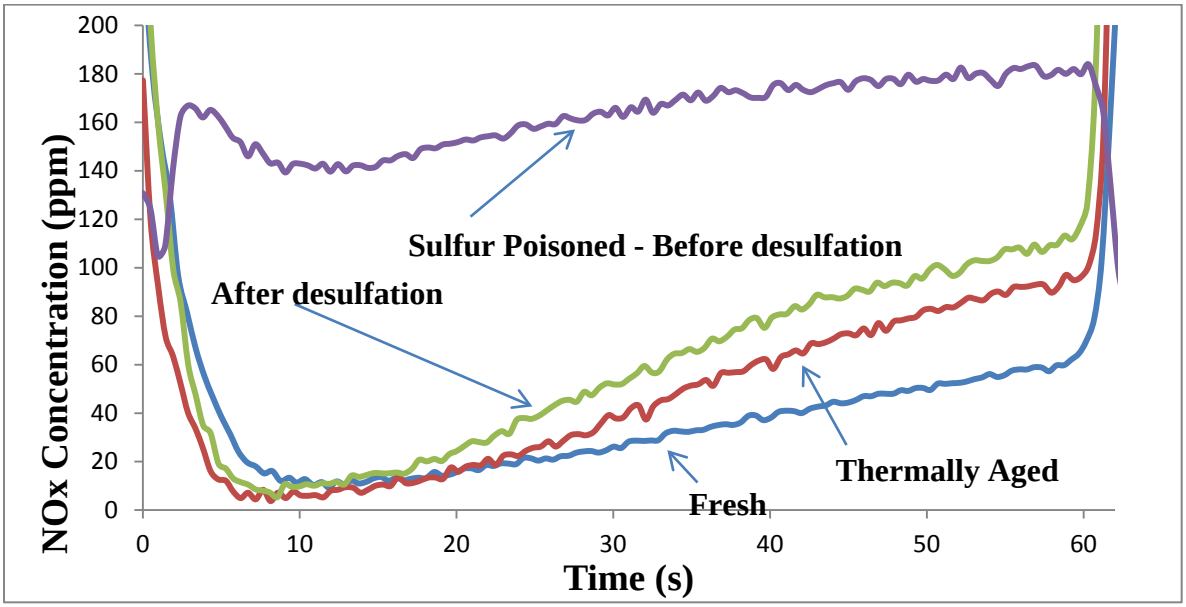

Figure 22: Short cycling NO_X (NO + NO_2) concentration profiles at 300°C for the fresh, thermally aged, sulfur exposed and desulfated catalyst; 200 ppm NO, 10% O_2, 10% CO_2, 10% H_2O, balance N_2 at 50,000 h^{-1} space velocity

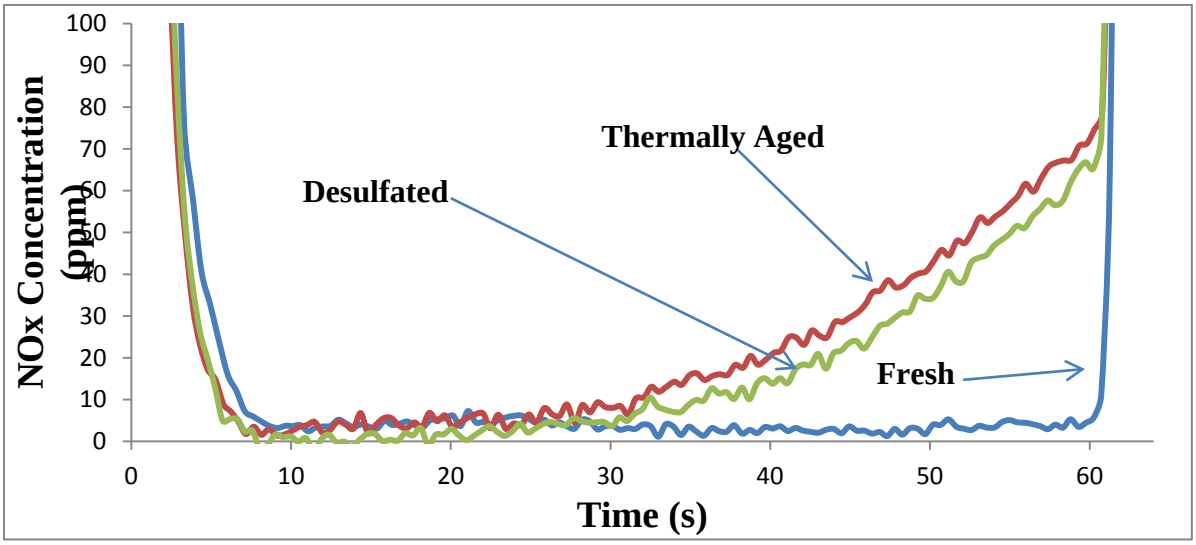

Figure 23: Short cycling NO_X (NO + NO_2) concentration profiles at 400°C for the fresh, thermally aged, sulfur exposed and desulfated catalyst; 200 ppm NO, 10% O_2, 10% CO_2, 10% H_2O, balance N_2 at 50,000 h^{-1} space velocity

After the catalyst was exposed to sulfur and then desulfated, the NO_X conversions were slightly lower. At 400°C, there was little difference in the trapping ability, as shown in Figure 23, but at 300°C an observable difference was still noted. These data suggest that not all the sulfur was removed during desulfation. The sample was previously thermally aged at 750°C (desulfation was done at 700°C), so the temperature exposure during desulfation should not affect subsequent performance. The extent and temperature of the desulfation protocol may not result in complete removal of the S species. As stated in the introduction section, bulk $BaSO_4$ decomposes at around 1600 °C [97] yet such a temperature would damage other components in the LNT catalyst; in addition this is simply an unrealistic exhaust temperature [106]. In the past, a rich environment at temperatures between 500°C and 830°C proved reasonable for significant desulfation of standard LNTs [29, 128 – 130]. Sulfate/sulfite reduction is more efficient when using H_2 as the reductant as opposed to CO [29, 87, 91]. Interestingly, past research also shows that even when H_2 is used, if there is no Pt present, less S is removed [31]. The authors suggested that sulfate species migrate to the Pt site where H_2 dissociates for desulfation to occur. It was also suggested that H_2 must spillover from Pt to reduce the sulfate species. The catalyst used in this study does not include Pt. It is difficult to tell if the absence of Pt hindered H_2 reacting with the sulfate species on this perovskite-based sample, however the data do suggest that sulfates were not completely removed.

As shown in Table 11, the amount of NO_X trapped increased from 200 to 400°C when the catalyst was fresh, thermally aged and desulfated, which follows the NO oxidation extent

trend. The best trapping performance was observed at 400°C for all cases; while the catalyst was fresh the best performance occurred with 45 µmoles stored. Once the catalyst was thermally aged, 42 µmoles were stored and after sulfur poisoning and desulfation, 44 µmoles were stored. Pd does not seemingly play a significant role in NO oxidation thus any Pd sintering may not affect the overall trapping performance. However, sintering of the washcoat/perovskite component can also create less surface area for NO oxidation and less NO_2 created for storage on the thermally aged catalyst. Lower NO oxidation extents were observed (Figure 20) and there are slightly lower trapping values after the catalyst was thermally aged. Lower trapping values when the catalyst was desulfated after S poisoning suggest Ba-sulfate formation and not all of it regenerated, which has been noted in literature [28, 91]. A typical lab-style desulfation procedure for a $Pt/Ba/Al_2O_3$ LNT catalyst is a temperature-programmed reduction where the temperature is ramped at 10°C/min to 700°C in a rich environment [94]. In this literature study, at 700°C $BaSO_4$ decomposition was observed and release of S from Al_2O_3 was observed at 600°C. Although S release from the Al_2O_3 occurred at lower temperatures, this was problematic for the trapping component. The authors noted that the S species that were released from the washcoat could readsorb to the Ba trapping sites thus decreasing the NO_X trapping ability. This effect was also seen with $CeSO_4$, which decomposes at lower temperatures than $BaSO_4$, where the S readsorbed and deactivated the trapping sites [131]. The same trend is suggested for this perovskite sample that includes Ba as a trapping component and a build-up of Ba-sulfates can ultimately reduce NO_X trapping and conversion performance. Lower amounts of NO_X trapped once the catalyst

was thermally aged and desulfated ultimately led to lower amounts of NO_X converted as discussed above. Furthermore, the amounts of stored NO_X that were reduced typically decreased with thermal aging and further decreased after desulfation (Table 11). This trend indicates that there was loss of Ba/reduction site interaction either through sintering of the perovskite or Pd and/or Rh components.

Short cycling experiments were also conducted after sulfur poisoning (only at 200 and 300°C) and the data are also listed in Table 11. The effects of sulfur poisoning without desulfation significantly decreased the amount of NO_X stored (as seen in Figure 22), overall NO_X converted and stored NO_X that was reduced. At 200°C, 2.4 μmoles and 11 μmoles and at 300°C 8.7 μmoles and 39 μmoles of NO_X were stored before and after desulfation, respectively. This effect can also be seen in Figure 24 where after desulfation at 200°C there was significantly more storage. As expected, this shows a build-up of sulfates inhibiting NO_X trapping. The presence of extensive sulfur on the surface also decreased NO oxidation, and ultimately regeneration and NO_X conversion. Thus not only was trapping negatively affected via sulfate formation, but the oxidation/reduction ability was also negatively impacted.

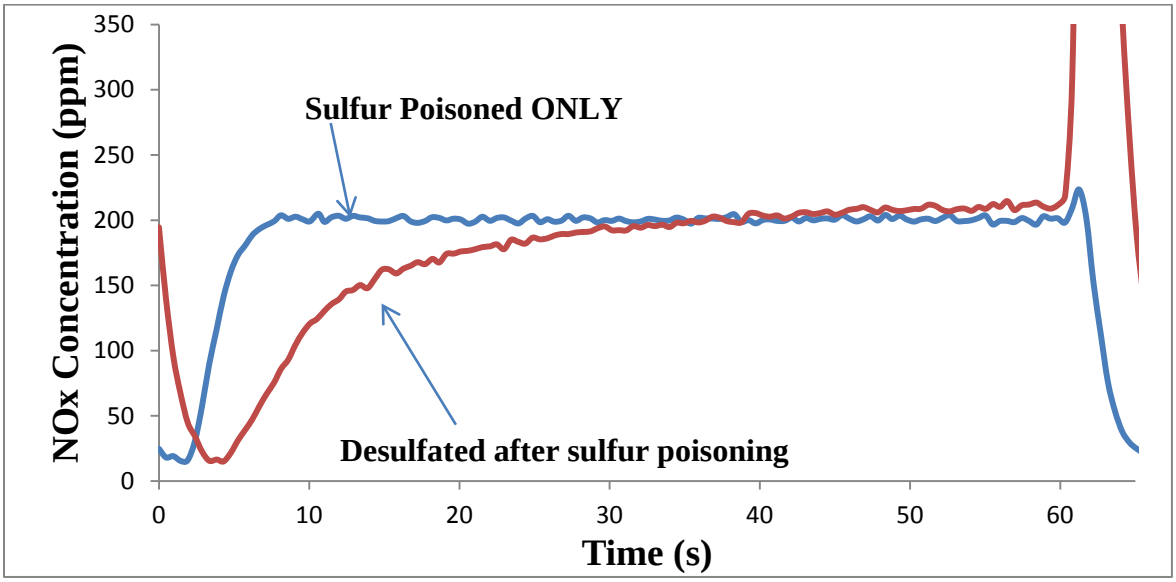

Figure 24: Short cycling NO_X (NO + NO_2) concentration profiles at 200°C before and after the catalyst was desulfated from sulfur poisoning; 200 ppm NO, 10% O_2, 10% CO_2, 10% H_2O, balance N_2 at 50,000 h^{-1} space velocity

Figure 25 shows the 500°C NO_X concentration profile as a function of time for three cases; fresh and after the catalyst was thermally aged and desulfated after sulfur poisoning. There is a non-monotonic NO_X concentration change during trapping with respect to time for all cases; a trend that has been seen previously over a commercial LNT catalyst [111]. The authors suggested that the exothermic oxidation reactions occurring during the regeneration phase formed a temperature wave that moved through the catalyst creating this non-monotonic profile. The heat that was generated moved across the solid at a slow rate surpassing the time of the regeneration phase and emerged into the lean phase. Once the reaction was in the lean phase an increase in the solid temperature led to a decrease in trapping again attributed to the instability of the nitrates at high temperatures. The effects of thermal aging and S exposure followed by desulfation follow the same trends as mentioned

above. There is a loss in trapping performance. More NO_X was released from the fresh sample, but this was simply due to more being trapped in the previous lean phase.

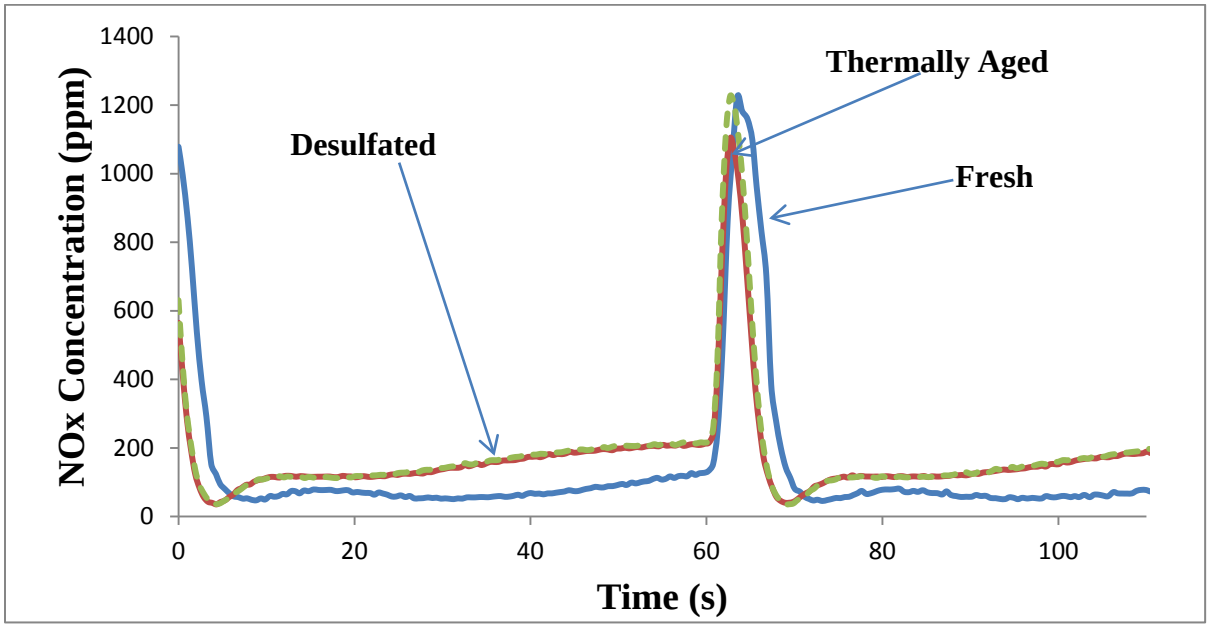

Figure 25: Short cycling NO_X ($NO + NO_2$) concentration profiles at 500°C for the fresh, thermally aged, sulfur exposed and desulfated catalyst; 200 ppm NO, 10% O_2, 10% CO_2, 10% H_2O, balance N_2 at 50,000 h^{-1} space velocity

While the short cycling experiments gave insight to the catalysts' abilities and limitations, the chemistry is difficult to isolate with such short time periods for the lean and rich phases. In order to investigate the LNT chemistry further, long cycles were performed; that is longer time periods in the lean and rich phases.

5.2.2 Long Cycles

A summary of the performance data obtained during the long cycle experiments on the fresh catalyst, after the catalyst was thermally aged and after the catalyst was desulfated after

sulfur poisoning at five different temperatures is presented in Table 12. The data are those of the third cycle of the CLEERS protocol, by which time cycle-to-cycle stability was reached.

Table 12: Long cycle storage and reduction performance results using NO as the NO_X source: 300 ppm NO, 10% O_2, 5% CO_2, 5% H_2O and a balance of N_2 in the lean phase (15 minutes); 625 ppm CO, 375 ppm H_2, 5% CO_2, 5% H_2O and a balance of N_2 in the rich phase (10 min)

Catalyst State	Temp (°C)	Total NO_X trapped (µmoles)	NO_X trapped (%) - at 20% BT	NO_X Released (µmoles) - no reductant	NO_X released (µmoles) - with reductant	NH_3 formed (µmoles) - with Reductant	N_2O formed (µmoles)	N_2 formed (µmoles)
Fresh	**200**	36	21	27	28	11	0	0
	288	137	56	36	70	44	3	17
	375	188	92	119	136	30	0.44	22
	463	93	55	90	90	0.1	0	3
	550	35	18	32	33	0.07	0	2
Thermally Aged	**200**	24	19	19	20	21	1	0
	288	123	63	37	64	36	3	16
	375	133	80	97	97	22	1	13
	463	65	42	65	63	0	0	2
	550	25	15	24	24	0	0	1
Sulfur Poisoned – Before Desulfation	**200**	14	7	7	7	9	0	0
	288	24	17	13	8	20	0	0
Desulfation – After	**200**	24	19	17	21	25	1	0

Sulfur Poisoning	**288**	132	63	36	81	43	2	4
	375	130	81	97	98	28	1	3
	463	66	42	66	65	0	0	1
	550	25	15	23	24	0	0	1

Again, the catalyst trapped the least amount of NO_X at the two temperature extremes for all three cases. At 550°C the amount of NO_X trapped differed only slightly between each of the instances, although there was a decrease in the amount trapped after thermal aging, with 35 µmoles, 25 µmoles and 25 µmoles stored when the catalyst was fresh, thermally aged and desulfated, respectively. Similarly, there was a difference after thermal aging at 200°C, with 36 µmoles, 24 µmoles and 24 µmoles stored when the catalyst was fresh, thermally aged and then desulfated, respectively. There were larger differences in trapping performance for the intermediate temperatures, and the concentration profiles as a function of time results data are shown in Figures 26-28.

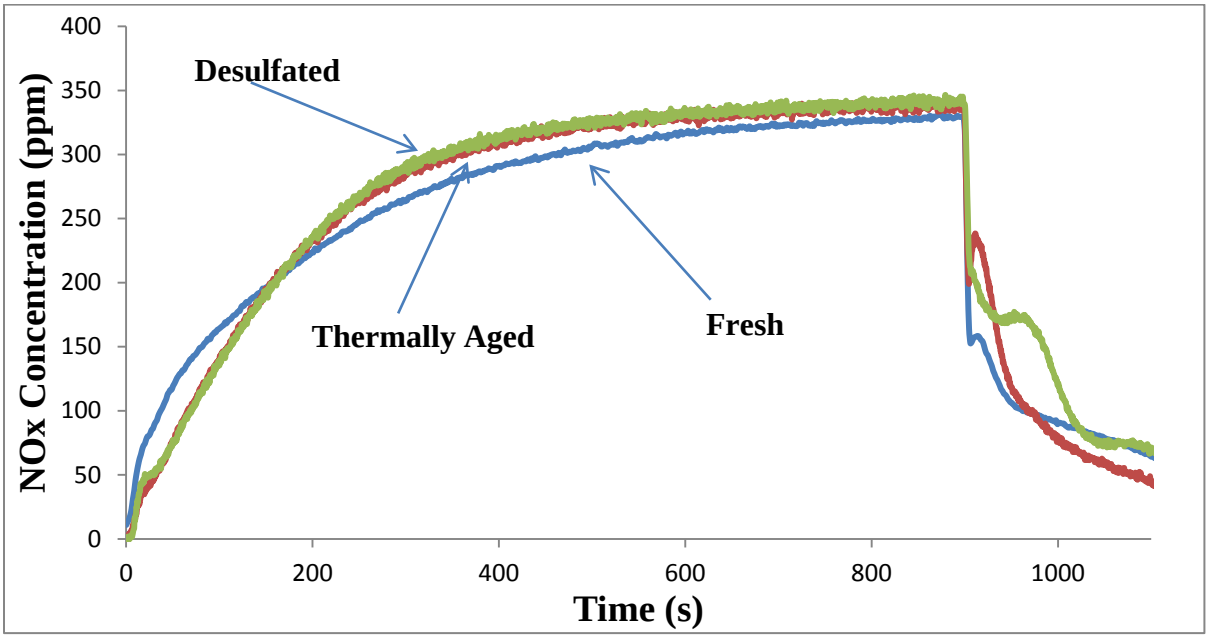

Figure 26: Long cycling NO_X concentration profiles at 288°C for the storage phase for the fresh, thermally aged, sulfur exposed and desulfated catalyst; 300 ppm NO, 10% O_2, 5% CO_2, 5% H_2O, balance N_2 at 30,000 h^{-1} space velocity

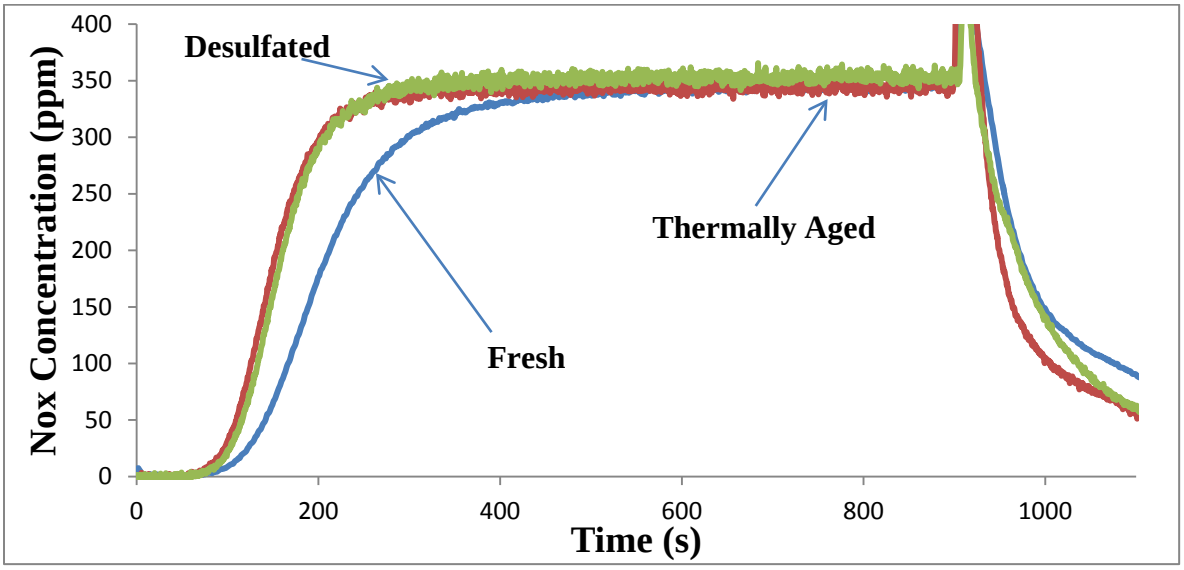

Figure 27: Long cycling NO_X concentration profiles at 375°C for the fresh, thermally aged, sulfur exposed and desulfated catalyst; 300 ppm NO, 10% O_2, 5% CO_2, 5% H_2O, balance N_2 at 30,000 h^{-1} space velocity

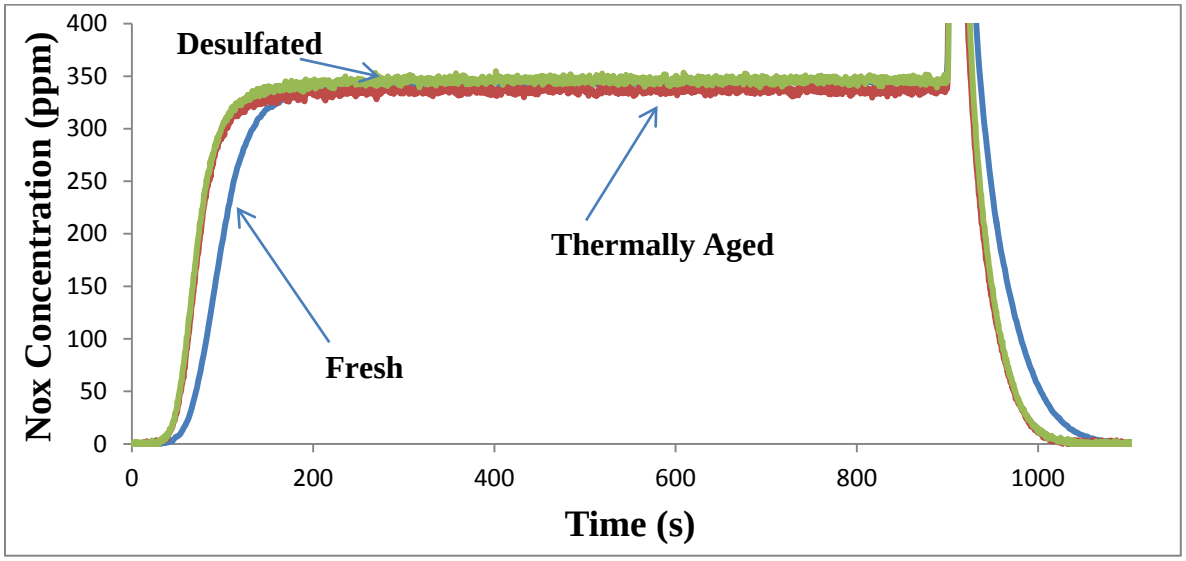

Figure 28: Long cycling NO_X concentration profiles at 463°C for the storage phase for the fresh, thermally aged, sulfur exposed and desulfated catalyst; 300 ppm NO, 10% O_2, 5% CO_2, 5% H_2O, balance N_2 at 30,000 h^{-1} space velocity

The smaller differences at the temperature extremes indicate that nitrate stability, at high temperature, and NO oxidation and nitrate diffusion, at low temperature, were still the critical factors. The best trapping performances when the catalyst was fresh and thermally aged were observed at 375°C, with 90 seconds and 75 seconds elapsed prior to slip and 188 and 133 µmoles trapped, respectively. Whereas the best trapping performance when the catalyst was desulfated after sulfur exposure was measured at 288°C (but just slightly better than at 375°C), with only 6 seconds elapsed prior to slip and 132 µmoles stored. At 463°C there was hardly any difference in storage performance once the catalyst was thermally aged and then when it was desulfated after sulfur exposure depicting again that enough S was removed after sulfur poisoning such that any remaining S was not a factor at this temperature. Figure 29 shows and compares the amount of NO_X trapped at all five temperatures when the catalyst

was fresh, thermally aged and desulfated after sulfur exposure. The lower performance after thermal aging at 288, 375 and 463°C again suggests sintering occurred, which decreased the catalyst's NO_X trapping ability. After desulfation the performance was nearly as good as it was after thermal aging during the long cycles, suggesting most of the S deposited and stored on the catalyst after sulfur poisoning was removed. Although the short cycling results demonstrate some was left, the amount remaining ultimately did not have much negative impact on the long cycle results.

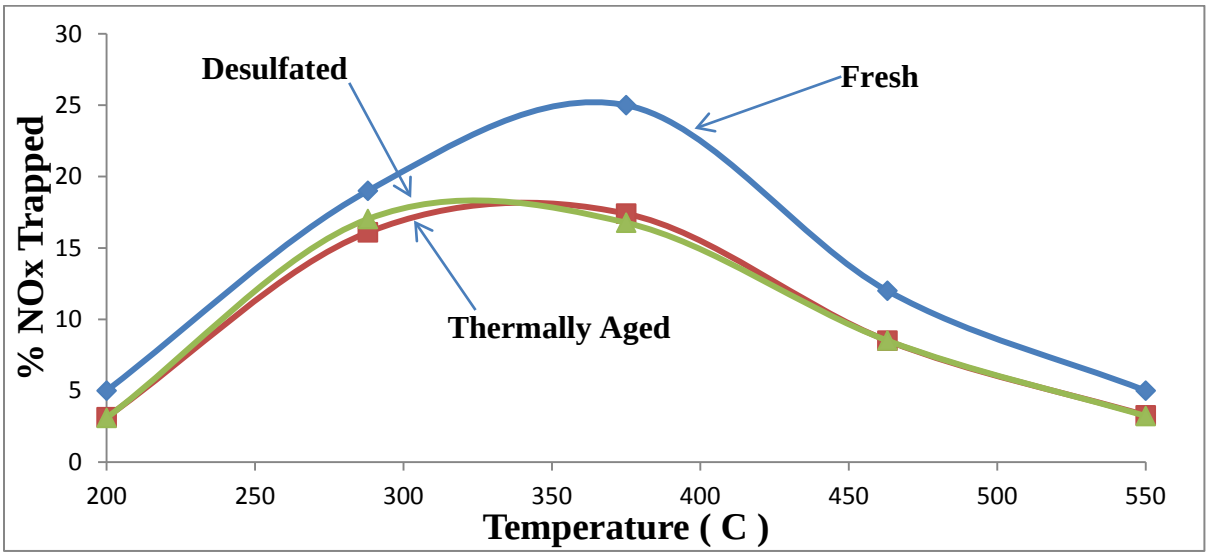

Figure 29: Long cycling NO_X storage comparison at 200, 288, 375, 463 and 550°C for the for the fresh, thermally aged, sulfur exposed and desulfated catalyst; 300 ppm NO, 10% O_2, 5% CO_2, 5% H_2O, balance N_2 at 30,000 h^{-1} space velocity

In terms of performance before and after desulfation, the amount of NO_X trapped at 200°C was 14 µmoles and 24 µmoles and at 288°C 24 µmoles and 132 µmoles, respectively. Sulfates formed on the storage component and blocked NO_X storage, but much was removed via the desulfation as the catalyst was restored to the thermally aged state.

Ba is the trapping component used in the perovskite catalyst formulation and is common in NSR catalysts. At high temperatures, trapping performance decreased as the temperature increased due to nitrate stability; something that has been observed in studies of $Pt/Ba/Al_2O_3$ catalysts [109, 110]. At low temperatures the decreased performance could possibility be due to a lack of regeneration, which has also been seen in previous work [113]. Similar limitations and questions arose in studies for Pt-based catalysts [107, 109]. In these previous studies leftover NO_X was observed on the surface of the catalyst even when reductant break through was observed, confirming a limitation due to regeneration. Yet another possibility is diffusion limitations as nitrates build up around the oxidation sites leading to poor trapping. Plots for the fresh perovskite catalyst long cycling experiments done at 200 and 288°C shown in Figure 15 show the first cycle (where the catalyst was previously cleaned and therefore NO_X-free) and the third cycle (where nitrate/nitrite build-up could have occurred) overlapped thus there was no build-up of nitrates on the surface between regenerations demonstrating trapping limitations and not regeneration limitations. It was therefore suggested that the poor trapping performance is caused by diffusion limitations as nitrates build up around the oxidation sites. As seen in Figure 30 the same comparison was completed on the catalyst after desulfation and the same conclusion stands, where the trapping abilities were the limiting factor and not regeneration.

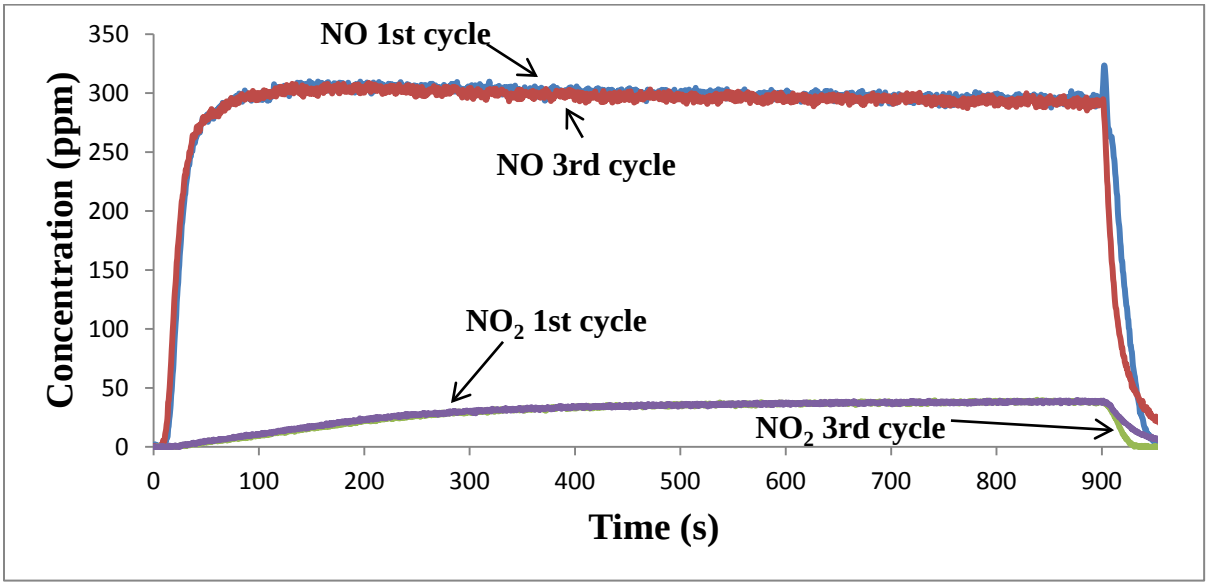

Figure 30: Long cycling 1st vs. 3rd cycles of NO_X storage at 200°C after the catalyst was desulfated after sulfur exposure. NO and NO_2 profiles shown; 300 ppm NO, 10% O_2, 5% CO_2, 5% H_2O, balance N_2 at 30,000 h^{-1} space velocity

In terms of the amount of NO_X trapped that was reduced during the regeneration phase, the best efficiency was observed at 288°C for the fresh catalyst as well as once the catalyst was thermally aged and desulfated after sulfur poisoning. Of the NO_X trapped 49%, 48% and 39% were reduced, respectively. This suggests some sintering of the catalyst component related to reduction, i.e. the Pd or Rh. Pd has been seen to increase sulfur resistance in a La-base perovskite catalyst [132]. This previous study suggested that the sulfur first reacts with the Pd and once that is completely covered lanthanum sulfates begin to form. However in this study, once the catalyst was exposed to sulfur then desulfated, a 10% decrease in performance was observed suggesting that there was still residual S left on the catalyst that inhibited regeneration. At 375°C only 28%, 27% and 25% and at and 200°C 22%, 17% and 13% of the trapped NO_X were reduced, when the catalyst was fresh, thermally aged and then

desulfated, respectively, and at the other temperatures reduction was quite poor for all cases. Yet at 375°C there was not much difference between the performances in all three cases. There was however a notable drop at 200°C after desulfation, as was observed at 288°C, suggesting the same effects occurred. Overall, at lower test temperatures lower regeneration performance is more evident due to sulfate formation, or residual sulfates left after desulfation. Also, and as stated previously, the perovskite sample is limited by diffusion with a build-up of nitrates around the oxidation/reduction sites, and it is possible sulfates around these sites can limit desulfation. Thus regeneration may not occur at sites further away from the oxidation/reduction sites which lowers performance, especially at lower temperature where diffusion limitations would be strongest.

Table 12 shows that at 550°C the amount of NO_X released is very close to the amount trapped when the catalyst was fresh and after thermal aging and desulfation after sulfur poisoning. At the higher temperatures this is in part due to a poor reduction rate relative to the nitrate decomposition rate. Similar trends were observed with a Pt-based commercial LNT catalyst [109] following the same CLEERS protocol as this study, where incomplete reduction was observed at 550 and 463°C and as discussed in Chapter 4. At all stages of testing, whether the catalyst was fresh, thermally aged or before and after desulfation, there was significant reductant consumption even when there was no NO_X reduction which must be related to reducing stored oxygen on the surface. Since the catalyst has measurable oxygen storage capacity (OSC), to be discussed below, competition arose between the stored oxygen and NO_X for the reductant. At both 463 and 550°C, neither N_2O nor NH_3 was

produced when the catalyst was fresh, thermally aged or desulfated, as expected given the lack of NO_X reduction. These trends are consistent with the Pt-based catalyst studied previously [109].

The data listed in Table 12 show that at 200, 463 and 550°C there was little to no difference in the amount of NO_X released when comparing the presence and absence of reductant during the regeneration phase in all instances; fresh, thermally aged and desulfated after sulfur exposure. The reason for such at high temperatures was discussed above. As shown in Table 12, at 200°C, reduction of stored nitrates occurs, with high selectivity to NH_3, when reductant was added when the catalyst was fresh. The same trend was seen after thermal aging and desulfation after sulfur exposure, however there was also an increase in NH_3 selectivity (discussed below). At 200°C, for the fresh catalyst, and after thermal aging, sulfur exposure and desulfation, the amounts of NO_X released were similar without reductant.

At 288 and 375°C over the fresh catalyst, nitrate decomposition was not as rapid and therefore there are still nitrates on the surface that can be reduced by the reductants. And when no reductant was added, these nitrates can still decompose thus resulting in some release. There was release without reductant present, but it was much slower than at higher temperatures, demonstrating the increase in stability of nitrates at these lower temperatures. Once the catalyst was thermally aged the trends at 288°C were the same. The amount of NO_X stored differed from the amount released with reductant thus NO_X was reduced. This is also evident in Table 12 with the amounts of N_2, NH_3 and N_2O produced listed. The data collected at this test temperature after thermal aging and when the catalyst was fresh differed only

slightly indicating small sintering effects. After desulfation similar trends were observed at this temperature as well, however the overall NO_X reduction performance was lower than both the fresh and thermally aged cases. While NO_X was trapped at this temperature, there was also a high NO_X release indicating again that regeneration was affected by sulfur exposure. Sulfates formed by sulfur poisoning can lower active surface area. A build up of lanthanum sulfates again has been observed to lower performance [132]. There was however a larger amount of NH_3 produced which will be discussed below. At 375°C the performance after thermal aging and desulfation after sulfur exposure was lower from that of the performance when the catalyst was fresh. The amount of NO_X released with and without reductant were the same. This suggests that at this temperature there was a slower reductant delivery rate than the rate of nitrate decomposition due to poor nitrate stability. Although this was true for when the catalyst was fresh at higher temperature it would seem that sintering did have an effect on nitrate stability once the catalyst was thermally aged. After desulfation the same results were seen; this doesn't suggest though that it was a result of the sulfur poisoning because damage was already done from thermal aging.

Little to no N_2O was formed during the regeneration phase in any case (fresh, thermally aged, sulfur exposure and desulfation) and at any of the temperatures. When the catalyst was fresh, at 375°C NH_3 release was delayed and not observed until after about 30 seconds from the onset of regeneration. A high NO_X to reductant ratio can be used to explain this delay in NH_3 breakthrough, as discussed in Chapter 4. This effect was also seen once the catalyst was thermally aged and also once it was desulfated from sulfur poisoning but with decreased

effect. In testing Pt-based LNT catalysts, reductant breakthrough typically coincides with NH_3 observed [109]. Over the fresh catalyst some NO_X was still left over on the surface as evident by the fact that NH_3 was still being released at the end of the regeneration phase. This was not seen once the catalyst was thermally aged where there was only 2-3 ppm of NH_3 coming out at the end of the regeneration phase. This suggests that less NO_X was left on the catalyst, possibly due to less trapped during the lean phase or less effective reduction of the NO_X remaining. The same results were found once the catalyst was desulfated after sulfur poisoning. With regards to CO breakthrough over the fresh sample, it was immediately observed after the onset of regeneration. The CO concentration decreased and then increased again near the end of the regeneration phase when NH_3 was also still being observed. These results suggest that surface NO_X species may be inhibiting the CO reaction with OSC, possibly through the OSC component, ceria, trapping NO_X [133]. Once the catalyst was thermally aged the same effect was observed, with CO breakthrough at the very beginning of the regeneration phase, then decreasing only to increase again. The results differed in that the second increase in CO concentration occurred at about 3 minutes into the regeneration phase once the sample was thermally aged whereas over the fresh catalyst it was at about 6 minutes into the regeneration phase. Again, the same results were found once the catalyst was desulfated after sulfur poisoning. The second increase in CO concentration occurring earlier in the thermally aged and desulfated cases suggest that less nitrates and stored oxygen were on the surface, thus less reductant was needed. As will be shown below, indeed there was somewhat less OSC and the data discussed above show less NO_X trapped. At 288°C over the

fresh catalyst, CO was also observed at the onset of regeneration, and then the outlet concentration decreased, again indicating surface nitrates inhibit consumption of CO in OSC or nitrate reduction. Here these results did not alter much once the catalyst was thermally aged and desulfated from sulfur poisoning.

In all, most of the trends were similar when the catalyst was fresh, thermally aged and desulfated after sulfur exposure, where a decrease in temperature led to a decrease in the amount of NO_X released relative to the amount of NO_X trapped. In all cases trapping was limited by both NO oxidation and nitrate formation diffusion at lower temperatures. Over the fresh catalyst at 463 and 550°C there are limitations due to nitrate stability. After thermal aging and desulfation this limitation was also seen at 375°C. NH_3 formation was observed with reductant breakthrough or high reductant to stored NO_X ratios. There was a substantially higher level of NO_X conversion during short cycling than long cycling in the middle operating temperature region. Short cycling led to better overall conversions due to more reductant readily available for reduction relative to all being consumed for OSC reduction, as well as less NO_X stored during the shorter lean phase.

5.3 Effects of Thermal Aging and Sulfur Poisoning on Water Gas Shift (WGS) Extent

A common reaction occurring during the regeneration step of LNT cycling experiments and in practice is the water gas shift (WGS) reaction [70, 77, 98, 120]. The WGS reaction occurs when both H_2O and CO are present via the following reaction: $CO + H_2O \rightarrow H_2 + CO_2$. The reductant gases consisted of a mixture of CO and H_2 during the regeneration phase and the

entire cycle included water. As such, the CO levels can drop and more H_2 can be formed and used as a reductant. Previous work shows that H_2 can more effectively reduce NO_X that is trapped in the lean phase of the cycle than can CO at lower temperatures [98, 121, 123], thus the more H_2 being used as a reductant the more efficient the entire process is. The extent of this effect can be altered by the catalysts exposure to thermal degradation and sulfur poisoning. The CO levels during the regeneration phase of the long cycling experiments, when the catalyst was fresh, thermally aged, and exposed to sulfur (before and after desulfation), were monitored and it was evident that WGS occurred. Results of the WGS experiments completed at 5 temperatures are listed in Table 13.

Table 13: WGS extent of fresh (bare and fully formulated), thermally aged, desulfated and sulfur poisoned catalyst at 200, 288, 375, 463 and 550 °C

Temp (°C)	BARE - FRESH	FULLY FORMULATED - FRESH	THERMALLY AGED	SULFUR POISONED WITH DESULFATION	SULFUR POISONED ONLY
	WGS Extent (%)	WGS Extent (%)	WGS Extent (%)	WGS Extent (%)	WGS Extent (%)
200	5	3	0	0	0
288	4	55	47	12	10
375	3	*	*	*	*
463	2	85	83	84	*
550	1	70	68	70	*
*Note: * Denotes that a WGS extent value was undetermined due to the fact that a CO value did not reach steady state when the rich phase was complete*					

The WGS data were obtained from the CO levels at the end of the regeneration phase of the 3rd long cycle. The data in Table 13 show that the WGS extent increased with an increase in temperature, but dropped between 463 and 550°C for all cases (fresh, thermally aged, before and after desulfation). Although the effect of temperature had the same trends for all cases, there were different effects caused by thermal aging and sulfur exposure (before and after desulfation) at each temperature. Past literature involving $Pt/Ba/Al_2O_3$ and $Pt/K/Al_2O_3$ catalysts showed that the WGS reaction occurs over the precious metal site [26, 70, 91, 120, 134, 135], thus any negative impact on precious metal site performance will likely consequently affect WGS extent. However it has also been shown that other components can promote the WGS reaction, specifically Ce (a component included in this perovskite LNT catalyst) has been proven to be a WGS promoter[91], thus sintering of other components of the catalyst can also decrease activity and in turn WGS extent as well. Table 13 shows that at the lowest temperature (200°C) the WGS extent was nil after thermal aging, and exposure to sulfur (both before and after desulfation) albeit the fresh catalyst started with a low WGS extent of only 3%. At 288°C decreased WGS extent was also observed after thermal aging, and exposure to sulfur (both before and after desulfation) relative to the fresh catalyst. As mentioned in the introduction section, sintering can lower the exposed precious metal surface area and the washcoat surface area (in this case the perovskite itself). However in order to lower the WGS extent, a WGS component must sinter; i.e. the Ce or Pd components or the perovskite washcoat itself. In order to distinguish which components were affected, between the Ce or Pd and perovskite, WGS extents of the fresh fully formulated perovskite catalyst

(which includes Ce and Pd) and the bare fresh perovskite catalyst (which does not include Ce or Pd) were compared. As seen in Table 13, the bare fresh perovskite catalyst had very low WGS extent. Alternatively, the fresh fully formulated perovskite catalyst proved to be active for WGS suggesting that sintering of the Ce or Pd component caused a drop in the WGS extent at 288°C. In a past study of a Pt-based LNT catalyst containing a Ce component, sintering (observed by a decrease in surface area) of the Ce component was found[136]. However, as seen in the OSC section below, at 288°C there was no loss in OSC activity after thermally aging the catalyst (OSC was almost fully recovered) which means that the OSC component, Ce, did not significantly sinter. It is suggested therefore, that Pd sintered, causing the 8% drop in WGS extent at 288°C. At higher temperature (463 and 550°C) there was no significant change in the WGS extent as seen in Table 13. Furthermore, the loss of Pd activity coincides well with the loss in reduction performance discussed above; further verifying that it is likely the Pd component that sintered.

After thermal degradation was performed on the catalyst, the catalyst was exposed to sulfur and then desulfated. Experiments were performed at 200 and 288°C before desulfation and after desulfation experiments were carried out at the same 5 test temperatures as when the catalyst was fresh. Table 13 shows that at 200°C the WGS extent was zero once the catalyst was thermally aged, once it was exposed to sulfur and then also once it was desulfated. This doesn't reflect that sulfur exposure itself lowered the activity of the catalyst but that after the catalyst was thermally aged the activity at 200°C was nil. Literature shows that the general catalyst formulation of Pt/alkali-alkaline-earth metal/Al_2O_3 are excellent sulfur traps [70,

137]. Literature on a Pt-based catalyst shows that sulfur poisoning in the lean phase (as was completed in this study) does not directly poison Pt itself but can be indirectly associated with poisoning by oxidizing SO_2 and other S species[106]. Sulfur can also be sorbed by other components in the catalyst and react to form sulfates, sulfites and sulfides on Pt-based catalysts and perovskite-based catalysts [83, 84]. At 288°C, while the values for WGS extent were the best when the catalyst was fresh, values differed once the catalyst was thermally aged and exposed to sulfur. As suggested above, thermal aging caused some sintering and deactivation of the Pd sites resulting in a lower WGS extent. However, poisoning the catalyst with sulfur led to a more significant drop in WGS extent. The desulfation process only restored some activity, with WGS at 12%, suggesting Pd was irreversibly poisoned. Note, the catalyst had been previously thermally aged to decouple any thermal aging effects related to desulfation (i.e. to directly compare S-poisoned versus desulfated performance). Sulfur uptake and release was measured and most or all of the sulfur stored was released. These data cannot distinguish which of the WGS components, Pd or Ce, irreversibly lost WGS activity with S exposure even after apparently significant S release. Yet again, in the OSC section below, OSC activity was recovered at 288°C showing Ce was not irreversibly damaged. It is suggested that the Pd sites were significantly impacted by sulfur, which lowered WGS extents at this temperature. Again, this coincides well with the loss in reduction performance noted also, where Pd can play a role in nitrate decomposition and released NO_X reduction, the latter of which decreased with aging.

5.4 Effect of Thermal Degradation and Sulfur Poisoning on Oxygen Storage Capacity (OSC)

The long cycling results, for temperatures of 200, 288, 375, 463 and 550°C, and the data obtained during the regeneration phases, over the fresh catalyst and the once the catalyst was thermally aged, suggest OSC was present. Stored O_2 competes for reductants, which could have otherwise been used to reduce stored NO_X. The amount of O_2 stored and the significant role in the regeneration phase it played was evaluated. The OSC of the catalyst when in its fresh state as well as after thermal aging and sulfur exposure (before and after desulfation) was quantified via CO consumption experiments to evaluate and compare the OSC competition. The catalyst was exposed to a lean gas stream consisting of 10% O_2, 5% CO_2, and a balance of N_2 for 60 seconds, and then the gas was switched to the rich gas stream consisting of 5% CO_2, 1% CO and a balance of N_2 for 90 seconds. H_2O was not included in this experiment in order to eliminate the WGS effect. The outlet CO concentrations were integrated and used to calculate the amount of O_2 being consumed.

Table 14: OSC for fresh (bare and fully formulated), thermally aged, desulfated and sulfur poisoned catalyst at 200, 288, 375, 463 and 550 °C

Temp (°C)	BARE - FRESH	FULLY FORMULATED - FRESH	THERMALLY AGED	SULFUR POISONED WITH DESULFATION	SULFUR POISONED ONLY
	O_2 Stored (µmoles)	O_2 Stored (µmoles)	O_2 Stored (µmoles)	O_2 Stored (µmoles)	O_2 Stored (µmoles)
200	50	61	60	57	49
288	60	114	112	112	88
375	75	312	307	305	*
463	145	408	403	410	*
550	185	442	441	450.1	*
*Note: * Denotes that a WGS extent value was undetermined due to the fact that a CO value did not reach steady state when the rich phase was complete*					

Table 14 lists the results from these experiments and shows that the amount of O_2 stored consistently increased with increasing temperature when the catalyst was fresh, thermally aged and exposed to sulfur (both before and after desulfation). When the catalyst was thermally aged, stored O_2 fell slightly, less by a couple of µmoles at each temperature, suggesting that slight sintering of the OSC component or an OSC promoter could have occurred, but did not hinder the OSC capabilities greatly. The effects of sulfur poisoning without desulfation (carried out only at 200 and 288°C) significantly decreased the OSC as seen in Table 14 for both temperatures. At 200°C, 61 µmoles, 60 µmoles and 49 µmoles and at 288°C 114 µmoles, 112 µmoles and 88 µmoles of O_2 were stored for the fresh catalyst,

once the catalyst was thermally aged and then exposed to sulfur poisoning, respectively. This shows that sulfur exposure decreased the OSC activity of the catalyst. It is possible that stored sulfates formed on the Ce OSC component as has been observed over a Pt-based LNT catalyst containing Ce [28], taking up surface area that could have otherwise been used to store O_2 hence a decrease in OSC. OSC experiments over the fresh fully formulated perovskite catalyst (which includes Ce) and the bare fresh perovskite catalyst (which does not include Ce) were compared. As seen in Table 14 the bare fresh perovskite catalyst had lower OSC values in comparison to the fresh fully formulated perovskite catalyst (which includes Ce). Thus the perovskite alone is not as active for O_2 storage as is the perovskite containing Ce suggesting that S species formed on the Ce component causing a drop in the OSC capabilities. Results of the OSC tests after desulfation are shown in Table 14, which show that at all five temperatures OSC was restored to the values found after thermally aging the catalyst. This suggests that the sulfur was in fact removed from the OSC related sites.

5.5 Effect of Thermal Degradation and Sulfur Poisoning on using NO_2 as NO_X Source

Typical LNT catalysts trap NO_2 more easily than NO, which includes rates of trapping as well as extents, as evident in literature [47 – 51, 56, 109]. In testing the catalyst in its fresh state, using NO_2 as the NO_X source rather than NO also significantly increased the amount of total NO_X trapped, as observed by comparing the values in Table 15. For example, at 200°C when the NO_X source was NO or NO_2, 36 and 178 µmoles of NO_X were trapped, respectively, and at 288°C, 137 µmoles and 353 µmoles of NO_X were trapped, respectively.

These results follow the same trends observed with Pt-based LNT catalysts, where limiting factors at low temperatures are NO oxidation and nitrate diffusion [107], as well as the increased NO_2 gas to solid phase equilibrium[113]. While the same trend was observed as seen in Table 15, there is less of an effect once the catalyst was thermally aged and once the catalyst was poisoned by sulfur both before and after desulfation when using NO_2 as a NO_X source instead of NO. For example once the catalyst was thermally aged at 200°C when the NO_X source was NO or NO_2, 28 and 34 µmoles of NO_X were trapped, respectively, and at 288°C, 134 µmoles and 150 µmoles of NO_X were trapped, respectively. As Ba is the trapping component, these data suggest that trapping reactions on Ba were negatively affected by the thermal aging and sulfur poisoning treatments. It is thought that NO_2 can sorb to sites both surrounding and further away from the oxidation sites [106]. And lower performance during long cycling experiments on the fresh catalyst was attributed to diffusion limitations, with a build-up of nitrates around the oxidation/reduction sites.

Table 15: Long cycle storage and reduction performance results using NO_2 as the NO_X source: 300 ppm NO_2, 10% O_2, 5% CO_2, 5% H_2O and a balance of N_2 in the lean phase; 625 ppm CO, 375 ppm H_2, 5% CO_2, 5% H_2O and a balance of N_2 rich phase

Catalyst State	Temp (°C)	NO_2 as NO_X source NO_X Trapped (µmoles)	NO as NO_X source NO_X Trapped (µmoles)	NO_2 as NO_X source NO_X Trapped - at 20% BT	NO as NO_X source NO_X Trapped - at 20% BT
Fresh	**200**	178	36	35	21
	288	353	137	67	56
Thermally Aged	**200**	34	28	21	19
	288	150	134	65	63
Sulfur Poisoned – Before Desulfation	**200**	15	14	7	7
	288	75	24	31	17
Desulfation – After Sulfur Poisoning	**200**	35	24	18	19
	288	148	139	63	63

With sulfur exposure, the same may occur – a build-up of sulfates around the oxidation sites, as well as sulfates forming on Ba sites far away from the oxidation sites. However, the trapping sites in proximity to the oxidation sites do not require gas-phase NO_2 to form nitrates, but oxidation of NO at those sites can lead to nitrate formation via a spill-over type mechanism. Similarly, reduction of the nitrates, to N_2, occurs via a spill-over type mechanism, either of NO diffusing to the reduction site, or H_2 dissociating and spilling over to the nitrate site. The loss of NO_2 enhancement suggests that this diffusion limitation may

have become more severe with aging, such that sites further away from the oxidation sites are no longer able to trap NO_X. During the experiment, three lean and rich cycles were performed in order to achieve cycle-to-cycle stability. As with the fresh catalyst, all three cycles overlay (at both 200 and 288°C) indicating it is not a regeneration-limited effect. This suggests again that limitations are not due to regeneration but to a loss of access to previously available trapping sites.

Chapter 6

Conclusions

A perovskite-based LNT catalyst was studied, which contained no Pt, but did contain Pd and Rh as part of the formulation. The NO oxidation kinetic study shows that the orders in NO, O_2 and NO_2 were 1.13 ± 0.25, 1.06 ± 0.06, and -1.01 ± 0.26, respectively. The activation energy was found to be 82 ± 11 kJ/mol for the fully formulated perovskite catalyst and 81 ± 11 kJ/mol for the bare perovskite catalyst. The similar Ea values, as well as conversions over both catalysts, suggest that the perovskite itself catalyzes the reaction and that Pd itself plays a nominal role in the reaction pathway. In terms of LNT performance, low temperature activity was limited by NO oxidation or surface diffusion and high temperature performance was limited by nitrate/nitrite stability. Using NO_2 proved to significantly enhance trapping ability. OSC was significant and therefore will contribute to reductant consumption competition between stored O_2 and stored NO_X. In comparing this perovskite-based catalyst to a Pt-based catalyst, most of the reaction chemistry observed was the same. However, the data suggest that the diffusion limitation was stronger on the perovskite, at low temperature regeneration was not a limiting factor for trapping, and that OSC consumption was initially inhibited by the presence of nitrates on the surface; all which differ from previous observations using a Pt-based LNT.

The same perovskite-based LNT catalyst was studied for its durability and limitations both before and after thermal degradation and S poisoning, and after desulfation to monitor its potential recovery from S poisoning. The NO oxidation kinetic study shows the activation energy (Ea) was 82 ± 11 kJ/mol for the fully formulated fresh perovskite catalyst, and after thermal aging the Ea was 78 ± 11 kJ/mol. The NO to NO_2 conversion trends when the catalyst was in a fresh, thermally aged and desulfated state were similar, however the conversion dropped after thermal aging possibly due to sintering of the Pd, Rh or more likely the perovskite itself. In terms of LNT performance, low temperature activity was limited by NO oxidation or surface nitrate diffusion and high temperature performance was limited by nitrate stability whether the catalyst was fresh, thermally aged or exposed to sulfur poisoning. After short and long cycling experiments the NO_X conversion and trapping abilities dropped once the catalyst was thermally aged which led to poorer overall reduction. After the catalyst was exposed to sulfur poisoning there was some drop in performance, and after desulfation there was still some performance loss, suggesting some (but not significant) S species remained on the catalyst even after desulfation. Using NO_2 proved to significantly enhance trapping ability over the fresh catalyst however this effect was not observed after thermal aging and S exposure. OSC was still significant, but there was a drop in the WGS extent, and coupled with the OSC results, the data suggest that the Pd component sintered during the thermal treatment, but was also severely impacted during S exposure.

Chapter 7

Recommendations

The goals for the research were to study NO oxidation, NO_X trap and reduction chemistry and limitations for the perovskite-based LNT catalyst in comparison to the standard Pt-based LNT catalyst. The goal also included the investigation of the effects of thermal degradation and sulfur poisoning on the perovskite-based LNT catalyst. The following are recommendations for future work:

1. Reductants used in this research were CO and H_2. What would be the effect of adding hydrocarbons to the reductant mixture? Would the amount of NO_X release and reduced change?
2. Would the amount of NH_3 formed be enough to feed a downstream SCR catalyst?
3. Would the thermal degradation results data be worse if the aging procedure was completed at a higher temperature and with a different gas mixture?
4. Sulfates were not measured after sulfur poisoning experiments and thus not identified exactly. What would be the results of BET and DRIFTS experiments after sulfur poisoning and before and after desulfation?

References

[1] DieselNet Technology, "Emission Control Catalysts," Ecopoint Inc. Revision, 2000. [Online]. Available: http://www.dieselnet.com/tech/cat_top.php. [Accessed July 2012].

[2] N. Miyoshi, S. Matsumoto, K. Katoh, T. Tanaka, J. Harada, N. Takahashi, K. Yokota, M. Sgiura and K. Kasahara, *SAE Technical Paper Series 950809 ,* 1995.

[3] N. Takahashi, H. Shinjoh, T. Iijima, T. Suzuki, K. Yamazaki, K. Yokota, H. Suzuki, N. Miyoshi, S. Matsumoto, T. Tanizawa, T. Tanaka, S. Tateishi and K. Kasahara, *Catalysis Today,* vol. 27, p. 63, 1996.

[4] W. S. Epling, J. Parks, G. Campbell, A. Yezerets, N. Currier and L. Campbell, *Catalysis Today ,* vol. 96, p. 21, 2004.

[5] W. S. Epling, L. Campbell, A. Yezerets, N. Currier and J. Parks, *Catalysis Review ,* vol. 46, p. 163, 2004.

[6] C. H. Kim, G. Qi, K. Dahlberg and W. Li, *Science,* vol. 327, p. 1624, 2010.

[7] J.C.Summers and J. S. A. Frost, "The 1990 Clean Air Act and Catalytic Emission Control for Stationary Sources," in *Catalytic Control of Air Pollution*, Washington, DC, ACS Symposium Series 495, American Chemical Society, 1992.

[8] The United States Environmental Protection Agency, "Air Trends: Basic Information," January 2012. [Online]. Available: http://www.epa.gov/airtrends/sixpoll.html. [Accessed July 2012].

[9] The United States Environmental Protection Agency, "Climate Change Basics," June 2012. [Online]. Available: http://www.epa.gov/climatechange/basics/. [Accessed July 2012].

[10] The United States Environmental Protection Agency, "Greenhouse Gas Emissions," June 2012. [Online]. Available: http://www.epa.gov/climatechange/ghgemissions/gases.html. [Accessed July 2012].

[11] The United States Environmental Protection Agency, "Sources of Greenhouse Gas Emissions," June 2012. [Online]. Available:

http://www.epa.gov/climatechange/ghgemissions/sources.html. [Accessed July 2012].

[12] W. A. Majewski and M. K. Khair, Diesel Emissions and Their Control, Warrendale, Pennsylvania: SAE International, 2006.

[13] Automobiletech, "Diesel Engine," 2012. [Online]. Available: http://www.automobilehitech.com/diesel-engine/. [Accessed July 2012].

[14] C. D. Cooper and F. Alley, Air Pollution Control: A Design Approach, 3rd Edition, Prospect Heights, IL: Waveland Press, 2002.

[15] Centers for Disease Control and Prevention, "Carbon Monoxide Poisoning," November 2011. [Online]. Available: http://www.cdc.gov/co/. [Accessed July 2012].

[16] Medscape, "Nitrous Dioxide Toxicity," March 2012. [Online]. Available: http://emedicine.medscape.com/article/820431-overview. [Accessed July 2012].

[17] CleanAIR SYSTEMS , "FAQs - General," 2011. [Online]. Available: http://www.cleanairsys.com/about/faqs/faq-general.htm. [Accessed July 2012].

[18] The United States Environmental Protection Agency, "Air Quality Trends," January 2012. [Online]. Available: http://www.epa.gov/airtrends/aqtrends.html. [Accessed July 2012].

[19] The United States Environmental Protection Agency, "Air Trends: Basic Information," January 2012. [Online]. Available: http://www.epa.gov/airtrends/sixpoll.html. [Accessed July 2012].

[20] Environmental Protection Agency, "Air Emission Sources: Nitrogen Oxides," July 2012. [Online]. Available: http://www.epa.gov/cgi-bin/broker?_service=data&_debug=0&_program=dataprog.national_1.sas&polchoice=NOX. [Accessed July 2012].

[21] R. M. Heck and R. J. Farrauto, Catalytic Air Pollution Control: Commercial Technology, 2nd Ed., New York, NY: John Wiley & Sons Inc., 2002.

[22] D. T. Guide, "Emission Control Catalysts," Ecopoint Inc. Revision , 2000. [Online]. Available: http://www.dieselnet.com/tech/cat_top.php. [Accessed July 2012].

[23] A. Berger, O. Hatling and D. Rodriguez-Ortiz, "Three Way Catalitic Converter," UC Berkeley, 2009. [Online]. Available: http://www.cchem.berkeley.edu/molsim/teaching/fall2009/catalytic_converter/bkgcatcon.html. [Accessed July 2012].

[24] G. Qi, C. W. Kim and W. Li, "Pt-free, Perovskite-based Lean NOx Trap Catalysts," in *DEER Conference*, Detroit, 2010.

[25] "Precious Metals Spot Prices and Charts," Northwest Territorial Mint, [Online]. Available: http://bullion.nwtmint.com/spot-price-charts.php. [Accessed July 2012].

[26] R. Farrauto and C. Bartholomew, Fundamentals of Industrial Catalytic Processes, 1st ed., New York, NY: Blackie Academic & Professional, 1997.

[27] F. Rohr, U. Gobel, P. Kattwinkel, S. Philipp and P. Gelin, *Applied Catalysis B: Environmental*, vol. 70, p. 189, 2007.

[28] C. Courson, A. Khalfi, H. Mahzoul, S. Hodjati, N. Moral, A. Kiennemann and P. Gilot, *Catalysis Communications*, vol. 3, p. 471, 2002.

[29] S. Poulston and R. Rajaram, *Catalysis Today*, vol. 81, p. 603, 2003.

[30] X. Wei, X. Liu and M. Deeba, *Applied Catalysis B: Environmental*, vol. 58, p. 41, 2005.

[31] Z. Liu and J. A. Anderson, *Journal of Catalysis*, vol. 228, p. 243, 2004.

[32] L. Lietti and P. Forzatti, *Catalysis Today*, vol. 52, p. 165, 1999.

[33] J. Butt and E. Petersen, Activation, deactivation and poisoning of catalysts, New York: Academic Press, Inc., 1988.

[34] S. GA, Introduction to Surface Chemistry and Catalysis, New York: John Wiley & Sons, Inc., 1994 .

[35] M. A. Pena and J. L. G. Fierro, *Chemical Reviews*, vol. 101, p. 1981, 2001.

[36] Mineralogy Database, "Perovkite Mineral Data," July 2012. [Online]. Available:

http://webmineral.com/data/Perovskite.shtml. [Accessed July 2012].

[37] L. Jana, S. Petra and M. Trojan, *Journal of Thermal Analysis and Calorimetry 93 (3): 823,* vol. 93, p. 823, 2008.

[38] W. R. Moser, Catalytic Chemistry of Solid State Inorganics, New York: New York Academy of Sciences, 1976.

[39] M. R. Levy, "Crystal Structure and Defect Property Predictions in Ceramic Materials," Department of Materials, Imperial College of Science, Technology and Medicine, London, 2005.

[40] J. McCarty and H. Wise, *Catalysis Today* , vol. 8, p. 231, 1990.

[41] H. Arai, T. Yamada, K. Eguchi and T. Seiyama, *Applied Catalysis,* vol. 26, p. 265, 1986.

[42] R. Spinicci, M. Faticanti, P. Marini, S. D. Rossi and P. Porta, *Journal of Molecular Catalysis A: Chemical* , vol. 197, p. 147, 2003.

[43] F. López-Suárez, M. Illán-Gómez, A. Bueno-López and J. A. Anderson, *Applied Catalysis B: Environmental* , vol. 104, p. 261, 2011.

[44] T. Harada, Y. Teraoka and S. Kagawa, *Applied Surface Science* , vol. 121, p. 505, 1997.

[45] X. He, M. Meng, J. He, Z. Zou, X. Li, Z. Li and Z. Jiang, *Catalysis Communications,* vol. 12, p. 165, 2010.

[46] X. Zhang, H. Li, Y. Li and W. Shen, *Catalysis Letters,* vol. 142, p. 118, 2011.

[47] D. Parker and B. Koel, *Journal of Vacuum Science and Technology A,* vol. 8, p. 2585, 1990.

[48] F. Rodrigues, L. Juste, C. Potvin, J. Tempère, G. Blanchard and G. Djéga-Mariadassou, *Catalysis Letters,* vol. 72, p. 59, 2001.

[49] S. Hodjati, K. Vaezzadeh, C. Petit, V. Pitchon and A. Kiennemann, *Catalysis Today,*

vol. 59, p. 323, 2000.

[50] S. Hodjati, C. Petit, V. Pitchon and A. Kiennemann, *Journal of Catalysis,* vol. 197, p. 324, 2001.

[51] N. Cant and M. Patterson, *Catalysis Today ,* vol. 73, p. 271, 2002.

[52] H. Ohtsuka and T. Tabata, *Applied Catalysis B: Environmental,* vol. 29, p. 177, 2001.

[53] H. Ohtsuka, *Applied Catalysis B: Environmental,* vol. 33, p. 325, 2001.

[54] A. Amberntsson, E. Fridell and M. Skoglundh, *Applied Catalysis B: Environmental ,* vol. 46, p. 429, 2003.

[55] S. Salasc, M. Skoglundh and E. Fridell, *Applied Catalysis B: Environmental,* vol. 36, p. 145, 2002.

[56] S. Mulla, N. Chen, W. Delgass, W. Epling and F. Ribeiro, *Catalysis Letters,* vol. 100, p. 267, 2005.

[57] B. M. Weiss and E. Iglesia, *Journal of Catalysis,* vol. 272, p. 74, 2010.

[58] H. Mahzoul, J. F. Brilhac and P. Gilot, *Applied Catalysis B: Environmental,* vol. 20, p. 47, 1999.

[59] F. Prinetto, G. Ghiotti, I. Nova, L. Lietti, E. Tronconi and P. Forzatti, *Journal of Physical Chemistry B,* vol. 105, p. 12732, 2001.

[60] S. Hodjati, K. Vaezzadeh, C. Petit, V. Pitchon and A. Kiennemann, *Applied Catalysis B: Environmental,* vol. 26, p. 5, 2000.

[61] S. Hodjati, P. Bernhardt, C. Petit, V. Pitchon and A. Kiennemann, *Applied Catalysis B: Environmental,* vol. 19, p. 209, 1998.

[62] L. Liotta, A. Macaluso, G. Arena, M. Livi, G. Centi and G. Deganello, *Catalysis Today,* vol. 75, p. 439, 2002.

[63] S. Erkfeldt, E. Jobson and M. Larsson, *Topics in Catalysis 2001,* vol. 16, p. 12, 2001.

[64] B. Westerberg and E. Fridell, *Journal of Molecular Catalysis A: Chemical,* vol. 165, p. 249, 2001.

[65] T. J. Toops, D. B. Smith, W. S. Epling, J. E. Parks and W. P.Partridge, *Applied Catalysis B: Environmental,* vol. 58, p. 255, 2005.

[66] F. Erik, S. Magnus, W. Björn, J. Stefan and S. Gudmund, *Journal of Catalysis,* vol. 183, p. 196, 1999.

[67] H. Mahzoul, P. Gilot, J.-F. Brilhac and B. Stanmore, *Topics in Catalysis* , vol. 16, p. 293, 2001.

[68] C. Narula, S. Nakouzi, R. Wu, C. Goralski and L. Allard, *AIChE Journal,* vol. 47, p. 744, 2001.

[69] H. Abdulhamid, E. Fridell and M. Skoglundh, *Topics in Catalysis* , vol. 30, p. 161, 2004.

[70] L. Limousy, H. Mahzoul, J. Brilhac, P. Gilot, F. Garin and G. Maire, *Applied Catalysis B: Environmental,* vol. 45, p. 169, 2003.

[71] R. Muncrief, K. Coym and M. Harold, in *18th North American Meeting of the North American Catalysis Society,* Cancun, Mexico, 2003.

[72] L. Zhaoqiong and J. A. Anderson, *Journal of Catalysis* , vol. 224, p. 18, 2004.

[73] A. Annika, P. Hans, E. Per and K. Bengt, *Applied Catalysis B: Environmental,* vol. 31, p. 27, 2001.

[74] W. S. Epling, G. C. Campbell and J. E. Parks, *Catalysis Letters,* vol. 90, p. 45, 2003.

[75] J. Coronado and J. J. Anderson, *Molecular Catalysis A: Chemical* , vol. 138, p. 83, 1999.

[76] O. Bailey, D. Dou and G. Denison, *SAE Technical Paper Series 972845.*

[77] Y. Li, S. Roth, J. Dettling and T. Beutel, *Topics in Catalysis* , vol. 16, p. 139, 2001.

[78] H. Abdulhamid and E. F. M. Skoglundh, *Applied Catalysis B: Environmental,* vol. 62,

p. 319, 2006.

[79] R. Burch, J. Breen and F. Meunier, *Applied Catalysis B: Environmental* , vol. 39, p. 283, 2002.

[80] A. Obuchi, A. Ohi, M. Nakamura, A. Ogata, K. Mizuno and H. Ohuchi, *Applied Catalysis B: Environmental* , vol. 2, p. 71, 1993.

[81] R. Burch, P. Millington and A. Walker, *Applied Catalysis B: Environmental* , vol. 4, p. 65, 1994.

[82] H. Hamada, Y. Kintaichi, M. Inaba, M. Tabata, T. Yoshinari and H. Tsuchida, *Catalysis Today* , vol. 29, p. 53, 1996.

[83] I. Rosso, G. Saracco, V. Specchia and E. Garrone, *Applied Catalysis B: Environmental,* vol. 40, p. 195, 2003.

[84] L. G. Tejuca and J. Fierro, "Poisoning of perovskite oxides by sulfur dioxide," in *Properties and Applications of the Perovskite-type Oxides*, New York, Marcel Dekker, 1993, pp. 145-170.

[85] Y. Zhu, R. Tan, J. Feng, S. Ji and L. Cao, *Applied Catalysis A: General,* vol. 109, p. 71, 2001.

[86] Y. Zhu, R. Tan, J. Feng, S. Ji and L. Cao, *Applied Catalysis A: General,* vol. 209, p. 71, 2001.

[87] J. Breen, M. Marella, C. Pistarino and J. Ross, *Catalysis Letters,* vol. 80, p. 123, 2002.

[88] K. Yamamoto, R. Kikuchi, T. Takeguchi and K. Eguchi, *Journal of Catalysis,* vol. 238, p. 449, 2006.

[89] N. Takahashi, A. Suda, I. Hachisuka, M. Sugiura, H. Sobukawa and H. Shinjoh, *Applied Catalysis B: Environmental,* vol. 72, p. 187, 2007.

[90] L. Lietti, P. Forzatti, I. Nova and E. Tronconi, *Journal of Catalysis,* vol. 204, p. 175, 2001.

[91] J. Li, J. Theis, W. Chun, C. Goralski, R. Kudla, J. Ura, W. Watkins, M. Chattha and R. Hurley, *SAE Technical Paper Series 2001-01-2503.*

[92] E. Fridell, H. Persson, L. Olsson, B. Westerberg, A. Amberntsson and M. Skoglundh, *Topics in Catalysis,* vol. 16/17, p. 133, 2001.

[93] A. Amberntsson, B. Westerberg, P. Engstrom, E. Fridell and M. .. Skoglundh, *Catalyst Deactivation,* vol. 317, 1999.

[94] S. Matsumoto, Y. Ikeda, H. Suzuki, M. Ogai and N. Miyoshi, *Applied Cataysis. B: Environmental,* vol. 25, p. 115, 2000.

[95] M. Takeuchi and S. Matsumoto, *Topics in Catalysis,* vol. 28, p. 151, 2004.

[96] B. Kucharczyk and W. Tylus, *Catalysis Today,* vol. 90, p. 121, 2004.

[97] R. Weast, CRC Handbook of Chemistry and Physics, 56th Ed., CRC Press, LLC, 1975.

[98] M. AL-Harbi and W. Epling, *Applied Catalysis B: Environmental,* vol. 89, p. 315, 2009.

[99] M. Molinier, *SAE Technical Paper Series 2001-01-0508.*

[100] S. Erkfeldt, M. Skoglundh and M. Larsson, *Catalyst Deactivation,* p. 211, 1999.

[101] C. H. Kim, G. Qi, K. Dahlberg and W. Li, "Supporting Online Material for Strontium-Doped Perovskites Rival Platinum Catalysts for Treating NOx in Simulated Diesel Exhaust," 2010 www.sciencemag.org/cgi/content/full/327/5973/1624/DC1.

[102] D. Uy, A. O'Neill, J. Li and W. Watkins, *Topics in Catalysis,* vol. 95, p. 191, 2004.

[103] M. Casapu, J. Grunwaldt, M. Maciejewski, M. Wittrock, U. G. bel and A. Baiker, *Applied Catalysis B: Environmental,* vol. 63, p. 232, 2006.

[104] P. Doggali, S. Kusaba, Y. Teraoka, P. Chankapure, S. Rayalu and N. Labhsetwar, *Catalysis Communications,* vol. 11, p. 665, 2010.

[105] M. Misono, *Catalysis Today* , vol. 100, pp. 95-100, 2005.

[106] W. S. Epling, J. Parks, G. Campbell, A. Yezerets, N. Currier and L. Campbel, *Catalysis Today,* vol. 96, p. 21, 2004.

[107] J. Segner, W. Vielhaber and G. Ertl, *Israel Journal of Chemistry,* vol. 22, p. 375, 1982.

[108] D. Bhatia, R. W. McCabe, M. P. Harold and V. Balakotaiah, *Journal of Catalysis,* vol. 266, p. 106, 2009.

[109] W. Epling, A.Yezerets and N. W. Currier, *Applied Catalysis B: Environmental,* vol. 74, p. 117, 2007.

[110] J. Kwak, D. Kim, T. Szailer, C. Peden and J. Szanyi, *Catalysis Letters,* vol. 111, p. 119, 2006.

[111] W. S. Epling, A. Yezerets and N. Currier, *Catalysis Letters,* vol. 110, p. 143, 2006.

[112] J. Wang, Y. Ji, V. Easterling, M. Crocker, M. Dearth and R. W. McCabe, *Catalysis Today* , vol. 175, p. 83, 2011.

[113] M. AL-Harbi and W. S. Epling, *Catalysis Letters,* vol. 130, p. 121, 2009.

[114] I. Nova, L. Lietti, L. Castoldi, E. Tronconi and P. Forzatti, *Journal of Catalysis* , vol. 239, p. 244, 2006.

[115] A. Amberntsson, H. Persson, P. Engström and B. Kasemo, *Applied Catalysis B: Environmental,* vol. 31, p. 27, 2001.

[116] V. Medhekar, V. Balakotaiah and M. Harold, *Catalysis Today,* vol. 121, p. 226, 2007.

[117] J. A. Pihl, J. P. II, C. Daw and T. Root, *SAE Technical Paper Series 2006-01-3441.*

[118] L. Cumaranatunge, S. Mulla, A. Yezerets, N. Currier, W. Delgass and F. Ribeiro, *Journal of Catalysis* , vol. 246, p. 29, 2007.

[119] P. Forzatti, L. Lietti and I. Nova, *Energy and Environmental Science* , vol. 1, p. 236, 2008.

[120] J. A. Botas, M. A. Gutiérrez-Ortiz and M. P. González-Marcos, *Applied Catalysis B:*

Environmental , vol. 32, p. 243, 2001.

[121] T. Szailer, J. Kwak, D. Kim, J. Hanson, C. Peden and J. Szanyi, *Journal of Catalysis,* vol. 239, p. 51, 2006.

[122] E. Tzimpilis, N. Moschoudis, M. Stoukides and P. Bekiaroglou, *Applied Catalysis B: Environmental,* vol. 87, p. 9, 2009.

[123] M. AL-Harbi, "Performance and Reaction Activity Changes of a NOX Storage/Reduction," *Master of Applied Science, Thesis, Chemical Engineering, University of Waterloo, Waterloo Ontario,* 2008.

[124] P. Engstrom, A. Amberntsson, M. Skoglundh, E. Fridell and G. Smedler, *Applied Catalysis B: Environmental,* vol. 22, p. 241, 1999.

[125] K. Taylor, *Catalysis Reviews* , vol. 35, p. 457, 1993.

[126] B. H. Jang, T. H. Yeon, H. S. Han, Y. K. Park and J. E. Yie, *Catalysis Letters* , vol. 77, p. 21, 2001.

[127] N. Fekete, R. Kemmler, D. Voigtla¨nder, B. Krutzsch, E. Zimmer, G. Wenninger, W. Strehlau, J. v. d. Tillaart, J. Leyrer, E. Lox and W. Muller, *SAE Technical PaperSeries, 970746, 1997.*

[128] J. Parks, A. Watson, G. Campbell and W. S. Epling, *SAE Technical Paper Series 2002- 01-2880.*

[129] J. Parks, J. Watson, W. E. G. Wagner, M. Sanders and L. Campbell, *SAE Technical Paper Series 2000-01-1012.*

[130] K. Yamazaki, T. Suzuki, N. Takahashi, K. Yokota and M. Sugiura, *Applied Catalysis B: Environmental,* vol. 30, p. 459, 2001.

[131] S. Erkfeldt, M. Larsson, H. Hedblom and M. Skoglundh, *SAE Technical Paper Series 1999-01-3504.*

[132] M. Koponen, T. Venalainen, M. Suvanto, K. Kallinen, T. Kinnunen, M. Harkonen and T. Pakanen, *Journal of Molecular Catalysis A: Chemical,* vol. 258, p. 246, 2006.

[133] Y. Ji, T. J. Toops and M. Crocker, *Catalysis Letters*, vol. 119, p. 257, 2007.

[134] C. Satterfield, Heterogeneous Catalysis in Industrial Practice, 2nd Ed., Malabar, FL: Krieger Publishing Company, 1996.

[135] C. Serre, F. Garin, G. Belot and G. Marie, *Journal of Catalysis*, vol. 141, p. 1, 1993.

[136] Y. Ji, C. Fisk, V. Easterling, U. Graham, A. Poole and M. Crocker, *Catalysis Today*, vol. 151, p. 362, 2010.

[137] L. Limousy, H. Mahzoul, J. Brilhac, F. Garin, G. Maire and P. Gilot, *Applied Catalysis B: Environmental*, vol. 42, p. 237, 2002.

[138] EasyCalculations, "T Distribution Critical Values Table". [Online]. Available: http://easycalculation.com/statistics/t-distribution-critical-value-table.php [Accessed July 2012]

Appendix A

Sample Statistic Calculations

All experiments, analysis and calculations have associated error. For example, in experiments such as the kinetic experiments, the data from the experiments were plotted and linear regression was used to find the best fitting slope. The slope was used for either the kinetic reaction order or to determine the activation energy. The error that was associated with the slope, or the standard error of the slope, was calculated. Below are the statistical error equations and calculations used finding the reaction rate order for NO in the NO oxidation experiment. A t-distribution was used to find the margin of error in the calculated slope.

Standard error of slope = SE = $\frac{\sqrt{\sum(y_i-\hat{y}_i)^2/(n-2)}}{\sqrt{\sum(x_i-\bar{x})^2}}$ (40)

Where:

y_i is the value of the observed dependent variable

$\hat{y}_i$ is the estimated value of the dependent variable

n is the number of observations

x_i is the value of the observed independent variable

$\bar{x}$ is the mean of the observed independent variable

The margin of error = calculated slope $\pm$ SE x t_{crit} (41)

Where:

t_{crit} is a factor that is found in tables

In the example, finding the reaction rate order for NO in the NO oxidation experiment, the experimental data was plotted and the equation of the line was found to be:

y = 1.13x - 24.83

with slope 1.13, which would signify that the reaction rate order for NO is 1.13. However the error associated with this number/slope was found using equations (40) and (41) above.

Sample calculations

Table 16: Standard Error of Slope

$\hat{y}$	$y_i - \hat{y}$	$(y_i - \hat{y})^2$	$x_i - \bar{x}$	$(x_i - \bar{x})^2$
-19.6159702	-0.065102576	0.00423835	-0.91081509	0.829584136
-18.831331	0.023989367	0.00057549	-0.21766791	0.047379321
-18.5787336	0.03040615	0.00092453	0.00547564	2.99826E-05
-18.3723465	0.118390111	0.01401622	0.18779719	0.035267786
-18.1978487	0.04373764	0.00191298	0.34194787	0.116928349
-17.913362	-0.154114816	0.02375138	0.5932623	0.351960159

n – 2 = 4

$\sum(y_i - \hat{y}_i)^2$ = 0.0454

$(\sum(y_i - \hat{y}_i)^2) \ / \ (n-2)$ = 0.0114

$\sqrt{(\sum(y_i - \hat{y}_i)^2) \ / \ (n-2)}$ = 0.107

$\bar{x}$ = 5.516

$\sum(x_i - \bar{x})^2$ = 1.381

$\sqrt{\sum(x_i - \bar{x})^2}$ = 1.175

SE = $\frac{\sqrt{\sum(y_i - \hat{y}_i)^2/(n-2)}}{\sqrt{\sum(x_i - \bar{x})^2}} = \frac{0.107}{1.175}$ = 0.09

The margin of error = calculated slope $\pm$ SE x t_{crit}

t_{crit} = 2.78 (found in t-distribution table [138])

The margin of error = 1.13 $\pm$ 0.09 x 2.78

The margin of error = 1.13 $\pm$ 0.25